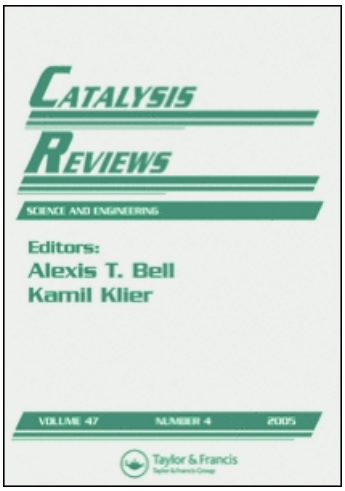

Catalysis Reviews
Publication details, including instructions for authors and subscription information:
http://www.informaworld.com/smpp/title~content=t713597232

Recent Advances in the Liquid-Phase Synthesis of Metal Nanostructures with Controlled Shape and Size for Catalysis

Natalia Semagina [a]; Lioubov Kiwi-Minsker [b]
[a] Department of Chemical and Materials Engineering, University of Alberta, Edmonton, Canada [b] Group of Chemical Reaction Engineering, Ecole Polytechnique Fédérale de Lausanne, Lausanne, Switzerland

Online Publication Date: 01 April 2009

To cite this Article Semagina, Natalia and Kiwi-Minsker, Lioubov(2009)'Recent Advances in the Liquid-Phase Synthesis of Metal Nanostructures with Controlled Shape and Size for Catalysis',Catalysis Reviews,51:2,147 — 217
To link to this Article: DOI: 10.1080/01614940802480379
URL: http://dx.doi.org/10.1080/01614940802480379

Catalysis Reviews, 51:147–217, 2009

ISSN: 0161-4940 print 1520-5703 online
DOI: 10.1080/01614940802480379

Recent Advances in the Liquid-Phase Synthesis of Metal Nanostructures with Controlled Shape and Size for Catalysis

Natalia Semagina[1] and Lioubov Kiwi-Minsker[2]

[1] Department of Chemical and Materials Engineering, University of Alberta, Edmonton, Canada
[2] Group of Chemical Reaction Engineering, Ecole Polytechnique Fédérale de Lausanne, Lausanne, Switzerland

Recent advances in the liquid-phase synthesis of metal nanostructures of different sizes and shapes are reviewed regarding their catalytic properties. The controlled synthesis of nanostructures is based on the colloid chemistry techniques in the solution, which use organic nanoreactors and a variety of stabilizers. Their catalytic activity and selectivity depend on the particle's shape and size, as shown for Suzuki and Heck coupling, hydrogenations, hydrogenolysis, oxidations, and electron-transfer reactions. The knowledge of a reaction's structure-sensitivity relationship is important for the rational catalyst design in view of process intensification. Nanostructures can be used *per se* and in supported form to meet the requirements of an eventual process.

Keywords Crystal surface, Metal nanoparticle, Shape effect, Size effect, Structure sensitivity

1. INTRODUCTION

During the last decades, catalysis by metal nanoparticles has attracted considerable attention due to the enhanced activity and selectivity of nanostructured materials. The unique features of metal nanoparticles, and thus, their catalytic properties, are significantly influenced by particle size, shape of the

Received 22 April 2008; Accepted 2 July 2008.
Address correspondence to Lioubov Kiwi-Minsker, Group of Chemical Reaction Engineering, Ecole Polytechnique Fédérale de Lausanne, Station 6, Lausanne CH-1015, Switzerland. E-mail: lioubov.kiwi-minsker@epfl.ch

crystal (cubic, tetrahedron, etc.), and the chemical nature of the microenvironment surrounding the nanoparticle (1–11).

Usually metal nanoparticles are prepared on a catalytic support (metal oxides, zeolites, carbon, solid polymer, etc.) (1–3, 12, 13). According to the Bradley's list modified by Aiken III and Finke (2), the synthesis involves either (i) transition metal salt reduction; (ii) thermal decomposition and photochemical methods (iii) ligand reduction and displacement from organometallics; (iv) metal vapor synthesis; or (v) electrochemical synthesis. However, the overwhelming majority of these techniques lack control over the nanoparticle size and shape. Moreover, the use of a support complicates catalytic studies due to possible internal diffusion limitations and/or strong metal-support interaction. On the contrary, colloidal methods using electrostatic ("inorganic") and/or steric ("organic") stabilization allow easy tuning of a nanostructure size and morphology.

Electrostatic stabilization occurs by the adsorption of ions on the electrophilic metal surface. This creates an electrical double layer, which results in a Coulombic repulsion force between individual particles. Steric stabilization is achieved by surrounding the metal center by layers of material that are sterically bulky, such as polymers or surfactant. These large adsorbates provide a steric barrier which prevents close contact of the metal particle centers (2). When the organic stabilizers form a spatially confined micro- or nanovolume, where nanoparticles may grow up to the restricted volume, one can speak about the engineered organic micro- or nanoreactors (emulsions, micelles, organized thin films, polyelectrolytes, etc.) (4, 5). The use of organic adsorbates and nanoreactors (templates) is the most efficient and easiest way to control metal nanostructure size and shape (4, 6).

The control over the nanoparticle size and shape is of fundamental importance for catalytic applications. Firstly, a high surface-to-volume ratio of nanomaterials provides high amount of active sites per metal mass. Secondly, there is a wide range of catalytic reactions, which rates for a given metal strongly depend on its surface characteristics. These catalytic reactions are called structure-sensitive (14–17) and include hydrogenations (18–21), oxidations (22, 23), Suzuki (24) and Heck (25) couplings, electron transfer reactions (26), etc. (27, 28). Most of these reactions have been studied in ultra-high vacuum using single metal crystals exhibiting definite crystallographic planes. However, these model catalysts are far away from the real catalytic systems (29). This "material gap" (29) is believed to be surpassed using stable nanostructures with desirable crystallographic orientations, which can be easily synthesized in a large scale. Crystal surface structure, in turn, depends on the size and shape of a nanoparticle.

The important requirement for the study of structure sensitivity is the preparation of a series of catalysts, which differ only in particle size and/or

shape. Heterogeneous catalytic particles of various sizes are typically prepared by using different precursors, supports, calcination conditions, producing catalysts which are intrinsically different one from another not only in size. Colloid preparation techniques, at contrast, provide catalytic metal particles with size or structure variation without other perturbations and thus, they are excellent materials suitable for catalytic investigations (25). Application of colloidal techniques for preparation of nanoparticles of various shapes and sizes allows understanding of the relationships between surface physicochemistry and nature of the active sites involved in the structure-sensitive reactions. This fundamental knowledge has a significant potential for the preparation of an eventual catalyst for industrially important reactions since the optimal shape and size provide the highest reaction rates and selectivities.

The presented review on the use of various metal nanostructures in catalysis is divided into three major parts. The first one discusses the liquid-phase size and shape-controlled colloidal syntheses of nanospheres (nanocubooctahedrons), nanocubes, nanotetrahedrons, nanorods, and nanowires. In spite of a wider variety of "platonic crystals" and other different anisotropic structures (dodecahedrons, icosahedrons, etc. (30, 31)), only the mentioned structures are reviewed. The reason is that their surface structures unambiguously reveal the catalytic reaction active sites, as nanocubes and nanotetrahedrons contain only (100) and (111) facets, respectively, while majority of nanowires and nanorods are composed predominantly from (100) or (110). The spheres containing both (100) and (111) facets are also included into discussion due to their extensive application in structure-sensitive reactions, as the number of atoms on the facets depend a particle size. As these particles are intended to give the information about active sites, the surface statistics of each of a nanocrystal is included. Colloidal syntheses involving steric stabilization and nanoreactors are exampled mainly for Pd, Pt, Au, and Ag due to their use in structure-sensitive catalysis by metals. The review does not cover the size-controlled preparation and catalytic properties of metal nanoparticles inside solid supports, including cross-linked polymers and mesoporous solids. These have been the object of several detailed reviews and books (1, 5, 8, 9, 13, 32, 33). The goal was to review liquid-phase colloidal methods used to prepare catalysts for size and shape effect studies.

The second part of the review is devoted to the structure sensitivity studies of hydrogenations, oxidations, Suzuki and Heck coupling, hydrogenolysis, and electron transfer reactions. The focus is made on the studies involving various nanostructures synthesized by the colloid techniques. However, since this field of catalysis is just emerging, the studies using traditional supported catalysts or single crystals are also discussed when necessary. Finally, there are also some case studies on nanostructures used in gas- and liquid-phase reactions in unsupported and supported form, including

conventional and structured (arranged) (34) supports. Immobilization may alter the nanoparticle size and shape distribution in the supported catalyst compared to the unsupported one (35, 36), but typically the stabilized nanostructures do not follow any changes upon immobilization (37, 38).

2. METAL NANOSTRUCTURES: SURFACE STATISTICS AND SYNTHESIS

2.1. Nanospheres

Nanospheres (spherical, round, or near spherical particles) are the most widespread and studied nanoparticles since thermodynamic imposes that metal atoms nucleate and grow preferably into a spherical shape. Transition metal nanospheres mostly show a face-centered cubic (f.c.c.) structure in the form of cuboctahedrons with their surfaces bounded by a mix of (111) and (100) facets (39).

The model of an f.c.c. cubooctahedron is presented in Fig. 1a (40). By the symbol C_j a surface atom with j nearest neighbors is denoted (40). To differentiate between atoms with the same j but different in arrangement, upper indices $p, q, r, \ldots$ etc. are added. They denote serial numbers of $(z\text{-}j)$ missing atoms, where for $p, q, r, \ldots$ always the lowest possible number is chosen. The z atoms in the complete set of nearest neighbors are numbered as shown in Fig. 1b. The set of indices thus obtained are abbreviated by omitting p, if corresponding to 1; q, is corresponding to 2, etc. When all indices should be left out this way, the last one $(=z\text{-}j)$ is retained, e.g., $C_6^{1,2,3,4,5,6} \rightarrow C_6^6$,

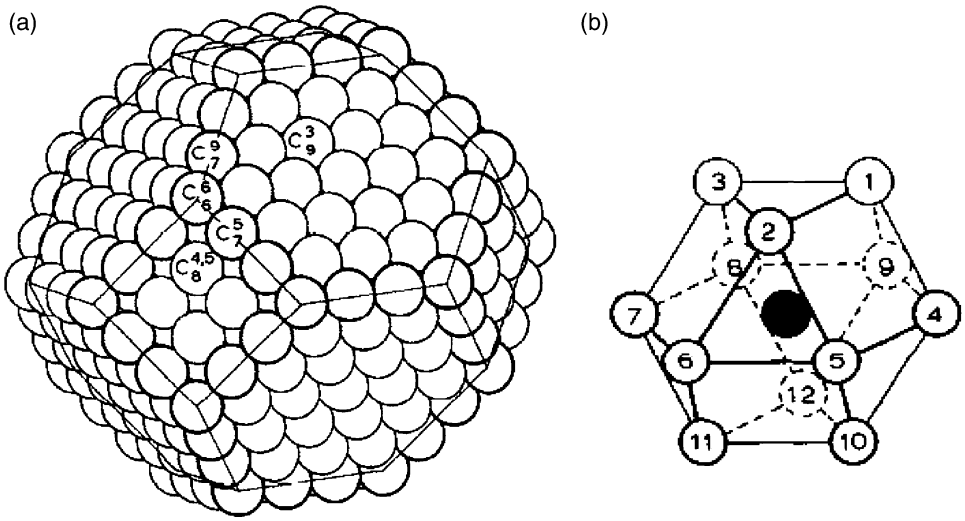

Figure 1: F.c.c. cubooctahedron (a) and (b) numbering of nearest neighbors in an f.c.c. structure. Reprinted from (40) with permission from Elsevier.

$C_8^{1,2,4,5} \rightarrow C_8^{4,5}$. To determine the surface statistics, i.e. the number of various surface atoms on a crystal with a given size, the dimensionless quantity d_{rel} is defined as the ratio of the diameter of a nanosphere typically found from transmission electron microscopy (TEM) or X-Ray diffraction (XRD) to the diameter the metal atom studied (40):

$$d_{rel} = d_{sph} / d_{at}. \quad (1)$$

For f.c.c. crystals total number of atoms N_T is determined as:

$$d_{rel} = 1.105 \cdot N_T^{1/3}. \quad (2)$$

In a series of geometrically similar crystals of different diameters, N_T is given by a polynomial of the third degree in m, with m being the number of atoms lying on an equivalent edge (corner atoms included). Number of surface atoms N_S is given by a polynomial of the second degree in m, while number of specific atoms by a polynomial of the 0^{th}, 1^{st}, or 2^{nd} degree in m, depending upon whether this type of atoms occurs on the corners on the edges or on the faces of the crystal. The surface atom statistics then depends on the size and type of a crystal. For an f.c.c. cubooctahedron it can be calculated using formulas presented in Table 1 (40). According to this, in order to change the fractions of various atoms on the particle surface, the size of a crystal should be varied: larger particles possess less fraction of "defect" (edge and corner) atoms, as visualized in Figs. 2 and 3.

Development of colloidal techniques for synthesis of nanospheres with a controlled size has been in focus of numerous studies in the past decades (2, 4–6, 41–43). Chemical or electrochemical reduction of metal ions proceeds in the presence of a stabilizer such as linear polymers, ligands, surfactants, polyelectrolytes, ionic liquids, which prevent the nanoparticles from aggregating and

Table 1: Crystal statistics for an f.c.c. cubooctahedron (40) with permission from Elsevier.

	M		
Number of metal atoms	**2**	**3**	**>3**
N_T	38	201	$16m^3-33m^2+24m-6$
N_S	32	122	$30m^2-60m+32$
$N(C_6^6)$	24	24	24
$N(C_7^9)$	0	12	$12(m-2)$
$N(C_7^5)$	0	24	$24(m-2)$
$N(C_8^{4,5})$	0	6	$6(m-2)^2$
$N(C_9^3)$	8	56	$8(3m^2-9m+7)$

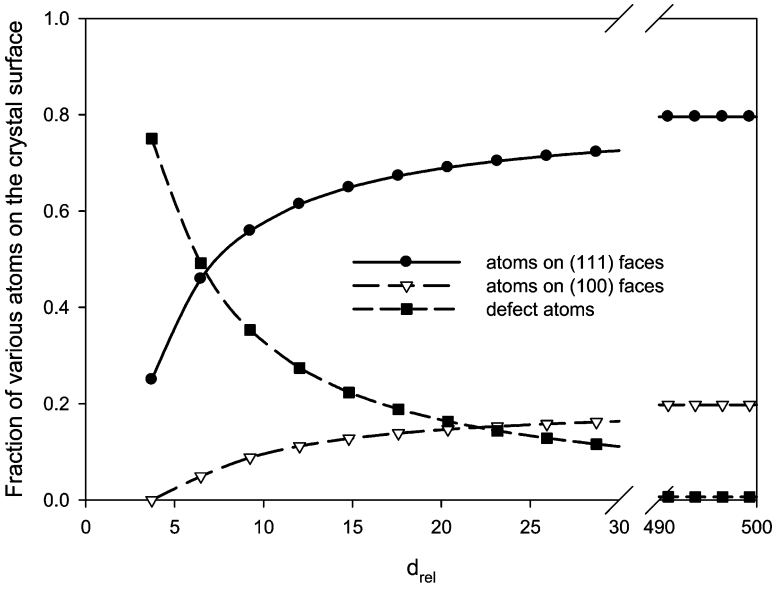

Figure 2: Variation of the fraction of various atoms on the surface of an f.c.c. cubooctahedon (40). Based on the data of Table 1 (40).

allow isolating the nanoparticles. In some cases, a stabilizing agent may also serve as a reducing agent, e.g., sodium citrate in colloidal gold (44) and silver formation (45). To control the particle size, the stabilizer, reducing agent, solvent, and other parameters have been varied. Below there are some examples of the colloidal synthetic methods to produce spherical nanoparticles used for the size effect studies in catalysis.

2.1.1. Linear Polymer as a Stabilizer

When a linear polymer is used as a protective agent, modification of the functional groups can offer a specific reactive field around the metal

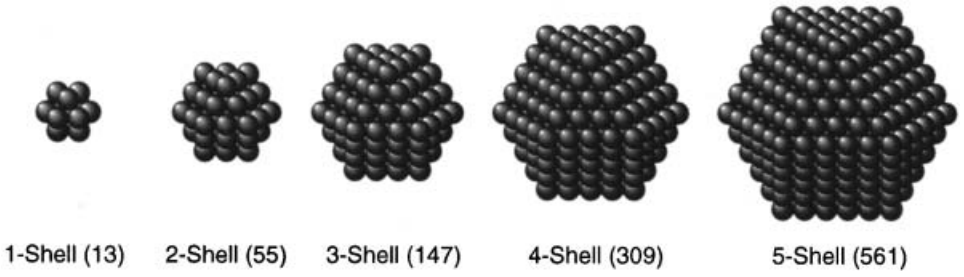

Figure 3: Shell structures of f.c.c. near spherical nanoparticles (cubooctahedrons) with the total number of atoms in the brackets. Reprinted with permission from (41). Copyright 1998, American Chemical Society.

nanoparticles that promotes the catalytic activity. Poly(N-vinyl-2-pyrrolidone) (PVP) has been successfully used to control the size of transition metal nanoclusters and their two-dimensional organization (24, 25, 41, 46–48). According to the Fourier transform infrared (FTIR) spectroscopy measurements, the carbonyl groups of PVP coordinate to the surface Pd atoms; part of the main chain of PVP is also expected to be adsorbed on the metal surface. The change in size of Pd nanoparticles occurs while varying the polymer concentration: the better is the stabilization (the higher the PVP concentration), the smaller are the Pd particles. The mean diameter of monodispersed Pd nanoparticles was controlled from 17 to 30 Å in a one-step synthesis by changing the amount of PVP and the type and/or the concentration of reducing alcohol. Although increasing the stabilizer concentration made the particle smaller, the lower size limit was controlled by the alcohol. Particles of smaller diameter were obtained in the order methanol > ethanol > 1-propanol, indicating that a faster reduction of $[PdCl_4]^{2-}$ provided smaller particles. 40% of alcohol in the solvent (water) was found to give the lowest particle size. As an example, Pd nanoparticles having a mean diameter of 24.4 Å (σ = 3.61 Å) were obtained at 20 vol.% of ethanol at PVP/Pd = 10, which corresponds to a 5-shell structure consisting of 561 atoms (Fig. 3) (41). However, it is quite difficult to synthesize monodispersed particle larger than 3 nm in a one-step synthesis. A stepwise growth can be employed, when the initially formed PVP-Pd nanoparticles (seeds) serve as the starting particles, which are refluxed with the Pd precursor in alcohol-water mixture, followed by a third and fourth growth. This procedure was shown to give a precise control over Pd diameters of 2.22, 2.79, 3.43, 4.12 nm (41), or 3.0, 3.9, 5.3, 6.6 nm (24), depending on the synthesis conditions. Pd particle size was also varied from 1 to 5.2 nm via PVP/Pd ratio during radiolytic (γ-rays) reduction (46). Spherical nanoparticles of other metals were prepared using PVP as a stabilizing agent as well, e.g., Pt nanoparticles of 1.7–7.1 nm diameter (47, 48).

As stabilizing agents for Au nanospheres, polyvinylalcohol (PVA) (49) and N-dodecil-N,N-dimethyl-3-amino-1-propan sulfonate (SB) (50) were reported. They allowed control over the nanoparticles size, which was between 4.3 and 10 nm, and 5.5 and 14.3 nm, respectively for each stabilizer. To prepare SB-stabilized nanoparticles, PVA-stabilized Au seeds were used. Particle size variation was achieved by varying concentration of $NaBH_4$ used for $HAuCl_4$ reduction (50).

2.1.2. Dendrimeric Stabilizers

Dendrimer templates have been also used to exert a high degree of control over the size of catalytically active nanoparticles in the <3 nm range (51, 52). Specifically, sixth-generation, hydroxyl-terminated polyamidoamine

dendrimers (G6-OH) at different Pd/dendrimer ratio were used to produce Pd nanoparticles of 1.3 ± 0.3, 1.4 ± 0.3, 1.5 ± 0.4, 1.7 ± 0.3, and 1.9 ± 0.2 nm. Such a precise control over the particles' size made them well-suited for studying the effect of particle size on a catalytic function (51).

2.1.3. *Stabilizing Ligands*

Size control of monodisperse Pd nanoparticle ranging from 1.7 to 3.5 nm was accomplished using thioethers as stabilizing ligands, in a one-step procedure. Modulation of the reaction temperature, time, solvent, and carbon chain length of the thioether provided control over the nanoparticle size and size distribution making them useful for size effect studies (53). Various stabilizing ligands are known to provide size control over metal nanoclusters, including 1,10-phenanthroline, polyoxoanions, 2,2′-bipyridine, tetraalkylammonium salts, etc. (2, 54). A representative example of a well-defined Schmid's cluster $Au_{55}(PPh_3)_{12}Cl_6$ is presented in Fig. 4 (2). It was prepared by passing diborane through a benzene solution of PPh_3AuCl. The diborane reduces Au(I) to Au(0) and complexes excess phosphine. Two-shell cubic close-packed Au metal core was produced, where twelve phosphine ligands occupy the twelve vertices and six chlorine ligands sit on the square faces of the cubooctahedron. A ligand-stabilized technique was extended, as well to produce Pt, Pd, Rh, Ru, and Co nanoclusters (2, 41). The mean diameters of Pd, Pt, Rh, and Pd/Pt nanoclusters stabilized by various ligands ranged from 1.3 to 3.2 nm if prepared by a single step, and from 2.2 to 4.0 nm if prepared by a stepwise growth method. The Stokes radii of metal nanoclusters stabilized by surfactants ranged from 1.7 to 2.1 nm, suggesting a thickness of the protective layer from 1.1 to 1.4 nm, whereas those stabilized by polymers gave much larger values, suggesting the formation of aggregates (54).

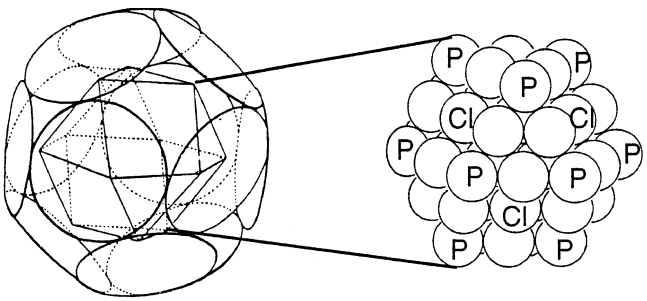

Figure 4: Ligand-stabilized nanocluster $Au_{55}(PPh_3)_{12}Cl_6$. The left image contains the metal core (internal cubooctahedron) surrounded by the phosphine ligand shell, while the right image shows the cubic close-packed Au_{55} metal core alone with the binding sites for P and Cl. Reprinted from (2) with permission from Elsevier.

2.1.4. *Microemulsion and Micellar Nanoreactors*

Another widespread technique for preparation of monodispersed spherical nanoparticles with a controlled size for catalytic applications is a microemulsion (ME) technique (37, 55–57). Water-in-oil (reverse) ME have been generally used for the synthesis of a variety of ultrafine metal particles (55) but there are also some examples of metal nanoparticle formation in normal microemulsions (oil-in-water) (58). The main advantage of ME as spatially confined nanoreactors of 5–100 nm size is their one-pot fabrication without sophisticated, time-consuming synthetic steps (4). The MEs allow obtaining monodispersed particles with a standard deviation from the average diameter of less than $\pm 10\%$. Monodispersity is thermodynamic in nature as a system has a minimum free energy at a definite volume fraction of the dispersed phase governing a droplet size (4, 6, 55). Metal salts are typically introduced into the droplets of dispersed phase of reverse ME and then reduced either by mixing with another reverse ME containing reductant (hydrazine), or by direct introduction of the reductant into the metal precursor-containing ME (e.g., hydrogen). The nucleation typically takes several minutes, after which the particles grow to their final sizes within several to tens of minute at room temperature. The final particle size depends on the nature of a surfactant, metal precursor, reducing agent, their concentrations, pH, temperature, and presence of a co-surfactant. A surfactant may be cationic like cetyltrimethylammonium bromide (CTAB) and cetyltrimethylammonium chloride (CTAC), anionic (sodium bis(2-ethylhexyl) sulfosuccinate, or docusate sodium salt, or aerosol OT, AOT) and non-ionic (Berol 02, which is nonylphenolethoxylate; Berol 050, which is pentaethyleneglycol dodecyl ether PEGDE; and NP-*X*, which is poly(oxyethylene)nonylphenol ether). CTAB and CTAC are often used with a co-surfactant such as n-hexanol (10 vol.% to hydrocarbon).

The most important factor influencing the size of final nanoparticles is a water-to-surfactant ratio ω_o: the higher the ratio, the bigger the particles. An example of a particle size variation from 3 to 18 nm depending on ω_o and TEM image of one of the samples of Pd nanoparticles obtained with a reverse ME technique are shown in Fig. 5 (59). These particles were prepared in water/AOT/hydrocarbon microemulsions, which are considered to be an ideal media to synthesize nanoparticles due to the well-established structural and dynamic properties of AOT reversed micelles, the surfactant's ability to solubilize relatively large amounts of water without a co-surfactant and the high stability of microemulsions (55, 59). The reverse ME technique allowed producing Pd, Pt, Au, Rh, Fe, and Cu nanoparticles of the controlled size, some of them were successfully used for catalytic applications, including size effect studies (55–57, 60, 61).

Metal nanoparticles stabilized in the micelles formed by amphiphilic block-copolymers attracted considerable attention in the past years due to the

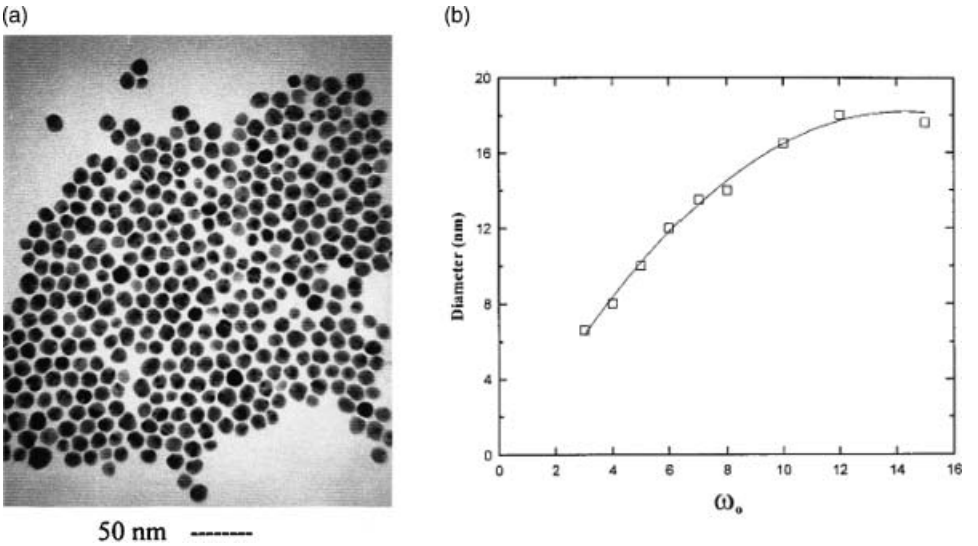

Figure 5: Pd nanoparticles prepared by a reverse ME technique: (a) particles at a water-to-surfactant ratio (ω_o) 5, and (b) effect of ω_o on the particle diameter. Reprinted from (59) with permission from Elsevier.

precise control over the particle size and application in catalysis (5, 62, 63). The nanoparticles may be stabilized in both the micelle corona and core. To synthesize nanoparticles, copolymers [e.g., poly(2-vinylpyridine), or polymethacrylic acid] must have functional groups, which could interact with the metal precursor, while the non-interacting copolymer [e.g., poly(ethylene oxide) or polystyrene] should provide solubility and stability of micelle in corresponding solvents (5). However, in spite of tremendous advances in metal nanoparticle stabilization in block-copolymer micelles and their high catalytic activity (5, 64), their applications in structure-sensitivity studies have not been reported. For these studies, the nanoparticles of several sizes should be synthesized in the same micellar system to prevent the influence of a functional polymer on the catalytic properties.

Interestingly, that due to thermodynamic reason, nanoparticles of other shapes easily transform into spherical particles during the course of a catalytic reaction by Ostwald ripening process, which is a mechanism of cluster growth in which atoms on the nanoparticle surfaces dissolve and deposit on the more stable surfaces of the other (larger, or spherical) nanoparticles (65). It was shown for PVP-stabilized Pt tetrahedrons used in Suzuki reaction, which transform to more stable bigger spheres (66).

Availability of techniques to produce spherical nanoparticles of various sizes makes them first candidates for structure sensitivity studies. According to the surface atom statistics, fraction of metal atoms with different geometrical and electronic characteristics changes with the particle size

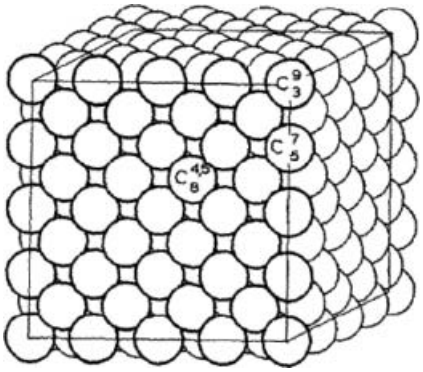

Figure 6: F.c.c. cube, m=5. Reprinted from (40) with permission from Elsevier.

(Fig. 2, Table 1). This results in different catalytic behaviour of nanoparticles of various diameters, as will be shown in Section 3.

2.2. Nanocubes

The model of a cube with m=5 (number of atoms on a cub's rib) and the crystal statistics are presented in Fig. 6 and Table 2, respectively (40). All the facets of the cube are (100) planes. An electronic microscopy image of gold nanocubes is shown as a representative example in Fig. 7 (67).

2.2.1. Platinum Nanocubes

Linear polymers have the potential to control not only the size but also the shape of metal nanoparticles. First shape-selective synthesis of f.c.c. platinum cubes, along with tetrahedrons was reported in 1996 (68). Selectivity to various morphologies was achieved by changing the ratios of sodium polyacrylate (PAA) to K_2PtCl_4: tetrahedrons formed at higher polymer-to-precursor ratio, compared to cubes. The final shapes of these particles were proposed to be determined by the relative growth on (100) and (111) faces. The

Table 2: Crystal statistics for an f.c.c. cube (40). Reprinted from (40) with permission from Elsevier.

	m		
Number of metal atoms	**2**	**3**	**>3**
N_T	14	63	$4m^3-6m^2+3m$
N_S	14	50	$12m^2-24m+14$
$N(C_3^9)$	8	8	8
$N(C_5^7)$	0	12	$12(m-2)$
$N(C_8^{4,5})$	6	30	$6(m-1)^2+6(m-2)^2$

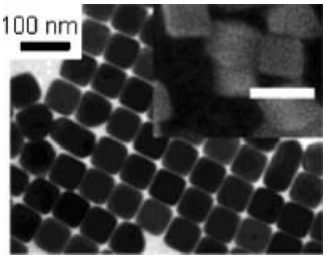

Figure 7: Electron microscopy images of Au nanocubes. Reprinted in part with permission from (67). Copyright 2004, American Chemical Society.

average size of the cubic particles was 11.0 $\pm$ 0.5 nm, with sizes ranging from 4 to 18 nm (68). Other sizes of the PAA-stabilized Pt nanocubes were reported later (26, 69, 70), e.g., 7.1 $\pm$ 0.2 nm (69). FTIR spectroscopy has revealed the binding geometry of polyacrylate capping material on cubic and tetrahedral platinum nanoparticles (71). It was suggested that the PAA capping material adsorbs on the Pt surface of the tetrahedral shape through the hydroxyl oxygen atom of the carboxylic acid moiety of the polyacrylate (linear adsorption configuration). On the cubic particle the adsorption was through both of the carboxylic oxygen atoms (bridge adsorption configuration). These two shaped Pt nanoparticles were synthesized by changing the starting ratio of the capping material to that of the Pt salt. The stabilizer adsorption mechanism and concentration were supposed to be the factors determining the final shape.

A comparison of the Pt nanoparticles shapes was carried out using PAA and PVP as stabilizing agents (72). Regardless of the kind of the polymer, the dominant shape was controlled by changing the reduction rate of Pt^{4+} using methanol or hydrogen. Cube formation was supposed to proceed from tetrahedrons via truncated octahedras as shown in Fig. 8. The role of the polymer consists in the selective blocking of (100) plane, resulting in faster growth rate of the protection-free (111) planes and cube formation. At high polymer concentrations, however, the particle shape is retained during the growth process; probably because the growth rates of the (111) and (100) planes are almost equal due to the complete protection of surface Pt atoms by the polymer interaction, resulting in tetrahedrons.

Platinum nanocubes with the average size of 12 nm were also produced with the yield of 52% by a reduction of K_2PtCl_4 with H_2 at 40°C in the presence of N-isopropylacrylamide (73, 74). Other shapes, such as irregular (11%), hexagonal (22%), spherical (11%), tetrahedral (1%), and others (3%) were observed. Successful synthesis of platinum nanocubes (4–8 nm) with the selectivity greater than 90% was reported using reduction of $K_2[Pt(C_2O_4)_2]$ by hydrogen (75). Oxalate played a role of a capping agent. Oxalate-stabilized Pt colloid was sensitive toward oxygen; during aging in air, oxidative decomposition of oxalate was catalyzed by the Pt nanoparticles, which led the Pt

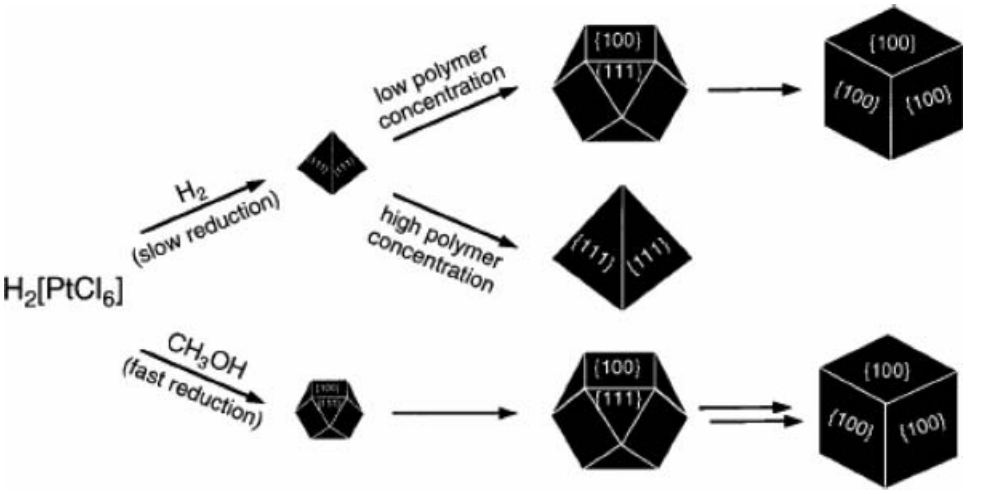

Figure 8: Proposed mechanisms for formation of Pt nanocubes and nanotetrahedrons. Reprinted from (72) with permission from Springer.

nanoparticles to aggregate into linear agglomerates. After a long period of air exposure, and treatment with hydrogen, these linear agglomerates transformed into Pt nanowires. Polyol reduction in the presence of silver ions allowed shape control of Pt nanocrystals, including cubes of 9–10 nm size (76). Addition of Ag^- enhanced the crystal growth rate along the (100) facets, producing cubes. The added ions could be easily removed after synthesis by precipitation giving pure platinum nanocrystals. They were assembled using the Langmuir-Blodgett method. The particles were evenly distributed on the substrate, and their surface coverage and density were precisely controlled by tuning the surface pressure. These Langmuir-Blodgett layers can serve as potential candidates for 2-D model catalysts as a result of their high surface area and the structural uniformity of the metal nanoclusters (76).

2.2.2. Silver Nanocubes

Polyol method was also used for the preparation of monodispersed Ag nanocubes by reducing $AgNO_3$ with ethylene glycol in the presence of PVP (77). There were single crystals characterized by a slightly truncated shape bounded by (100), (110), and (111) facets. Addition of sodium chloride during the synthesis (78) promoted the formation of truncated cubes. It was proposed (Fig. 9) that the defects inherent in twinned nuclei of silver led to their selective etching and dissolution by chloride and oxygen (from air), leaving only the single crystalline ones to grow into nanoscale cubes and tetrahedrons. A similar O_2/Cl^- etching of Ag nanospheres to other shapes including cubes was observed during the $AgNO_3$ reduction by $NaBH_4$ in the presence of

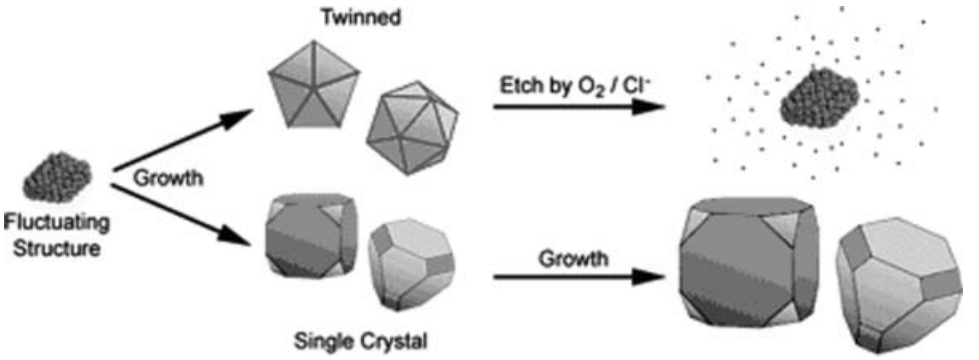

Figure 9: Formation of Ag cubes and tetrahedrons by polyol reduction in the presence of PVP, air and sodium chloride (78). Reprinted with permission from (78). Copyright 2004, American Chemical Society.

sodium citrate, followed by their conversion into sodium dodecyl sulfate (SDS)-stabilized Ag nanospheres, and the aging of the SDS-Ag in 0.01 M NaCl solution (79). SDS regulated the dynamics of the O_2/Cl^- etching of the Ag nanospheres and the reduction of the released Ag^+ by citrate ions in the same solution. Several silver nanostructures, including cubic ones, were produced by microwave-polyol (ethylene glycol) method with the assistance of Pt seeds and PVP (80).

2.2.3. Gold Nanocubes

Shape-selective synthesis of gold nanocubes (Fig. 7) involved the preparation of spherical Au seeds of 4 nm diameter and its addition to the aqueous solutions containing cetyltrimethylammonium bromide (CTAB), $HAuCl_4$, and ascorbic acid (weak reductant) (67). The morphology and dimensions of the nanoparticles depend on the reactant concentrations. The shape-selective synthesis is the outcome of the interplay between the faceting tendency of the stabilizing agent and the growth kinetics (rate of supply of Au^0 to the crystallographic planes). CTAB molecules bind more strongly to the (100) than the (111) faces, leading to their disappearance and the formation of (100) faces, thereby producing cubic shapes. Gold cubes with the edge length of 66 nm were produced with the yield of 85% at the concentrations of CTAB, seeds, Au precursor and ascorbic acid of $1.6 \cdot 10^{-2}$ M, $1.25 \cdot 10^{-8}$ M, $2.0 \cdot 10^{-4}$ M, and $6.0 \cdot 10^{-3}$ M, respectively (67). When the latter two concentrations were $4.0 \cdot 10^{-4}$ M and $6.4 \cdot 10^{-4}$ M, and $6.0 \cdot 10^{-5}$ M $AgNO_3$ was added to the growth solution, 70% of cubes were produced with the edge length of 90 nm. Silver nitrate allowed obtaining Au cubes even at much lower reductant concentration. About 3–7 wt% of Ag^- was found to be associated with Au/CTAB particles decreasing the charge density on Br^- and diminishing a repulsion between CTAB on Au surface; a possible catalytic effect of silver was declined (81).

Gold nanocubes of 150 ± 14 nm size were prepared with 95% yield via a polyol based method in nitrogen at 553 K using PVP, ethylene glycol (solvent and reductant), $HAuCl_4$ and $AgNO_3$ (31). Electron diffraction showed that the cube was a single domain with (100) surfaces. F.c.c. structure was proved by XRD. The intensity ratio between the (200) and the (111) diffractions was 1.93, which is significantly larger than the conventional bulk intensity ratio (0.53). This was a clear indication that the faces of these nanocubes, primarily composed of (100) planes, tend to preferentially orient parallel to the supporting substrates, thus giving a significantly high (200) diffraction intensity. Selective interaction of PVP and different surface planes of the gold nanocrystals enhances the growth rate along the (100) direction, reducing the growth rate along the (111) direction, which would result in the particles with tetrahedral or icosahedral shapes. Further, the introduction of silver ions significantly reduces the growth rate along the (100) direction and/or enhances the growth rate along the (111) direction, and ultimately cubic particles result. This proposed mechanism (31) is vastly different from (77) for the silver system, in which the interaction of the particles with PVP promoted the nanocube formation. The difference was attributed to the fact that the gold and silver systems interact differently with the polymer.

2.2.4. Palladium Nanocubes

Pd nanocubes were produced by a chemical reduction method of H_2PdCl_4 by ethanol in the presence of a polymeric stabilizer: PVP, polyvinyl alcohol (PVA) or polymethylvinyl ether (PMVE) at pH 7 (46). The synthesis was carried out at 353 K for 3 h in air atmosphere. Ratio of a stabilizer-to-Pd influenced the nanocube size, i.e., with the PVP/Pd increase from 1 to 40, the nanoparticle size decreased from 7.1 to 5 nm. PVP was claimed to be the most efficient stabilizer due to its two heteroatoms (oxygen and nitrogen). When PVA was used, the cube size increased from 5.0 nm (PVP-Pd) to 5.7 nm (PVA-Pd). Nanoparticles of other metals (Pt, Rh, Ru, Ni) reduced by ethanol also showed cubic shapes.

The above mentioned examples described nanocubes as single crystals. However, nanocubes may be formed as agglomerates of smaller particles, as reported for copper cubes (82). Cu(II) was reduced to Cu(0) in the presence of sodium oleate as a stabilizer. The resultant cubic Cu cages were aggregates of Cu nanoparticles with 200 nm in edge lengths and the inclusive nanoparticles were about 20 nm in size. Cu_2O cubes were proposed to be the reduction intermediates and served as spontaneous shape-controlled templates of the Cu cubes. The aggregates were stable for several hours, followed by the nanostructure transformation into Cu hollow spheres.

Several synthesized nanocubes were successfully implemented in catalysis, as will be discussed in the Section 3. As they exhibit only (100) facets,

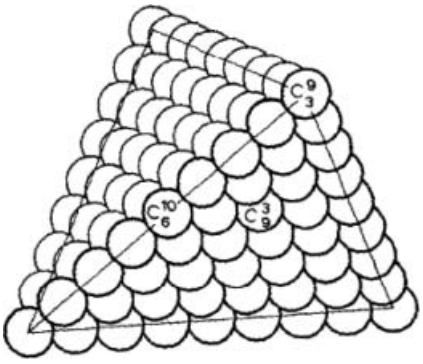

Figure 10: F.c.c. tetrahedron, m=9. Reprinted from (40) with permission from Elsevier.

they are particularly important for structure sensitivity studies for the reactions taking place on particular crystal planes.

2.3. Nanotetrahedrons

The model of an f.c.c. tetrahedron with 9 atoms on the tetrahedron's rib and the crystal statistics are presented in Fig. 10 and Table 3, respectively (40). Transmission (TEM) and scanning (SEM) electron microscopy images of gold nanotetrahedrons are exampled in Fig. 11 (31, 67). All the facets of the tetrahedron are (111) planes; edges and corners of tetrahedral particles are more "sharp" compared to the cubic ones (65). In literature, tetrahedrons are sometimes refereed as triangles (due to the microscopically observed shape). The tetrahedrons should be distinguished from flat nanoprisms (31, 83).

2.3.1. Platinum Nanotetrahedrons

Pt tetrahedrons can be prepared according to the mechanism presented in Fig. 8 and stabilized by various stabilising polymers using methanol or hydrogen reduction as was described for cubic particles (26, 66, 68–70, 72). As

Table 3: Crystal statistics for an f.c.c. tetrahedron (40). Reprinted from (40) with permission from Elsevier.

Number of metal atoms	*m*				
	2	**3**	**4**	**5**	**>5**
N_T	4	10	20	35	1/6m(m+1)(m+2)
N_S	4	10	20	34	$2m^2-4m+4$
$N(C_3{}^9)$	4	4	4	4	4
$N(C_6{}^{10})$	0	6	12	18	6(m−2)
$N(C_9{}^3)$	0	0	4	12	2(m−2)(m−3)

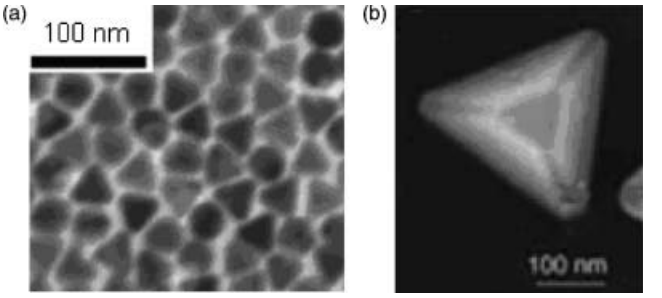

Figure 11: (a) TEM image of Au nanotetrahedrons. Reprinted in part with permission from (67). Copyright 2004, American Chemical Society. (b) SEM image of Au tetrahedrons (31). Copyright Wiley-VCH Verlag GmbH & Co. KGaA. Reproduced with permission from Wiley and author (P. Yang).

an example, the monodispersed tetrahedral nanoparticles were prepared with the PVP of M_W of 360,000 and K_2PtCl_6 as a precursor, and they had an average size of 5.0 $\pm$ 0.1 nm. 55 $\pm$ 4% of the particles were regular tetrahedrons, 22 $\pm$ 2% were distorted tetrahedrons, and 23 $\pm$ 2% of near spherical particles were also present (66).

2.3.2. Gold Nanotetrahedrons

Evolution of size and shape was studied during colloidal crystallization of oleylamine-stabilized gold nanoparticles (84). The addition of dodecanethiol to the particles in chloroform led to their aggregation and formation of amorphous, single-crystalline, polycrystalline, and core-shell (with an impurity nucleus) type clusters. Three different growth mechanisms were identified using dynamic light scattering and scanning electron microscopy: direct nanoparticle aggregation, cluster aggregation, and heterogeneous aggregation. All crystalline structures exhibited f.c.c. or icosahedral packing and were terminated by (100) and (111) planes, which led to truncated tetrahedral, octahedral, and icosahedral shapes (Fig. 12). Importantly, most clusters in this system grew by aggregation of 60–80 nm structurally nonrigid clusters that formed in the first 60 s of the experiment.

Gold nanotetrahedrons (Fig. 11a) were synthesized using the seed-mediated technique described for cubes using CTAB and ascorbic acid but at different reactant concentrations (67). Tetrahedrons (triangles) with the edge length of 35 nm were produced with the yield of 80% at the concentrations of CTAB, seeds, Au precursor and ascorbic acid of $1.6 \cdot 10^{-2}$ M, $1.25 \cdot 10^{-7}$ M, $2.0 \cdot 10^{-4}$ M, and $6.0 \cdot 10^{-3}$ M, respectively. The formation of small tetrahedrons under these conditions was attributed to an order-of-magnitude higher seed concentrations compared to the production of bigger cubes.

Au tetrahedrons of 210 $\pm$ 20 nm size (Fig. 11b) were prepared with 70% yield using the polyol process described above for the cube production (31). The

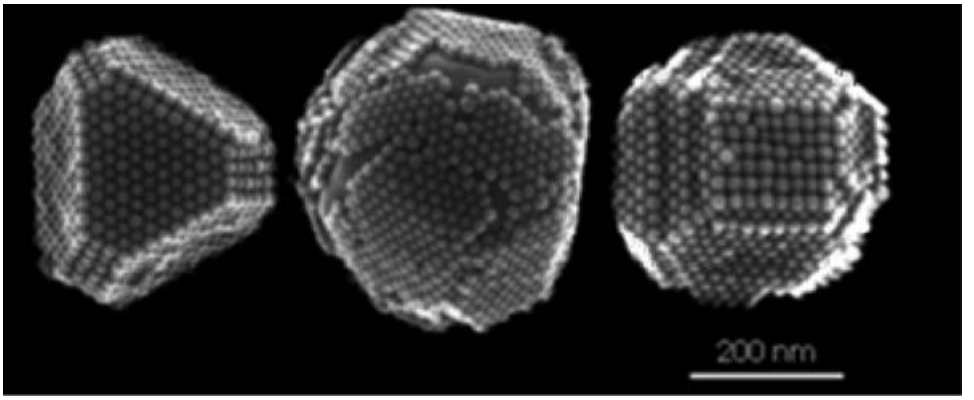

Figure 12: Truncated tetrahedral, octahedral, and icosahedral gold nanocrystals grown during colloidal crystallization of oleylamine-stabilized gold nanoparticles. Reprinted with permission from (84). Copyright 2007, American Chemical Society.

triangles were produced without addition of $AgNO_3$ which led to the cube formation. PVP enhances the growth rate along the (100) direction, reducing the growth rate along the (111) direction, which result in tetrahedron formation with (111) planes. Electron diffraction of a single tetrahedron showed that the particle was single crystalline, with the top and bottom covered with (111) surfaces. The formation of flat nanoprisms [as proposed for silver (83, 85)] was discarded: the sides of the particles were clearly slanted representing tetrahedras with a truncated corner, or partially developed tetrahedras. The fact that the surfaces of these particles were dominated with (111) planes, which make then energetically favourable compared to prisms.

Anisotropic gold nanoparticles could be also synthesized by photoinduced synthesis in ionic liquid (86) 1-butyl-3-methylimidazolium tetrafluoroborate ([BMIM][BF_4]) without any additional capping agent. The [BMIM][BF_4] served as a reaction medium, template, and capping agent. Variation of the reaction time and reactant concentrations allowed control over the particle shape (triangles and hexagons were obtained).

2.3.3. Silver Nanotetrahedrons

Silver tetrahedrons were produced by the method described for the cube formation using polyol method via O_2/Cl^- etching of Ag nanospheres (Fig. 9) (78). Silver truncated triangles, along with truncated rectangles and near spherical particles were prepared by reducing a high molar concentration of $AgNO_3$ (up to 0.735 M) with glycerol in the presence of *m*-phenylenediamine (87). Silver triangles were also produced in the presence of CTAB: it was postulated that the crystal growth of the silver nanoparticles with sizes of more than 10 nm proceeded through an adhesion of small-sized particles followed by a subsequent coalescence process under the reaction conditions.

As will be shown in the subchapter 2, tetrahedrons were used in several catalytic reactions and exhibited high activity due to (111) facets and high fraction of edge atoms. They also readily change shape under reaction conditions to spherical particles.

2.4. Nanorods and Nanowires

In the most cases, the surface statistics of rods and nanowires may be assumed to be identical to that one of cubes, as majority of rods exhibit predominately (100) facets (35) similar to cubes. The nanorods are typically characterized by an aspect ratio, which is the length divided by the width. In the literature, nanorods and nanowires are often called as one-dimensional (1-D) metal nanostructures, in which the short axis of the material is in the 1–100 nm regime but the long axis is up to microns long. The nanomaterials with aspect ratios between 1 and 5 are called sometimes as "short nanorods" (or nanobars), materials with aspect ratios between 5 and 25 "long nanorods", and higher-yet-aspect-ratio materials "nanowires", although this classification is not uniform in the literature (88).

2.4.1. Gold Rods and Wires

A seed-mediated approach was developed to produce gold nanorods according to the scheme presented in Fig. 13 along with the TEM images of short and long nanorods (88). The synthesis is performed in water, in air, and at room temperature and thus is amenable, in principle, to scaling up without the use of specialized equipment or organic solvent. The seeds can be stabilized by citrate, thiols, and surfactants. In the growth solution, ascorbic acid is used as reductant and CTAB as a stabilizer. Bromide may be the most important part of the directing surfactant CTAB, as when bromide is replaced with chloride, no nanorods form (88, 89). Addition of silver ions significantly increases rod yield but limits the achievable aspect ratios to 5 (90).

Electron diffraction revealed that the gold rods were penta-tetrahedral twinned single crystals. The side faces were found to be (100) or (110) or a combination of both: the nanorod ends consisted of five tetrahedra making a ring, to expose five triangular (111) faces at the end [Fig. 14 (91)]. How this general structure of gold nanorods may be different, depending on the presence of additive ions, is still emerging (88). For example, rods obtained with silver addition might have a different crystallography, with (111) facets on the long side (90).

Several mechanisms were proposed for the growth of gold nanorods using CTAB. Nanorods appear to grow longer briefly, then "fill out" and grow wider, during the course of the reaction (90). In one of the first proposed mechanisms

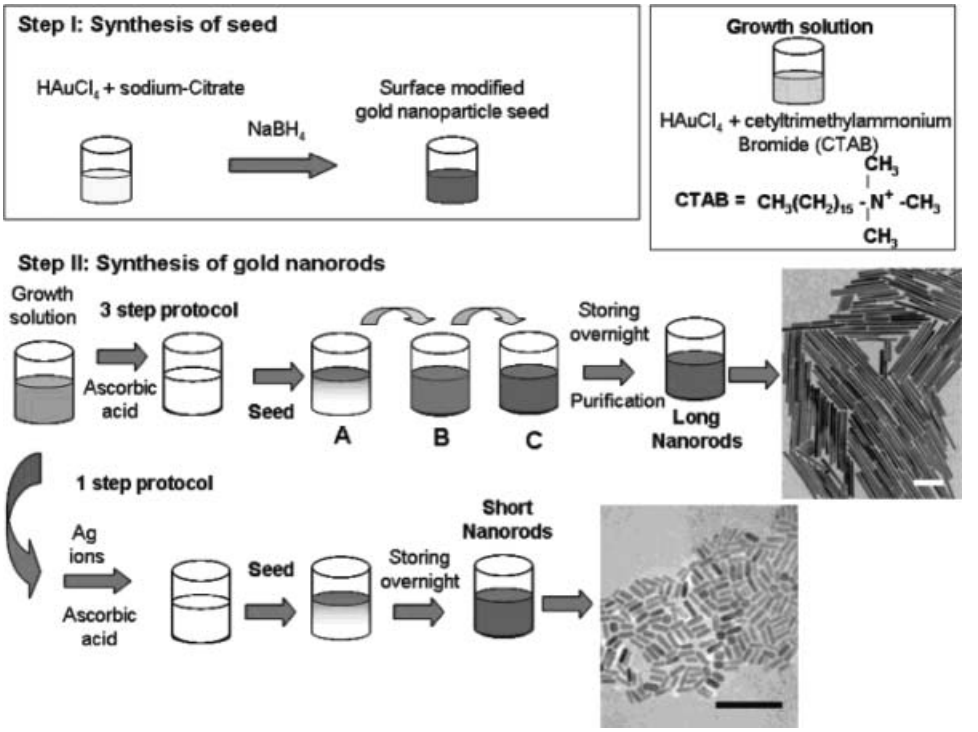

Figure 13: Scheme of the seed-mediated growth of gold nanorods. Scale bar is 200 nm. Reprinted with permission from (88). Copyright 2006, American Chemical Society.

the surfactant forms a soft template, to which the surfactant-capped seed attach and growth starts by diffusing the gold atoms into the template (92). Later, this mechanism was discarded in favor of the following (88). Surfactant-containing Au(I) complexes, such as $[AuBrCTA]^+$, are specifically incorporated into the (100) side edges, whereas non-complexed ion-pairs or Au(0) atoms/clusters are added to the (111) end faces. The discrimination between sites

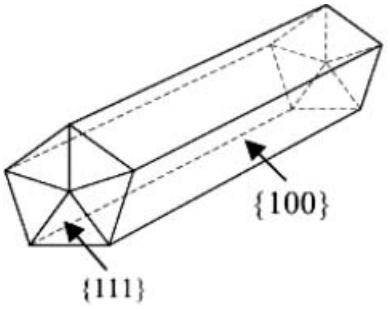

Figure 14: Elongated cyclic penta-tetrahedral twin model of gold nanorods with (111) end faces and (100) side faces. Reproduced from (91) by permission of the Royal Society of Chemistry.

could be due to the increased stability of the close-packed (111) surfaces as compared to the edge sites, which contain numerous defects (91). The presence of silver might form silver bromide at the gold surface and slow down the subsequent gold growth step. The slower kinetics results in single crystalline growth of the gold nanorods and the rod morphology comes from a silver bromide layer on the (111) faces of the gold nanocrystal, leading to gold reduction on other faces producing a rod with (111) facets on its long side (90). In an electric-field directed mechanism of the silver-free growth, Au(I) ions are bound to the CTAB micelles and are transported to the seed surface. The flux is maximized at points of highest curvature (at the tips of the rods), where the electrical double layer gradient is highest. This leads to the preferential attachment of ions on the tips, leading to the elongation of the particles (93).

Effect of reactant concentrations during growth was also studied for seed-mediated gold nanorods (90). The rod length decreased with an increase in the seed concentration for a given concentration of Au(III) ion due to its smaller quantity per seed. Au^{3+} concentration shows a strong effect on the amount and dimensions of gold nanorods depending on both $[Au]_{seed}$ and [CTAB]. The ends of the rods appeared more rounded with the decrease in $[Au^{3+}]$. The rod length can be decreased by increasing ascorbic acid concentration due to the very fast formation and supply of growth units (Au^0) to the seeds in the presence of a large excess of reducing agent. Decrease in CTAB concentration leads to the decrease of the rod length with increase of the width, however, the yield of rods drops significantly upon CTAB concentration making this route not suitable for the synthesis of short rods with high yield.

In order to increase the aspect ratio of the gold nanorods, cosurfactant benzyldimethylhexadecylammoniumchloride (BDAC) was used in combination with CTAB (BDAC/CTAB molar ratio of 2.7) without silver (81). It allowed increasing the aspect ratios from 1.5–4.5 to 4.6–10. The elongation of nanorods upon aging was observed only in the binary surfactant mixture of BDAC and CTAB. The elongation effect of the silver ion was not observed in the case of pure BDAC or large ratios of BDAC/CTAB mixture. Using a growth solution containing BDAC, only nanospheres were formed and silver ions did not show any effect on elongation. This was an indication that CTAB monomers are required for growth of nanorods and that these monomers are more influenced by the silver ions. A probable reason could be that the chloride counterion from BDAC has smaller size and polarizability than the bromide ion, thus a weaker bonding could be expected in Ag-Cl relative to that in Ag-Br (81).

Some more examples of Au nanorods synthesis follow. A room-temperature oxalate reduction method was reported recently for gold nanowires production. Oxalate served as the reducing and capping agent along with PVP as the co-capping agent. As the concentration of oxalate was increased, the rate of reduction as well as particle growth was found to increase as well.

The formation of the Au nanowire was due to the bridging nature of the oxalate di-anion. Polycrystalline Au nanowires were formed with a preferential growth of the (111) facet (94). Growth of colloidal gold nanowires (along with nanostars) was shown to be induced by Pd doping (95). Using a combined solution of aqueous $HAuCl_4$ and triethylamine at room temperature, gold threads were obtained. Triethylamine acted not only as a stabilizer and a reducing agent, but also as a precursor to build the alkane-like material upon which the gold thread was formed. Initially, some reduced gold nanoparticles were self-organized into one-dimensional nanowires, which then developed into three-dimensional microscale threads (96). The nanowires can be also developed as an assembly of nanocrystals, e.g., using a room-temperature approach via agitating Au hydrosol in a toluene-aqueous mixture without templates (97). The nanowires were uniform in diameter of $\sim$ 5 nm and consisted of coalesced face-centered cubic nanocrystals. Toluene molecules passivated the gold surfaces during nanoparticle coalescence, rendering the nanowires hydrophobic and enabling their transfer into the toluene layer.

2.4.2. *Silver Rods and Wires*

Silver nanowires can be produced by a "hot-solution" approach based on the seed-mediated polyol process (98, 99). Such synthesis was reported to result in Ag nanowires with diameter is in the range of 30–40 nm and length up to $\sim$50 μm (100). The first step of this process involved the formation of Ag (or Pt) nanoparticles by reducing $AgNO_3$ (or $PtCl_2$) with ethylene glycol at 160°C. These Ag (or Pt) nanoparticles could serve as seeds for the heterogeneous nucleation and growth of silver (formed by reducing $AgNO_3$ with ethylene glycol) because of their close match in crystal structure and lattice constants. In the presence of PVP, the growth of silver could be directed into a highly anisotropic mode to form uniform bicrystalline nanowires with aspect ratios as high as $\sim$1000. Both morphology and aspect ratios of these silver nanostructures could be varied from nanoparticles and nanorods to long nanowires by adjusting the reaction conditions, including the ratio of PVP to silver nitrate, reaction temperature, and seeding conditions. The nanowires exposed predominantly (100) facets as presented in Fig. 14 (100). The importance of PVP for nanowires production was proven by the use of other coordination agents, such as poly(ethylene oxide) (PEO) and poly(vinyl alcohol) PVA (99). There seems to be a selectivity between the metal surfaces and the functional groups of the coordinating polymer. Only PEO had the same function as PVP to promote the formation of Ag nanowires, albeit the yield and uniformity of PEO-Ag nanowires were much worse as compared to PVP-Ag. This implies the importance of O-Ag coordination bond in nanowire formation. The oxygen atoms in PVA can easily form intramolecular hydrogen

bonds due to the strong interactions between hydroxyl groups. These hydrogen bonds may cause the PVA molecules to fold into coils inhibiting the O atoms interaction with silver surfaces.

Microwave treatment was also used during the polyol synthesis in the presence of Pt catalyst and PVP (101). When $AgNO_3$ was reduced by ethylene glycol in the presence of Pt seeds and PVP, a mixture of one-dimensional silver nanorods with nanowires and three-dimensional spherical, triangular-bipyramidal, and cubic nanoparticles were produced within a few minutes. The average diameter, length, and yield of these products were a function of concentration of Pt, PVP, or $AgNO_3$, heating time, and/or microwave power. Longer and thicker 1-D structures could be prepared by using 1-D products as seeds and repeating the reduction of $AgNO_3$ in ethylene glycol under microwave irradiation.

The morphologies of the silver nanowires prepared by the polyol process were found also to depend strongly on temperature and molar ratio PVP/$AgNO_3$ (102). Silver nanowires were obtained at the ratio of 1.5, while at the ratio of 3, nanopolyhedra formed. The diffraction revealed abundance of (111) facets on the nanowires, indicating that in this case Ag nanowires had the tendency to grow as bicrystals twinned along the (111) planes, showing (111) crystal faces at their surfaces. This, however, contradicts to the previous observations of (100) abundance (100), probably, due to the change in the preparation conditions.

Seedless, surfactantless approach was developed resulting in Ag nanowires with a high yield, albeit with no good control over the aspect ratio (diameter 25–32 nm; length up to 12 μm) (103). Silver nitrate was reduced to silver metal at 100°C by sodium citrate in the presence of NaOH. Hydroxide ion concentration is a key parameter for producing nanowires. This again suggests that the adsorbed ions block reactions on one face of a growing nanocrystal and control the crystal shape (88).

2.4.3. Platinum and Palladium Rods and Wires

Pt and Pd nanorods and nanowires were also reported to be synthesized with PVP stabilizer. Single-crystal nanowires of platinum of ~100 nm in length and ~5 nm in diameter have been synthesized by reducing H_2PtCl_6 with ethylene glycol in the presence of PVP and a trace amount of Fe^{3+} or Fe^{2+} (104). The iron ions had dual functions in the synthesis: they induced aggregation of Pt nanoparticles into larger structures that served as the nucleation sites, and they greatly reduced the reaction rate and supersaturation level to induce anisotropic growth. Formation of Pt nanowires was also reported to proceed after air-aging of oxalate-stabilized Pt nanocubes (4–8 nm) as discussed above (75).

A seed-mediated technique with CTAB developed for Ag and Au nanostructures was successfully extended to palladium (35, 105). Various morphologies were obtained going from 0-D nanocrystals (cubes, icosahedral multiply twinned particles) to 1-D (nanorods) and 2-D nanocrystals (triangular nanosheets). Palladium nanorods were obtained in a relatively high yield and presented a well-defined 5-fold symmetry similar to that reported previously for Ag and Au. They exposed preferentially (100) facets. Embedding the $PdCl_4^{2-}$ precursor inside CTAB micelles was found to be a key parameter to decrease the rate of reduction of palladium allowing a kinetic-controlled growth regime leading to nanorods. Shifting the experimental conditions to a thermodynamic-controlled growth regime led to the formation of cubic (~80%) or icosahedral (~100%) particles (105). Palladium single-crystal nanobars bounded by (100) facets and nanorods with their side surfaces enclosed by (100) and (110) facets (Fig. 15) were synthesized under kinetically controlled conditions, while the cubic symmetry was broken (39). One-dimensional growth could be induced and maintained through an interplay of the following processes: (i) speedy reduction of the precursor to ensure prompt addition of atoms to the seed; (ii) chemisorption of bromide on the seed to promote the formation of (100) and (110) facets; and (iii) localized oxidative etching on one specific face of the seed to initiate preferential growth on this face. Experimentally, the anisotropic growth was achieved by varying the type and concentration of reducing agent, as well as by adjusting the reaction temperature. This methodology developed for Pd has also been extended to both Au and Pt. As expected for a kinetically controlled product, the anisotropic nanostructure evolved into the thermodynamically favoured shape during an aging process.

Use of nanorods and nanowires in catalytic reactions is rather scarce but some successful examples will be reported in Section 3. Note that in

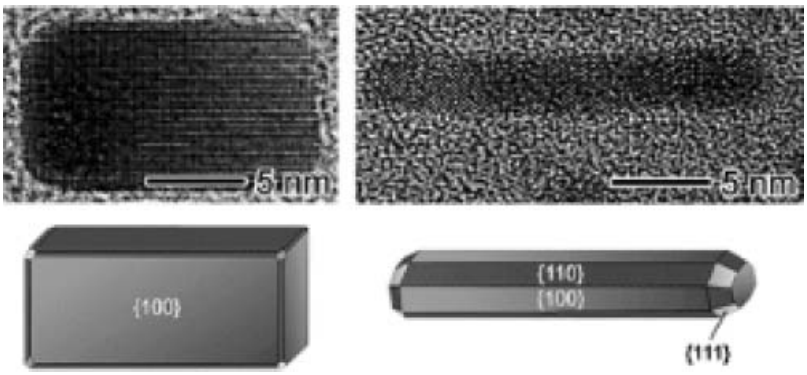

Figure 15: Palladium nanobars and nanorods (39). Reprinted with permission from (39). Copyright 2007, American Chemical Society.

combination with cubes their application in structure-sensitive reactions can be very useful to determine active sites. While cubes expose only (100) facets. nanorods can have some atoms on (111) facets with the majority being on the (100) planes.

3. STRUCTURE SENSITIVITY OF CATALYTIC REACTIONS

3.1. Nature of Structure Sensitivity in Catalysis by Metals

The phenomenon of structure sensitivity is related to the mechanism of a heterogeneous catalytic reaction which involves a substrate adsorption followed by its chemical transformation on an active site (14–16). A surface atom, or a combination of atoms, should possess definite geometrical and electronic properties to act as an active site. Electronic ("ligand") effect reveals itself in the nature and strength of a bond between the *d*-band orbital of the surface site with the molecular orbital of reactant and product. According to the Sabatier's principle, an intermediate formed by a reactant at the surface must be stable enough to be formed, but not too stable since it must decompose yielding the products. Geometric ("ensemble") effect implies that the reactant needs for adsorption sometimes multiple atoms with a specific arrangement (18, 106). Structure sensitivity of a variety of the reactions was first studied using model catalysts, which were single metal crystals. Ideal surfaces allowed the direct correlation between activity and surface atomic ensembles. For example, in alkane isomerization, (100) planes are significantly more active for n-butane and isobutene conversion (Fig. 16). The changes in reaction rates occur when steps and kinks appear on the surface (29). As shown above, nanoparticles of various morphologies and sizes represent various fractions of different crystallographic orientations together with edge and vertex atoms. Thus, they possess different activities in structure-sensitive reactions.

Structure sensitivity studies use a turnover frequency (TOF) as a measure of a nanostructure activity. TOF calculations are based either on active particle metal dispersions determined by CO and/or H_2 chemisorption, or on the total surface atom number estimated using metal crystal statistics and particle size found by electron microscopy or X-ray diffraction. When all atoms on a nanoparticle surface possess necessary properties to catalyze a reaction, then the turnover frequencies of the reactions carried out with nanoparticles of different sizes and shapes will stay constant [Fig. 17, curve 1 (17)]. Such reactions are considered to be *structure-insensitive*, or *intrinsically size/shape-independent*. For other reactions, the differences between the surface atoms located on different facets, edges or corners, become crucial for a catalyzed reaction, and not all atoms constitute the active sites. TOF for such reactions will depend on the nanoparticle structure, which, in turn, is a function of a particle's size and shape. Such reactions are *structure-sensitive*.

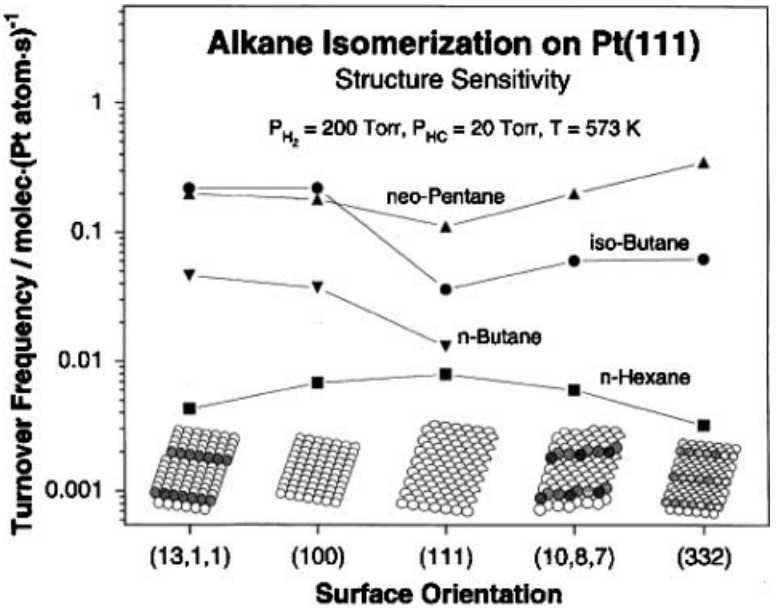

Figure 16: Structure sensitivity in alkane isomerization reactions catalyzed over platinum single-crystal surfaces. Reprinted from (29) with permission from Elsevier.

The TOF of a structure-sensitive reaction may vary in different ways (Fig. 17). It may decrease with the particle size decrease, when large particles are more active than small ones (curve 2). This is called a negative particle size effect (or antipathetic size dependence); or it may increase for decreasing particle sizes, when smaller particles are more active than larger ones (curve 4). This is

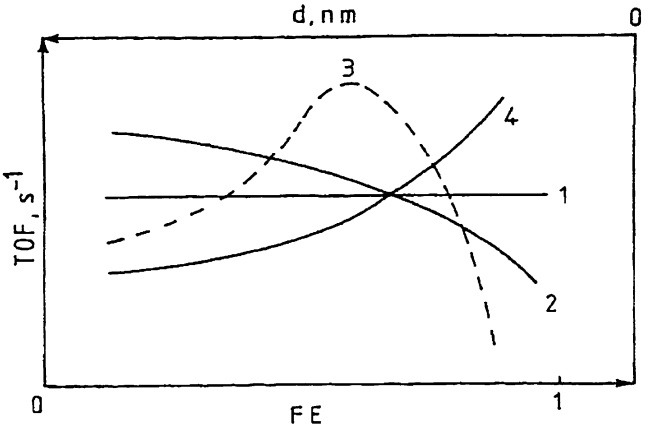

Figure 17: Turnover frequency (TOF) variation with the particle size d or the fraction exposed (FE) for structure-insensitive (curve 1) and structure-sensitive reactions (curves 2–4). Reprinted from (17) with permission from Elsevier.

called a positive particle size effect. The TOF may go through a maximum, for instance, if small particles exhibit a negative effect and larger ones positive effect. In this case, an intermediate size particles will have maximum specific activity (curve 3) (17).

Apart from the single metal crystals used for structure sensitivity studies (29), till recently, the conclusion of a structure sensitivity has been based on size effect studies using near spherical (cubooctahedral) nanoparticles of different diameters. Qualitative explanation of the size effect was based on the fact that the relative ratio of surface atom types (vertex, edge, and facets atoms) changes with varying particle size. Large particles possess mainly large crystal planes with atoms of high coordination number, whereas metal atoms with low coordination numbers constitute small particles (40, 18). Besides, the proportion of atoms located on different facets changes with the particle size as well (Fig. 2). In the last several years, structure sensitivity and observed size dependence was explained for some reactions on a quantitative basis, as will be exampled below. Using surface atom statistics, it is possible to estimate the amount of atoms with different geometric and thus electronic properties separately, followed by TOF calculation—not per total surface atoms, but per specific atoms. If the TOF does not change with the particle size, then these atoms may be considered as active sites. The reaction itself is then *structure-sensitive* but *intrinsically size-independent* contrary to the *observed (apparent) size dependency*. If this approach for a TOF calculation does not give a constant value for various particle sizes, then the reaction is *intrinsically structure-sensitive and size-dependent*. This phenomena is usually observed for small particles (with up to five shells around a central atom in the metal crystal), which are constituted mainly from low coordinated edges and corners without pronounced terraces. Another reason may be due to the catalytic activity of an ensemble of several atoms, which appears only in a definite interval of particle sizes. Structure sensitivity studies may be complicated by side reactions taking place on the catalyst surface (107) and by a carbon layout formation discussed in more details below.

The advances in colloidal preparation of metal nanostructures open new opportunities in the study of structure-sensitive catalytic reactions (6, 24, 51). Nanostructures of various shapes and sizes have become a powerful tool in revealing the reaction active sites due to a predominance of definite surface atoms on some nanostructures. For example, all terrace atoms of tetrahedrons belong to (111) facets, while of nanocubes to (100) terraces. In comparison, near spherical particles comprise of surface atoms of several types that complicates the structure sensitivity studies. Once an active site is found, colloidal techniques might make it possible to synthesize a catalyst containing mostly active sites. In the following, we provide some examples of structure-sensitive reactions carried out with various nanostructures.

3.2. Hydrogenations

3.2.1. Hydrogenation of Multiple Carbon-Carbon Bonds

Among structure-sensitive reactions, catalytic hydrogenations of multiple carbon-carbon bonds are of special interest due to their high importance in bulk and fine chemical production (18, 108). Until recently, most studies have been performed with near spherical Pd nanoparticles.

Numerous investigations have been carried out on Pd size effect in alkyne and alkadiene hydrogenations (18, 19, 109, 110). Highly electronegative alkynes bind to metals with a back-donation of the metal d electrons to the empty π^*-antibonding orbitals of the molecule, making the bonding to the metal stronger as compared to olefins. Possible reactive intermediates during hydrogenation of alkynes are presented in Fig. 18. Both π-adsorbed (I) and doubly σ-bonded (II) structures have been considered for the adsorbed acetylenes (111). Intermediates III-V have been proposed for the product development. While III lies on the pathway to the olefin, IV and V have been suggested as additional species leading to the fully reduced product. V is valid only for mono-substituted acetylenes. On Pd(100) acetylene coordinates to four atoms, while di-σ bridging coordination to either one or two adjacent metal centers with extra π interaction to the side atoms was proposed for Pd(111) and Pd(110) (29). This difference in surface intermediates on different surfaces gives rise to the structure sensitivity of alkyne hydrogenations.

Data on the side effects in hydrogenation of alkynes and alkadienes are rather controversial, although most studies showed that an increase in the metal dispersion decreases TOF. Antipathetic TOF dependence of acetylene on size was shown for a number of supported catalysts. The specific activity of Pd/α-Al_2O_3 catalysts was found to decrease by one order of magnitude as the dispersion increased from 10% to 76% (112). A drop of TOF was found for carbon nanofiber – deposited Pd nanoparticles of less than 3-nm diameter

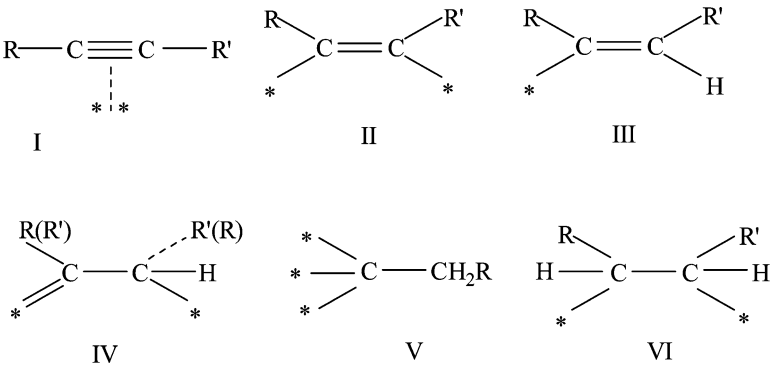

Figure 18: Possible reactive intermediates during hydrogenation of acetylenes. Reprinted from (111) with permission from Elsevier.

(113). These low activity of small metal particles is usually explained by the strong complexation of the highly unsaturated electron-rich alkyne to the electron-deficient atoms with low coordination number present on small particles, i.e., by a change in acetylene adsorption strength with a particle size (18, 112, 113). However, this electronic effect disappears when the particle size exceeds $\sim$ 5 nm, as there is no profound difference in the surface atoms statistics for bigger particles. Nevertheless, TOF of acetylene hydrogenation continues to increase above this limit. As was shown for polydispersed Pd/SiO_2 catalysts, TOF increases with an average particle size increase from 4.2 to 26.2 nm (19). When ME-derived monodispersed Pd nanoparticles of 8, 11, and 13 nm diameter were used for the size effect studies, TOF reached a constant value at 11 nm (114). Selectivity to ethylene stayed constant independently on the particle size (19, 114). Geometric effect allowed explaining this behaviour. Carbonaceous deposits produced during gas-phase hydrogenation form two types of catalytic sites: **A** sites representing small spaces and **E** sites representing large spaces of Pd between the carbonaceous deposits (Fig. 19). The **A** sites adsorb acetylene and hydrogen but, due to steric hindrance, do not adsorb ethylene. Consequently, these sites are involved in the conversion of acetylene, producing ethylene and small amounts of ethane, and they are inactive in the hydrogenation of ethylene. Instead, the **E** sites adsorb all reactants and are responsible for the hydrogenation of ethylene (115). As these sites are similar in nature (the regions of Pd surface between carbon), the overall selectivity to ethylene does not change (19). Thus, the active sites involve the relatively large ensembles of Pd surface atoms. Taking into account that the coverage of the surface by carbon is very high, it was suggested that the ensemble (geometric) effect was responsible for the structure sensitivity of this reaction (19, 114).

The importance of carbonaceous deposits in the alkyne hydrogenation structure sensitivity was discussed in terms of the surface and/or subsurface carbon ($Pd\text{-}C_x$) (116, 117), which builds up within the initial reaction stage. The deposit diminishes the Pd surface available for the adsorption of

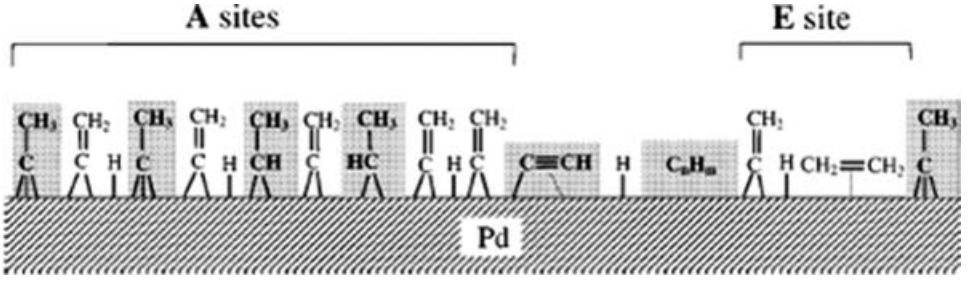

Figure 19: Pd surface during hydrogenation of acetylene and ethylene. The carbonaceous deposits (gray rectangles) create A and E sites. The reacting forms of acetylene, ethylene, and hydrogen are between the deposits. Reprinted from (115) with permission from Springer.

acetylene. The formation of the Pd-C_x phase itself is a structure-sensitive reaction, and it is not effective on the (111) facet of Pd (117). At higher particle size, the fraction of atoms on (111) planes increases leading to lower carbon deposition. Indeed, the maximum concentration of carbon in Pd at the steady state of the reaction decreases with increase of crystalline size (116). Thus, on smaller particles the ratio between surface C and Pd is higher, o the available surface for acetylene hydrogenation is diminished and consequently the observed TOFs are smaller (114).

Some studies also showed the importance of β-PdH phase in acetylene hydrogenation, which disappears with decreasing the metal particle size (118). This phase was claimed to be responsible for the direct alkyne hydrogenation to alkane (106), while some reports did not find this detrimental effect (18, 119). In addition, this phase often can hardly be stable under the reaction conditions: the partial pressure of hydrogen necessary to obtain a stable β-PdH phase during the reaction has to be one order of magnitude higher than the equilibrium pressure of hydrogen above the β-PdH phase at the same temperature (116).

Recent studies of 1,3-butadiene hydrogenation over Pd-Al_2O_3/NiAl(110), Pd(111) and Pd(110) single crystal catalysts revealed that TOF does not change with the particle size being normalized per number of Pd atoms in the incomplete (111) facets (20, 120). The reaction, therefore, was proposed to be structure-sensitive but size-independent for the particle size above 4 nm. Hydrogenation takes place preferentially on the (111) facets of these Pd nanoparticles. Pd nanoparticles <4 nm exhibited rather open surfaces and approached the reactivity of a Pd(110) single crystal. The latter crystals showed ~5-fold higher activity than Pd(111) probably due to the stronger bonding of 1,3-butadiene to Pd(111), which reduces the surface hydrogen concentration. By-product distribution also changes with Pd nanoparticle structure: Pd(111) crystals exhibit lower selectivity to the isomerization products but higher one to the alkane. Alkadiene-blocking effect on hydrogen adsorption was proposed to explain differences in selectivity. Critical hydrocarbon coverage below which hydrogen better perforates the alkadiene layer, depends on the particle size and reflects a size-dependent binding energy of alkadiene.

Alkene hydrogenations have been typically considered as structure-insensitive reactions. Using well-defined Pd/Al_2O_3 model catalysts, where the particle size was varied in a controllable manner, the size effect in ethylene and trans-2-pentene hydrogenation was studied (121). Ethylene was adsorbed as a π-bonded species irrespectively of the surface composition explaining its hydrogenation structure insensitivity. Other hydrocarbons, beginning with propene, adsorb in a less distorted geometry (π-bonded) in a second layer on the top of the most strongly bound di-σ-bonded species. Thus,

π-bonded pentene are not in direct contact with Pd and desorbs intact, and hydrogenation proceeds only via di-σ-bonded species, which are favored on the terrace sites of large particles. Pentene hydrogenation is thus structure-sensitive (121). PVP-stabilized Pt nanoparticles with the sizes between 1.7 and 3.6 nm also confirmed structure insensitivity of ethylene hydrogenation (47).

Structure sensitivity studies of alkyne hydrogenations in liquid phase do not suffer from carbonaceous deposit formation as in gas phase but may be complicated by mass transfer effects, especially when supported particles are used in the catalytic experiments. For the first time, the size effect in a liquid-phase alkyne Pd-catalyzed hydrogenation was shown for 1-butyne hydrogenation over polydispersed Pd/SiO_2 and Pd/Al_2O_3 catalysts (122). Lower selectivity and more than 10-fold decrease of TOF were observed when the metal dispersion increased from 20 to 100%. However, due to the particles' polydispersity and presence of the support, "one particle size effect" could not be evaluated. It was recently studied using monodispersed unsupported Pd spherical nanoparticles of 6, 8, 11, 13, and 14 nm diameter isolated from a reverse ME in 1-hexyne hydrogenation (56). A 15-fold TOF increase was observed with increase of the particles diameter from 11 to 14 nm (Fig. 20a). For particles above 14 nm, TOF approached the value of the Pd black catalyst. The 15% dispersion was found to be crucial, below which a drastic TOF increase occurred and approached a value of Pd black at the dispersions of ~12%. The higher crucial particle dispersion of 20% reported for the supported Pd catalysts in 1-butyne hydrogenation (122) can be explained both by the particles' polydispersity masking the true size effect and by the smaller size of the substrate molecule. The latter is of high importance as the observed size dependence was ascribed to the geometric and not to an electronic effect. There is no marked difference in the surface structure of the particles of 11- and 13-nm diameter, whereas the TOF was an order of magnitude higher for the 13-nm particles compared to the ones of 11 nm, confirming that the electronic effect is negligible in 1-hexyne hydrogenation for the particles more than 6 nm size. For the same Pd nanoparticles in acetylene hydrogenation, TOF does not change once the particles are of 11-nm size (114) contrary to 14 nm in hexyne hydrogenation. This again confirms the geometric factor governing the size sensitivity: larger 1-hexyne molecules require more space for adsorption on Pd surface than acetylene.

The by-product distribution in 1-hexyne hydrogenation characterized by the ratio of initial selectivities to 2-hexenes/n-hexane decreased 5-fold with particle diameter from 6 to 11 nm and remained constant for bigger particles (Fig. 20b) (56). Small particles (less than 11 nm) were prompted to form isomers (2-cis- and 2-trans-hexenes); the hydrogenation to hexane was observed only for particles bigger than 11 nm. It was supposed that hydrogenation requires specific ensembles of surface atoms constituting

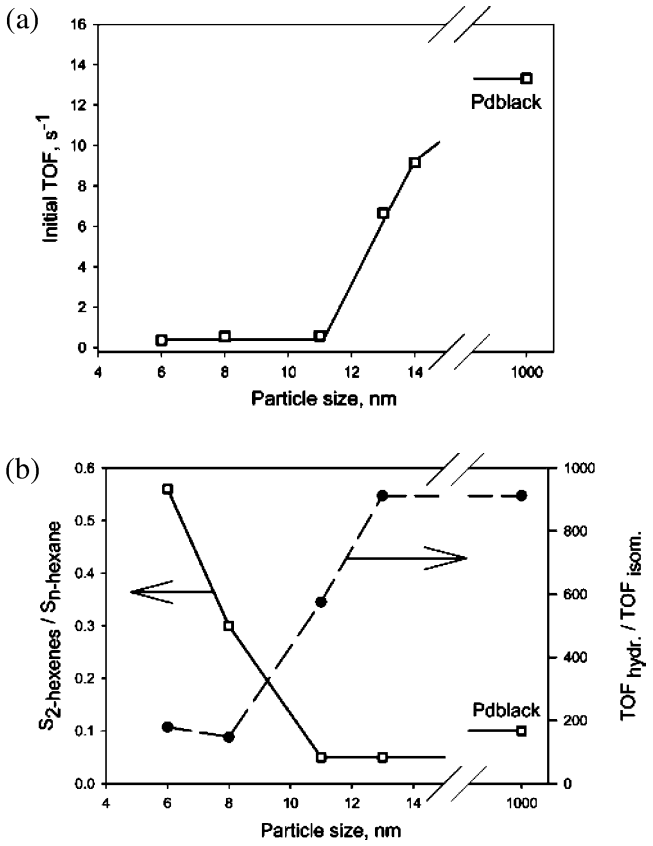

Figure 20: Size dependence of TOF (a) ratio of the product selectivities on the Pd particle size in 1-hexyne hydrogenation. Reprinted with permission from (56). Copyright 2007, American Chemical Society.

active centers, which only appear at particle sizes above 11 nm. It was in line with a hypothesis that there are several active sites on Pd surface, and the largest ensemble is required for π-adsorbed or di-σ-adsorbed flat-lying alkynes, which are the precursors for the alkene formation (18). For the formation of oligomers, alkyne can be adsorbed in a perpendicular mode dissociatively, which requires a small active center existing even at small nanoparticles.

Liquid-phase 1,3-butadiene hydrogenation was carried out over anisotropic Pd nanostructures synthesized by seed-mediated method using CTAB and deposited on Al_2O_3 (35). The catalyst was comprised by 40% of rods and by 60% of multi-twinned particles (MTP). The rods exposed preferentially (100) facets due to the stabilization effect of CTAB. The MTPs were supposed to be formed from six tetrahedrons with (111) surfaces. Higher TOF was observed for spherical particles of 1.5-nm diameter, however, compared to an isotropic catalyst, anisotropic Pd catalysts were found highly selective for the

hydrogenation of buta-1,3-diene into butenes without further hydrogenation into butane. Moreover, further hydrogenation of but-1-ene into butane was reduced while but-2-enes were hardly converted. Finally, an unusual high level of cis-but-2-ene isomer was observed. Comparing catalysts with rods and MTPs of different sizes, it was supposed that the observed effects were due to the reaction proceeding on (100) surfaces; however, no quantitative basis was provided.

A correlation between a spherical Pd nanoparticle size and TOF for the hydrogenation of allyl alcohol was found for the particle size between 1 and 2 nm (51). The hydrogenation reaction is sensitive to both the electronic and geometric properties of the catalytic Pd nanoparticles, both of which change quickly in the size range of 1.3–1.9-nm diameter. Analysis indicated that the hydrogenation kinetics are dominated by electronic effects for the smallest particles (<1.5 nm diameter) and by geometric effects for larger particles (1.5–1.9-nm diameter). For the hydrogenation of allyl alcohol over dendrimer-encapsulated Pd nanoparticles, all terrace atoms were found to be the active sites for nanoparticles larger than 1.5 nm as TOF calculated per number of these atoms did not change (Fig. 21) (51).

Hydrogenations of functionalized alkynes were also found to be structure-sensitive. Shape change allowed controlling activity and selectivity in 2-butyne-1,4-diol hydrogenation (46): cubic Pd nanoparticles stabilized by PVP were compared to the spherical particles produced by radiolytic reduction. Pd cubes were more active and selective in the hydrogenation reaction that revealed its structure sensitivity. Influence of the nanoobject size on TOF was opposite for the two catalysts: higher spherical particle size led to higher TOF, while the highest TOF was observed for the smallest nanocubes. Selectivity to 2-butene-1,4-diol in both cases increased with the particle size showing the

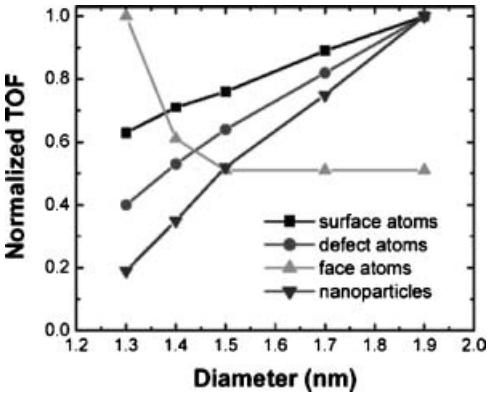

Figure 21: Dependence of TOF on size of dendrimer-encapsulated Pd nanoparticles in allyl alcohol hydrogenation. TOFs were calculated per different possible active sites. Reprinted with permission from (51). Copyright 2006, American Chemical Society.

existence of selectivity/activity optimum depending on the catalyst structure and size.

Spherical Pd nanoparticles were tested also in another acetylenic alcohol hydrogenation. Pd nanospheres of 7.5 nm size prepared by electrostatic stabilization exhibited a 6-fold higher activity and 14%-higher selectivity in hydrogenation of 2-methyl-3-butyn-2-ol (MBY) in comparison with 2.5 nm particles (123, 124).

Recently, size-controlled synthesis of Pd nanospheres allowed determining structure sensitivity but size independence of MBY hydrogenation (57). The particles under study included spherical monodispersed AOT-stabilized particles of 6, 8, 11, and 13 nm isolated from a reverse microemulsion (57). The unsupported particles were used, and their initial activity and selectivity were correlated with surface atom statistics. From Fig. 22a one can see that when initial TOF was calculated per total number of surface atoms in the catalysts, it changed with size. However, the apparent size sensitivity of MBY hydrogenation disappeared when TOFs were recalculated per number of C_9^3 atoms on (111) facets, i.e., atoms surrounded by 9 nearest neighbors with 3 missing ones (40). These atoms were proposed to be the active sites for the reaction performed over the AOT-stabilized Pd nanospheres (57). Alkene selectivity did not depend on the particle size, while the by-product distribution varied (57) in the same manner as for Pd catalysts in 1,3-butadiene hydrogenation (101): the more atoms are located on Pd(111) facets, the lower the ratio of isomerization to the saturated products. Pd(111) is known to bind the unsaturated substrate stronger as compared to Pd(110) (125) which reduces the surface hydrogen concentration leading to the suppressed alkane formation (20). In addition, Pd(100) does not hydrogenate alkenes but isomerizes them while showing absolute selectivity to alkene in an alkyne hydrogenation due to the strong metal-hydrogen bonding on Pd(100) (126).

These examples demonstrate the importance of the shape and size control for catalysis. A necessity to create a catalyst consisting of (111) faces for alkyne hydrogenations have been discussed earlier in the 1980s, when (111) surface of Pd single crystals showed the highest selectivity in 2-hexyne hydrogenation, while (110) plane was responsible for isomerization and olefin hydrogenation (127). However, it was noted, that even the "ideal" surface of (111) single crystal does not give 100% selectivity to alkene, as 5% of byproducts are formed directly from the adsorbed alkyne. In addition, the (111) surface is surrounded by edges and the surface itself become cracked after the reaction course. Practically, a nanostructure with predominant (111) planes should perform efficiently in alkyne hydrogenation. Considering tetrahedrons with four (111) planes, the highest TOF per total surface atom should be obtained at the largest particles with the reduced fraction of edges, but this would lead to low reaction rate per total Pd. The nature of a stabilizer

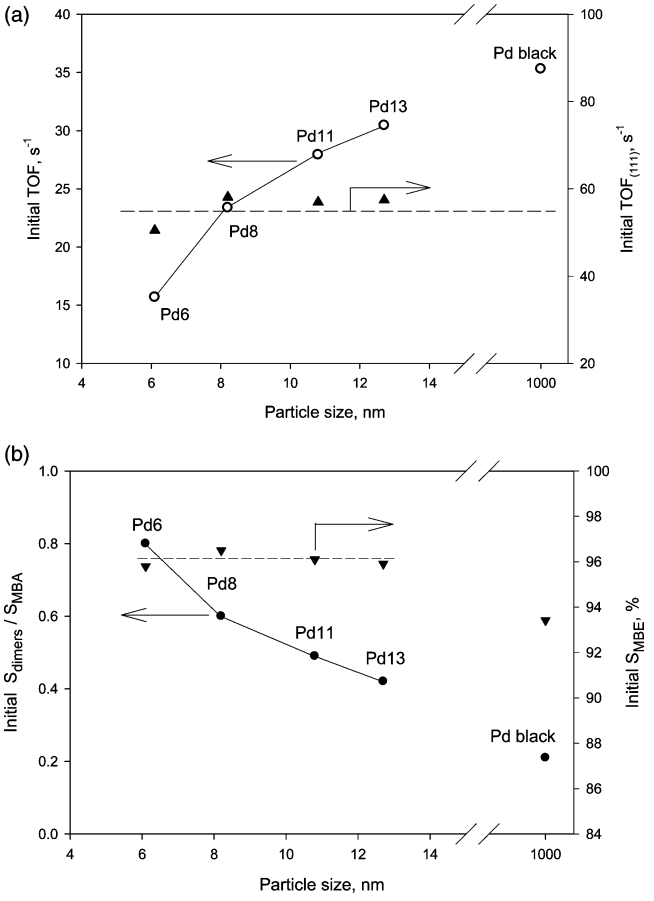

Figure 22: Structure sensitivity of 2-methyl-3-butyn-2-ol hydrogenation: (a) dependence of TOF calculated per total surface atoms on size and shape of Pd nanospheres and its independence if calculated per surface atoms on Pd(111) facets; (b) size dependence of the selectivities to 2-methyl-3-buten-2-ol (MBE), dimers and 2-methylbutan-2-ol (MBA). Reprinted from (57) with permission from Elsevier.

also affects the nanoparticle performance, e.g., Pd nanoparticles of similar diameters, but stabilized by PVP or 1,10-phenanthroline, exhibited very different catalytic activities for the hydrogenation of 1,3-cyclooctadiene: a strongly interacting ligand like 1,10-phenanthroline, or tetraoctylammonium halide, can disturb the hydrogenation (54). Therefore, an optimum has to be found for a given reaction and catalyst.

3.2.2. Other Hydrogenation Examples

Studies of hydrogenation of 2,4-dinitrotoluene to 2,4-diaminotoluene over Pd/SiO_2 catalyst revealed higher activity of larger Pd particles that was

correlated with the ability to form a palladium β-hydride phase which acts as a reservoir for activated hydrogen (palladium β-hydride formation increases with the Pd particle size (118)). Different crystallographic planes were shown to alter selectivity during hydrogenation of α,β-unsaturated aldehydes (21, 128). Closed-packed planes such as Pt(111) were selective for C=O bond hydrogenation due to repulsive interactions between the methyl groups attached to the C=C bond and the surface. Corrugated surfaces such as Pt(110) were more selective for hydrogenation of the conjugated C=C bond due to suppressed repulsive interactions.

A comprehensive study of Co particle size effects in the Fischer-Tropsch reaction (CO hydrogenation) was carried out using carbon nanofiber supported catalysts (129). The particles ranged in size between 2.6 and 27 nm and were supported on inert carbon nanofibers. At 35 bar, TOF increased with the particle size up to 8 nm. C_{5+} selectivity decreased from 85 to 51 wt.% with the particle size decrease from 16 to 2.6 nm. No CoO or Co carbide species were found, and the size effect was ascribed to structure sensitivity in combination with CO-induced Co nanoparticle surface reconstructurion. A size effect in CO hydrogenation was also studied using Rh nanoparticles prepared in a microemulsion and deposited on alumina (130). TOF increased four-fold by increasing the particle size from 5 to 30 nm. It was ascribed both to electronic and ligand effects in CO dissociation, which needs at least two well-separated sites into which the released carbon and oxygen can be accommodated, therefore, a sufficiently large Rh ensemble is needed. Methane selectivity decreased with increasing particle size, while higher hydrocarbons were favored on larger rhodium particles, as it is easier to accommodate higher hydrocarbons on large metal particles.

Apparent size effect in hydrogenations was shown to arise from a side reaction poisoning active sites for the main reaction (107). For example, active sites on highly dispersed metal particles can facilitate decarbonylation, as seen from the studies of 3-methyl-crotonaldehyde hydrogenation over Pt(111), (110), (553) surfaces (21, 131). Pt(110), which has a furrowed structure and hence a greater number of low coordination atoms, exhibits the highest selectivity to decarbonylation products. The same effect of the sites inhibition by produced CO was found for citral hydrogenation (107).

3.3. Heck reactions

Heck reactions catalyzed by soluble palladium compounds have been thoroughly revised in the past decade in terms of intrinsically active catalytic species. Palladium nanoparticles were reported to be dominant active catalysts formed *in situ* from a Pd(II) precursor (132). Another discussed topic in the area is that the nanoparticles are only precatalysts: nanoparticles

formed *in situ* are followed by oxidative addition of aryl halide to nanoparticle surface (133). This leads to Pd atom leaching, which is the source of very active molecular catalysts.

Ex situ prepared stabilized colloidal Pd (6, 134–137) and Ru (138) nanoparticles have gained considerable attention due to their high activity and recyclability. Pd equidimensional nanoparticles of mean sizes from 1.7 to 3.7 nm stabilized by PVP were used as a catalytic probe to study structure sensitivity of Heck coupling of *p*-bromobenzaldehyde with butyl acrylate (25). Much lower reaction rate was found when Pd precursor was used without a polymer that allowed suggesting the reaction does not occur via solution-phase catalysis by leached Pd species. A quantitative relationship was found between the initial reaction rates over various stabilized Pd nanoparticles and the number of low-coordinated ("defect") Pd surface atoms calculated using statistics for f.c.c. cubooctahedron (40) (Fig. 23). Initial reaction rates did not vary being calculated per number of the defect atoms. The Pd-metal catalyzed Heck coupling of aryl halides with olefins was thus claimed a structure-sensitive reaction with low-coordinated atoms as active sites.

This finding (25) is in the agreement of the results obtained for supported Pd catalysts in Heck coupling of acyl chloride with enol ethers (139). A single turnover (STO) reaction sequence was used to characterize the catalysts with respect to the numbers of alkene saturation sites, double bond isomerization sites and hydrogenation inactive sites. When a series of STO characterized catalysts were used to promote a Heck reaction, a linear relationship between the reaction rate and the amount of the alkene saturation sites on each catalyst was found. These sites are the coordinately unsaturated corner atoms and adatoms on the metal surface. The single atom active sites are the only ones having a sufficient number of orbitals available for interaction with both aryl species and the enol ether at the same time. However, the use of the supported catalysts did not allow direct correlation of the reaction rates with surface atom number based on the crystal statistics. This again shows an advantage of the unsupported colloidal nanoparticles of the controlled size and monodispersity in structure sensitivity studies (25).

3.4. Suzuki reactions

For the first time the structure sensitivity of Suzuki reactions was shown using PVP – stabilized Pd nanoparticles with mean diameters of 3.0, 3.9, 5.2, and 6.6 nm prepared via the step-growth reaction (24). The size effects of the Suzuki reaction between phenylboronic acid and iodobenzene in aqueous solution was investigated. Again, the surface statistics of equidimensional nanoparticles was estimated assuming that PVP-Pd nanoparticles were cubooctahedral in shape with a cubic close packed structure. When TOF of

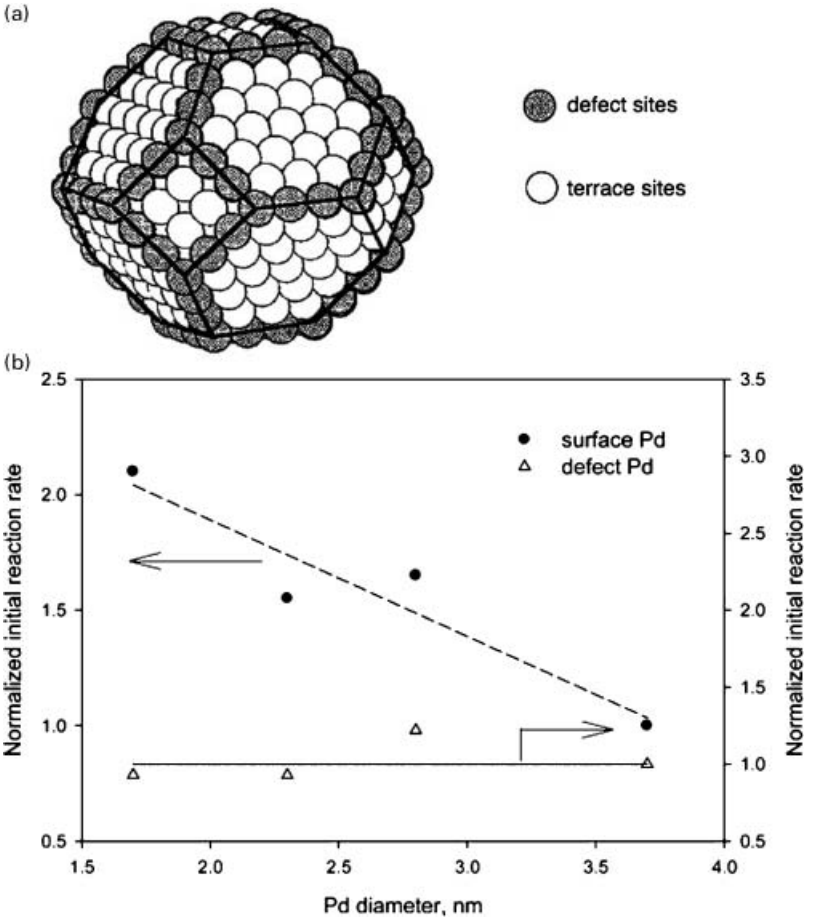

Figure 23: Structure sensitivity of a Heck reaction: (a) low-coordinated defect Pd surface atoms as active sites; (b) initial reaction rates normalized to that of the catalyst with the largest crystallite size and calculated per total surface Pd atoms and per defect atoms. Reprinted with permission from (25). Copyright 1999, American Chemical Society.

the reactions with different Pd sizes were calculated per total surface atoms, they changed by more than a factor 2 in the size range studied (Fig. 24a), indicating the reaction structure sensitivity. When defect (vertex and edge) atoms were assumed to be the active sites and used for TOF calculation, the dependence of TOF on the particle size almost disappeared, except for Pd nanoparticles of 3.0 nm (Fig. 24b). The lower catalytic activity for the smaller nanoparticles might be due to stronger adsorption of the reaction intermediates on the particles surface acting as the reaction inhibitor. Authors excluded the effect of the stabilizer by changing PVP/Pd ratio after the different size Pd nanoparticles were prepared. The catalytic activity remained the same for the nanoparticles with various PVP/Pd ratios indicating that the

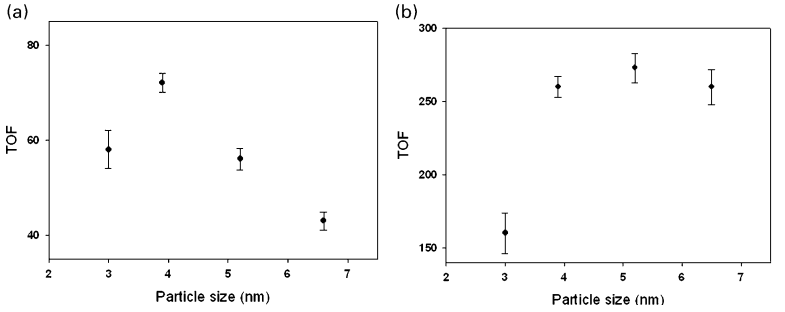

Figure 24: Turnover frequency as a function of Pd nanoparticle size in the Suzuki reaction between iodobenzene and phenylboronic acid. The TOF is calculated on the basis of (a) total number of surface atoms and (b) total number of defect (vertex and edge) surface atoms. Reprinted with permission from (24). Copyright 2002, American Chemical Society.

stabilizer does not play an important role. Thus, similarly to Heck reactions, the active sites for Suzuki coupling are single Pd defect atoms.

The study of the spherical particle stability during the Suzuki reaction was carried out using 2.1 ± 0.1 nm PVP-stabilized Pd nanoparticles (140). The nanoparticles become larger after the first run and the size distribution broadens. This effect is due to the Ostwald ripening process, which is a mechanism of cluster growth in which atoms of the smaller nanoparticle dissolve and deposit on the surfaces of more stable larger nanoparticles (65). During the first reaction run the Ostwald ripening takes place mostly during the first 3 h (Fig. 25). It was attributed to the enhanced formation of biphenyl in this time period, which poisons the active sites. After the second run, the nanoparticles were found much smaller and monodispersed due to the

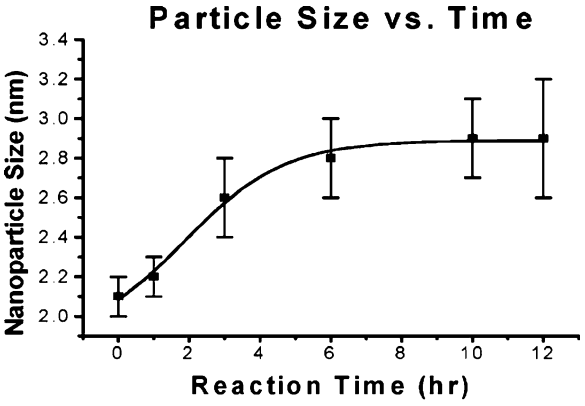

Figure 25: Growth of PVP-Pd nanoparticles during the first run of Suzuki reaction between phenylboronic acid and iodobenzene. Reprinted in part with permission from (140). Copyright 2003, American Chemical Society.

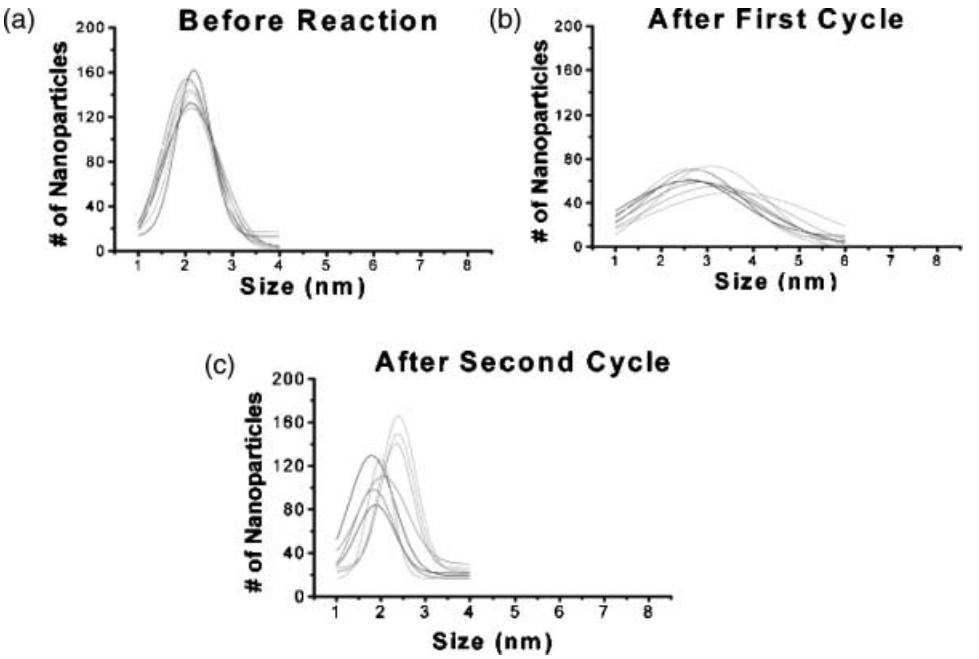

Figure 26: Size and size distribution of PVP-Pd nanoparticles grown during two cycles of the Suzuki reaction between phenylboronic acid and iodobenzene. Reprinted in part with permission from (140). Copyright 2003, American Chemical Society.

precipitation of the large nanoparticles as Pd black keeping the smaller particles in the solution (Fig. 26) (140).

The nanoparticles preparation and the nature of a stabilizer were shown to play an important role in the metal structure changes during the Suzuki reaction (65). For a comparison with the PVP-stabilized Pd spheres (140), poly(amido amine) PAMAM-OH generation 4 dendrimer-Pd nanoparticles of 1.3 ± 0.1 nm were studied (141). After the first cycle, the average size of the dendrimer-Pd nanoparticles increased by 54% (compared to 38% for PVP-Pd particles). After the second cycle, the dendrimer-Pd nanoparticles continued to increase in size by 35%, while the PVP-Pd nanoparticles decreased by 24%. The strong encapsulating of the PAMAM-OH generation 4 dendrimer-Pd nanoparticles could make the rate of transformation to the full nanoparticle size slow, resulting in a large excess of Pd metal atom concentration in solution, and thus, in the continuous growth of the nanoparticles during the catalytic reaction. Study of the changes in size occurring during refluxing of the both types of Pd nanoparticles in individual reactants did not reveal any difference between the samples, indicating that the reaction mechanism is insensitive to the capping material used. The ratio of the yield of biphenyl formed in the second cycle to that in the first cycle was higher for the dendrimer-Pd nanoparticles catalyzed reaction than for the PVP-Pd

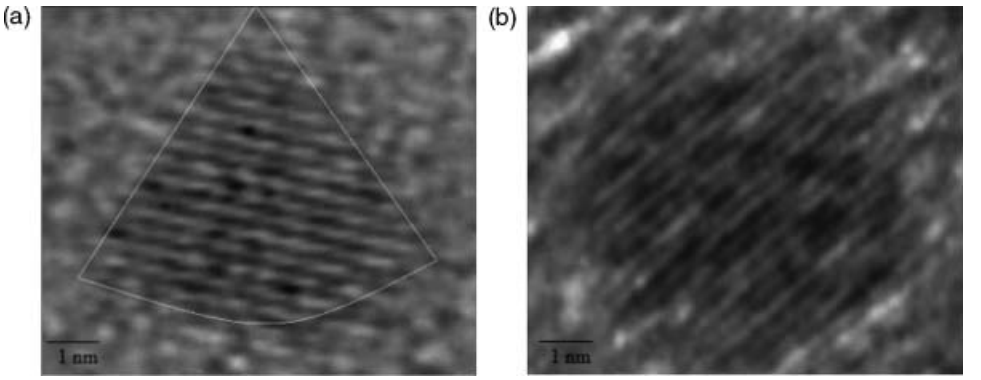

Figure 27: High resolution TEM images of the PVP-Pt tetrahedra before the Suzuki reaction (a) and after being transformed to a larger sphere (b). Reprinted with permission from (66). Copyright 2005, American Chemical Society.

nanoparticles. This could be due to the greater stability of the dendrimer-Pd nanoparticles and the increase in its size during the reaction. The presence of excess dendrimer was found to severely diminish the catalytic activity of the dendrimer-Pd nanoparticles and also diminished the change in the Pd nanoparticle size during the catalysis (141).

An elegant study of the catalytic activity and stability of tetrahedral PVP-stabilized Pt nanoparticles in the same Suzuki reaction revealed the change of the particle morphology during the reaction course to larger spherical (cubooctahedral) particles (Fig. 27) (66). The monodispersed tetrahedrons of 5.0 ± 0.1 nm size transform to the near spherical particles of 5.2 ± 0.1 nm size after the first reaction run, and to bigger 5.7 ± 0.2 nm spheres after the second run. Tetrahedrons consist of (111) facets and sharp edges and corners. The defect unstable atoms tend to dissolve and transform the nanotetrahedrons to the more stable spheres growing by Ostwald ripening process. Remarkably, that the nanoparticles lose their catalytic activity at recycling (66) since the Pt spheres formed are not active in the Suzuki reaction. Thus, the tetrahedral shape is catalytically active shape compared to a spherical one. This qualitatively confirms the hypothesis that the edge and corner atoms are the active sites: the fraction of these defect atoms in the initial tetrahedrons is 0.32, while in the formed spheres 0.11, explaining the reduced activity. Moreover, the authors (66) claim that the difference in activities of tetrahedral and spherical particles may come from the facet structure, i.e., the spherical (cubooctahedral) particles are composed of numerous (100) and (111) facets, and the tetrahedrons only of (111) facets. The number of Pt neighbors for (111) surface is 6, being 4 for (100) facets, leading to different electron densities of the two surfaces and different reactivity.

The influence of the chemical environment on the change of tetrahedron morphology during the Suzuki reaction was studied by refluxing Pt

nanoparticles in individual reactants (65, 66). The shape transformation occurs when the nanoparticles are refluxed in solvent, sodium acetate and iodobenzene. In the presence of phenylboronic acid the nanoparticles remain tetrahedras with the same size. The acid was supposed to bind to the particle surface acting as a stabilizer. This hypothesis was confirmed by the FTIR study of the mode of binding of the reactants on the Pd nanoparticle surface. It showed that the phenylboronic acid adsorbs on the nanoparticle surface and then interacts with the iodobenzene present in the solution (142). The large change in the B-O stretching frequency of phenylboronic acid from 1348 to 1376 cm^{-1} in the presence of sodium acetate and palladium nanoparticles strongly suggests that the mode of binding of phenylboronic acid to the Pd nanoparticle surface involves a B-O-Pd type of bonding. The phenylboronic acid needs to be in the deprotonated form in the presence of sodium acetate (phenylboronate anion) to bind to the palladium nanoparticle surface. No changes in the characteristic bands of iodobenzene were observed.

In summary, the reviewed studies showed that the change of different metal structures and their morphology during the catalytic reaction may be correlated with the catalytic activity. Studies of the influence of individual reactants on the particle shape/size may give an insight on the reaction mechanism.

3.5. Hydrogenolysis

Shape dependence of butane hydrogenolysis was studied over Pt and Rh nanowires and nanoparticles synthesized in mesopores of FSM-16 with a pore size of 2.7 nm (27). The Pt nanowires were produced by photoreduction of H_2PtCl_6 in FSM-16 (5 wt% Pt) in the presence of water/2-propanol vapors. In contrast, a H_2-reduction of H_2PtCl_6/FSM-16 at 673 K resulted in Pt nanoparticles within FSM-16. Pt nanowires (diameter 2.5 nm, length 50–300 nm) exhibited a 36 times higher TOF than Pt nanospheres of 3 nm. Ethane was produced over nanowires by secondary C-C bond cleavage, while spheres cleaved only terminal bonds producing methane and propane. The nanowires' behaviour was ascribed to the preferential exposition of (110) facets which atoms are supposed to be the active sites. The Pt nanowires could be extracted from the mesopores using $[NBu_4]Cl$ in benzene/ethanol (143).

Structure sensitivity studies of ethane hydrogenolysis were performed using Pt spherical nanoparticles in the size range of 1.7–7.1 nm stabilized by PVP and deposited on SBA-15 silica with pores of 9 nm. The reaction was structure-sensitive with smaller particles demonstrating higher specific activity. TOF for ethane hydrogenolysis increased monotonically with increasing metal dispersion, while the apparent activation energy increased linearly with Pt particle up to a size of ~4 nm and then remained constant.

Coordinatively unsaturated metal atoms present in small particles were suggested to be more active for C_2H_6 hydrogenolysis than the low index planes that dominate in large particles (47, 48). Changes of Pt (111) and (110) surfaces during olefin hydrogenolysis were monitored by scanning tunnelling microscopy (144).

Influence of the particles size on the product distribution during hydrogenolysis of methylcyclopentane (MCP) was shown for 10 nm Pt nanoparticles prepared by high vacuum evaporation of platinum onto either alumina or silica films followed by high temperature annealing and reduction. The main products were 2-methylpentane, 3-methylpentane and n-hexane. The product distribution was found to depend on Pt dispersion: lower n-hexane formation (10–12%) was ascribed to the large particle size (145, 146). However, it was found that the MCP hydrogenolysis consists of two parallel reactions (i) occurring on the platinum surface and producing mainly 2-methylpentane and 3-methylpentane and (ii) occurring on the phase boundary platinum/support and producing additional n-hexane (147). Lower Pt dispersion in this case means higher support/metal ratio and increase in hexane production. This shows that the use of stabilized Pt nanostructures without any support would be beneficial to study the reaction structure sensitivity.

3.6. Electron-Transfer Reactions

Comprehensive studies of the size- and shape-dependent nanocatalysis of electron-transfer reactions were performed for the Pt-catalyzed reaction between hexacyanoferrate(III) ions and thiosulfate ions forming tetrathionate and hexacyanoferrate (II) ions (6, 26, 65, 69, 70, 148–151). A study of the reaction kinetics using Pt spheres of various sizes and different concentrations allowed determining the process rate-limiting step. The particles were stabilized in aerosol-OT/water/heptane reverse microemulsion, were monodispersed and ranged between 2.2 and 8.4 nm (151). The authors concluded that the catalysis was controlled by processes at the particle surface rather than by diffusion. However, no correlation of the reaction rate with the particle size was provided.

The size-dependent catalytic behaviour of Pt spheres were studied for the nanoparticles ranging between 10 and 80 nm prepared in a reverse microemulsion (150). The maximum reaction rate was observed for the particle diameter of 38 nm. The activation energies for the reaction catalyzed by platinum nanoparticles of 12 and 30 nm are about 18 and 4.8 kJ/mol, respectively, indicating that the catalytic efficiency of 12-nm-diameter platinum particles is less than that of 30 nm particles. It was supposed that for smaller particles, a downward shift of Fermi level with a consequent increase of band gap energy takes place. As a result, the particles require more

energy to pump electrons to the adsorbed ions for the electron transfer reaction. This leads to a reduced reaction rate catalyzed by smaller particles. On the other hand, for nanoparticles above diameter 38 nm, the change of Fermi level is not significant. These particles exhibit less surface area for adsorption as the particle size increased. As a result, the catalytic activity is also decreased with increased particle size.

Spherical PVP-stabilized Pt nanoparticles of 4.9 ± 0.1 nm were found to decrease in size and increase their monodispersity during the electron-transfer reaction (149). Interestingly that the size did not change in the presence of thiosulfate which bond to the Pt surface and acted as a stabilizer, but did decrease in the presence of only the hexacyanoferrate. This was proposed to result from the dissolution of surface Pt atoms via complexation with the strong cyanide ligand. Thus, the studies of the particles stability in individual reactants allowed authors to propose the reaction mechanism, which involves the thiosulfate ions binding to Pt, followed by reaction with hexacyanoferrate ions from the solution. Carrying out the reaction with the nanoparticles pre-exposed to thiosulfate resulted in very small change in the size distributions of the nanoparticles, thus suggesting that thiosulfate ions bind to the nanoparticle surface and inhibit desorption of Pt atoms by hexacyanoferrate(III) ions. The activation energy of the reaction was also determined for various catalyst concentrations. The activation energy was found to decrease linearly with increasing nanoparticle concentration during both the first and second cycles. This suggests that the nature of the catalytic particles changes with the concentration due to aggregation. The type of catalytic particles changes as new sites created at the intersection of the aggregated nanoparticles are formed. As a result, it is possible that atoms at these sites are more catalytically active, giving rise to a reduction in the activation energy that is observed in the more concentrated nanoparticle solutions.

The change of the Pt nanoparticle shapes in the reaction of interest was also observed for the PVP-capped tetrahedrons and polyacrylate-capped cubes (26, 70). The high resolution TEM images of Pt tetrahedral and cubic particles before and after the electron-transfer reaction is presented in Fig. 28 (26). Distorted tetrahedrons and distorted cubes are formed due to the dissolution of Pt atoms from the corners and edges of initial tetrahedrons and cubes, respectively [Fig. 29a (65)]. Spheres do not change the shape. The shape change of tetrahedrons is faster compared to that one of cubes as tetrahedral particles have sharper corners and edges and also have a bigger fraction of these defect atoms. Interesting observation comes from Fig. 29b that a change in the activation energy follows the change in shape. The authors concluded that for comparable size nanoparticles, the near spherical particles were of modest catalytic activity but were the most stable. The correlation of the

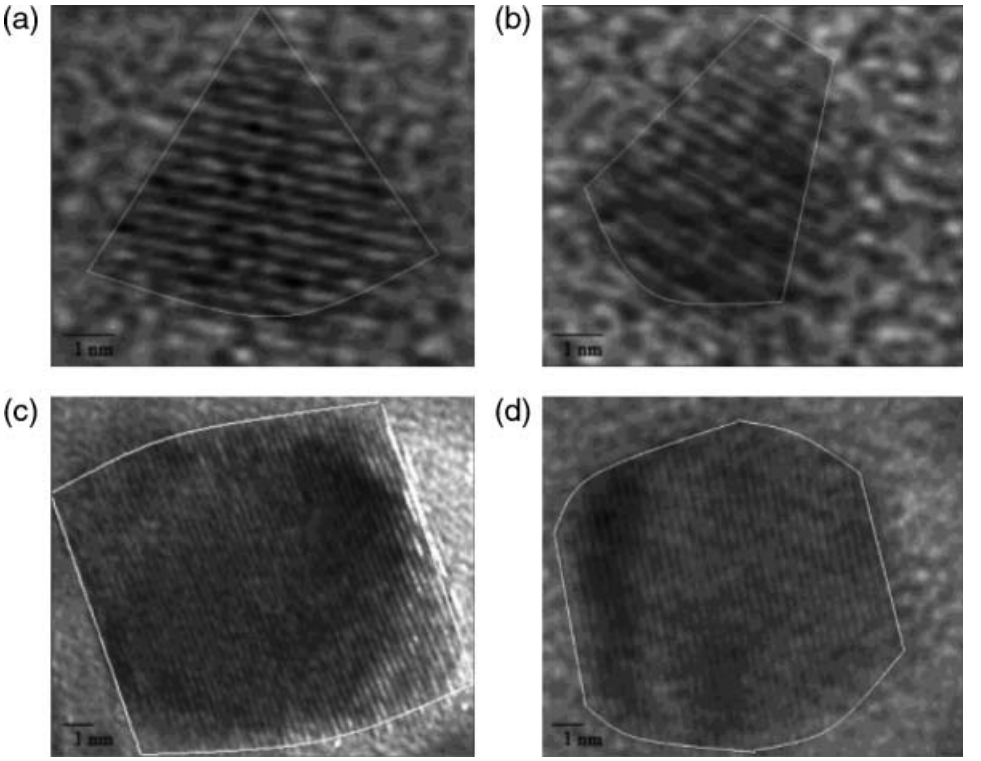

Figure 28: High resolution TEM images of Pt tetrahedron before (a) and after (b) the electron-transfer reaction, and of a cube before (c) and after (d) the reaction. Reprinted with permission from (26). Copyright 2004, American Chemical Society.

catalytic activity with fraction of surface atoms on corners and edges of Pt tetrahedrons, spheres, and cubes showed that as this fraction increased, the rate constant also increased (69) (Fig. 30). The tetrahedral Pt nanoparticles

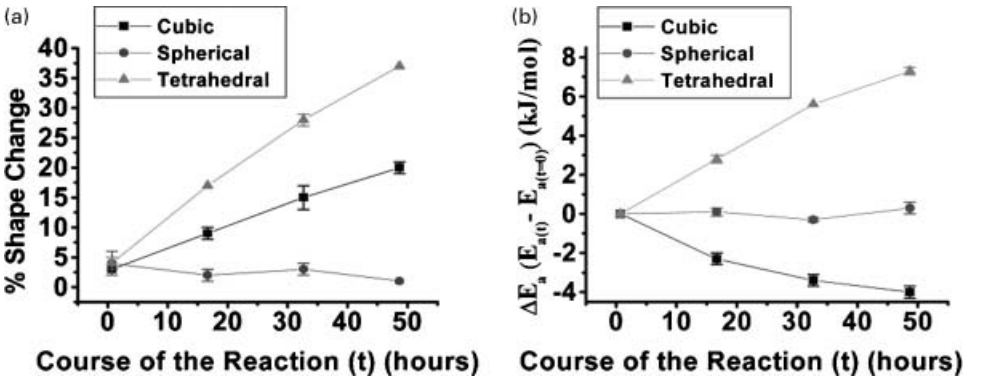

Figure 29: Percent change of shape (a) and activation energy (b) during the electron-transfer reaction. Reprinted with permission from (65). Copyright 2005, American Chemical Society.

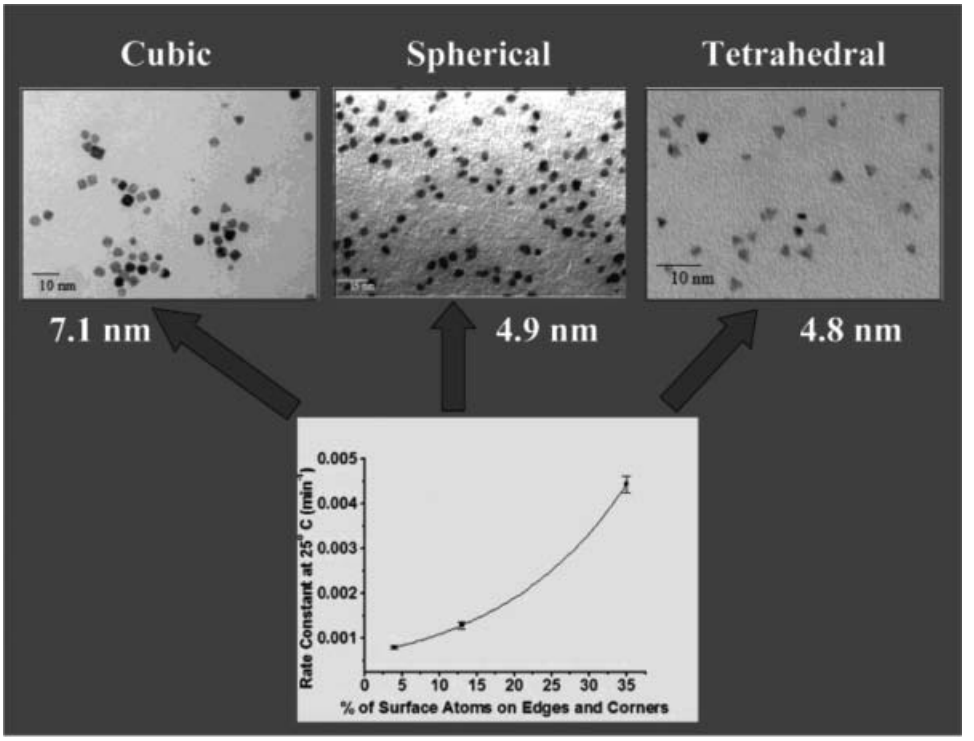

Figure 30: Correlation of catalytic activity of various Pt shapes in the electron-transfer reaction with the fraction of metal atoms on the corners and edges. Reprinted with permission from (65). Copyright 2005, American Chemical Society.

have the highest fraction of defect surface atoms and they were the most catalytically active.

As for the spherical particles (149), reactant influence on the cube and tetrahedron shape was studied (26). The presence of just hexacyanoferrate ions in the solution with the nanoparticles was found to increase the amount of distorted tetrahedral and distorted cubes present much more than during the reaction. The presence of only the thiosulfate ions did not seem to affect the size or shape. This might be a result of capping ability of this anion protecting the nanoparticles similar to the spherical Pt nanoparticles. This suggests that the mechanism of the reaction is not dependent on the shape of the nanocatalyst.

3.7. Oxidations

Carbon monoxide and methanol oxidations are the most vigorously studied oxidative structure-sensitive reactions catalyzed mostly by platinum, gold, or palladium. Most of the studies were performed for the nanoparticles

on an oxide or carbon support prepared via impregnation with the metal precursor.

3.7.1. CO oxidation

The effect of the Pt particle size on the kinetics of CO electrooxidation were studied for the particle sizes from 1 to 30 nm (22, 152). TEM analysis revealed that Pt crystallites were not perfect cubooctahedrons, and that large particles had "rougher" surfaces than small particles, which had some fairly smooth (111) facets. The importance of "defect" sites for the catalytic properties of nanoparticles was probed in infrared reflection-absorption spectroscopy experiments by monitoring how the vibration frequencies of atop CO (ν_{CO}), as well as the concomitant development of dissolved CO_2 were affected by the number of defects on the Pt nanoparticles. It was found that defects play a significant role in CO "clustering" on nanoparticles, causing CO to decrease/increase in local coverage. The observed deviations were accompanied by CO_2 production, which increased with the number of defects on the nanoparticles in the order $1 \leqslant 2 < 5 \ll 30$ nm (22). It was suggested that the catalytic activity for CO adlayer oxidation was predominantly influenced by the ability of the surface to dissociate water and to form OH_{ad} on defects rather than by CO energetics. Chronoamperometric and rotating disk electrode studies showed that in the back sweep of CO bulk oxidation, the activity increased with decreasing particle size, that is, with increasing oxophilicity of the particles. The adsorbed OH (at the same potential the surface coverage with OH increases by decreasing the particle size) was shown to behave as an educt species and promote the CO oxidation reaction (152).

A series of PVP-stabilized Pt nanoparticles of different size distributions was employed for CO electrocatalytic oxidation (153). The electrodes have been prepared from aqueous Pt colloids and glassy carbon (GC). The effect of platinum particle size of Pt/GC catalyst electrode on the electrocatalytic oxidation of carbon monoxide has been investigated. The voltammetry showed that a higher potential was needed for the oxidation of absorbed carbon monoxide with a decrease of the platinum particle size for particle sizes larger than 1 nm. But for particle sizes smaller than 1 nm, the potential remained constant while the activity decreased with decreasing the size (153). 1 nm Pt nanoparticles were also studied in hydrogen oxidation reaction (154). Experimental and computational data showed that upon reducing the diameter of Pt nanoparticles down to 1 nm, a collapse in the crystalline structure occurs spontaneously and this causes a decline in the catalytic activity.

For CO oxidation on nanometer-sized palladium nanoparticles a mesoscopic stochastic model was developed (155). The reaction rate oscillations are

of a stochastic nature, because of considerable internal noise in such mesoscopic systems. The performance of the stochastic oscillations underwent a maximum with the variation of the particle size at a given CO partial pressure, which demonstrated the occurrence of particle size resonance. Such a phenomenon was shown to be robust to the change of CO pressure. These results implied that there exists an optimal particle size for the CO oxidation over nanometer-sized palladium. However, no experimental data were reported.

Another theoretical study using density functional calculations was performed for catalytic CO oxidation by a gold nanoparticle (156). Gold is usually considered to be catalytically inert (very noble). The surface of gold cannot adsorb most of molecules from the gas phase. Yet it has been found that nanometre size gold particles supported on different oxides can act as catalysts even below room temperature. The density functional calculations showed that even an isolated Au_{10} cluster should be able to catalyze the CO oxidation reaction below room temperature. The extraordinary reactivity can be traced back to special reaction geometries available at small particles in combination with an enhanced ability of low coordinated gold atoms to interact with reacting molecules.

CO oxidation at room temperature was studied using gold nanoparticles synthesized on activated carbon fibre fabrics (157). The particles of 2.5–5 nm showed high catalytic performance, while 9-nm particles were not active. Similarly, the optimal Au size for CO oxidation was reported to be 3 nm (158, 159). A series of Au/TiO_2 catalysts with different gold sizes was prepared by a sequence of calcination steps and studied in CO oxidation (160). For Au particles with mean particle size, d, in the range of 2–10 nm, the measured TOF at 298 K varied as $d^{-1.7 \pm 0.2}$ and $d^{-0.9 \pm 0.2}$ for the 7.2 and 4.5 wt% Au/TiO_2 catalysts, respectively. Variation between samples emphasized the conclusion that the activity is sensitive to many factors that may mask the true structure dependence. It was suggested that the observed decrease in activity with increasing particle size beyond 2 nm was controlled by the population of low-coordinate sites, rather than by size-dependent changes in overall electronic nature of the nanoparticle (160).

Particle size and substrate effects in CO electro-oxidation on titania- and carbon-supported Au nanoparticles of mean diameters <6.5 nm was studied in acidic environment (0.5 M $HClO_4$). The activity of the particles prepared by physical vapor deposition was compared with that one of bulk, polycrystalline gold. Carbon-supported gold exhibited activity for CO oxidation only at potentials similar to that observed for bulk gold. Decreasing the particle size below $\sim$2.5 nm resulted in a sharp decay in catalytic activity. Titania-supported gold exhibited catalytic activity at overpotentials significantly below those of bulk gold, and the activity was strongly particle-size-dependent.

A maximum in activity was observed at ~3.0 nm, and a sharp reduction in activity was observed below ~2.5 nm. The results highlighted two important effects. Titania was responsible for a strong substrate-induced activity for CO electrooxidation on gold particles. In addition to the induced activity at low overpotentials, this titania-supported gold was also shown to exhibit activity at high potentials where normally the oxidation of the gold poisons the reaction. The second observation was that the oxidation is inhibited on particles below 2.5 nm in size, irrespective of the support (161).

A correlation between size, electron structure and activity in CO oxidation was made for Au nanoparticles deposited onto a SiO_2/Si(100) wafer by Ar^+ ion implantation of 10-nm thick gold film (162). The intrinsic catalytic activity of the gold particles increased with decreasing size. When an Au/FeO_x interface was created by FeO_x deposition on large gold nanoparticles, a significant increase in the rate of the CO oxidation was observed. These data were regarded as an experimental verification of the correlation between the catalytic activity and valence band density of gold.

3.7.2. Methanol and Formic Acid Oxidation

Structure sensitivity studies of methanol and formic acid oxidations have attracted considerable attention in the past decade as these reactions are of interest for the direct methanol fuel cell (DMFC) and direct formic acid fuel cell (DFAFC).

A recent study reported on the shape-controlled synthesis of triangular gold nanoprisms (70–110 nm size) and nanoperiwinkles (150–230-nm size) for electrocatalytic methanol oxidation (163). The nanostructures were synthesized using 5-hydroxytryptamine as a reducing/stabilizing agent at room temperature. Their X-ray diffraction profiles revealed that they were composed of mainly a Au(111) lattice plane. The nanostructures were self-assembled retaining their morphologies on a three-dimensional silicate network derived from (3-mercaptopropyl)trimethoxysilane. Their spectral and electrochemical properties have been investigated. The nanoparticles on the silicate network showed excellent electrocatalytic activity toward oxidation of methanol and reduction of oxygen. Their electrocatalytic activity was higher than the spherical gold nanoparticles, probably, due to high Au(111) content.

Different sized f.c.c. platinum nanoparticles supported on carbon were prepared using 1-hexanethiol as a surfactant and heated to various temperatures to vary the particle size (23). The average platinum particle size as determined from XRD data was found to be ~2.00, ~2.56, ~4.23, ~4.52, ~2.13, ~2.77, ~4.29, and ~4.62 nm. X-ray photoelectron spectra of all catalysts indicated that most (>70%) of the platinum nanoparticles have zero

oxidation state and a small amount (<30%) have (+4)-oxidation state. Increase of the heating temperature resulted in an enlargement of platinum particle size, a positive shift in the binding energies of Pt(0) and Pt(IV), and a decrease in catalytic activity in the methanol oxidation (23). Pt(111) plane is the most active for methanol oxidation, and its fraction on the surface increases with the particle size increase, probably, causing the observed phenomena (164).

Nanoparticle size effects on methanol electrochemical oxidation on Pt/C catalysts was studied using differential electrochemical mass spectrometry under both potentiodynamic and potentiostatic conditions (165). While the particle size effect in this reaction is usually regarded as a reflection of different Pt-CO and Pt-OH bond strengths for different particle sizes, the authors (165) focused mainly on the mechanism of methanol dehydrogenation on platinum which is crucial for the optimization of the methanol electrooxidation efficiency by favouring the CO_2 formation pathway. It was found that the partitioning of the methanol precursor among the end products on supported platinum nanoparticles is strongly dependent on particle size distribution. Also, it was postulated that the coupling among particles of different sizes via soluble products must be considered in order to understand the particle size effects on the observed trends of product formation. An optimum particle size range for efficiently electrooxidizing methanol to CO_2 was found between 3 and 10 nm, and loss in efficiency was mostly related to the partial oxidation of methanol to formaldehyde on either too small or too large particles.

Along with the methanol oxidation activity, Pt nanoparticle size effects in the range of 2–9 nm were studied for formic acid and formaldehyde electrooxidation (166). The TOFs on the larger nanoparticles ($d > 4$ nm) were similar to those observed on polycrystalline Pt. The rates of methanol electrooxidation decreased for Pt nanoparticle below 4 nm, but in formic acid electrooxidation the rates increased markedly for $d < 4$ nm, while in formaldehyde electrooxidation no sensitivity to the Pt nanoparticle size was observed. The extent of chemisorbed CO formation from all three reactants, as deduced from voltammetric and infrared spectral data, diminished with particle diameter, the CO coverages for a given nanoparticle size being in the order methanol < formic acid < formaldehyde. These nanoparticle-size-dependent electrocatalytic reaction and CO adsorption were suggesting the Pt site "ensemble effect", where reactant dehydrogenation to form CO, and also in the case of formaldehyde and methanol to yield the reactive intermediate during CO_2 production, was impeded by the sharply decreased availability of contiguous Pt terrace sites for $d < 4$ nm. The markedly enhanced electro-catalyic rates for formic acid oxidation on the smaller nanoparticles were attributed to the lack of a "Pt site ensemble" required for this process, coupled with decreased CO poisoning: unlike the other two reactions, oxygen addition (from coadsorbed -OH) was not required to produce CO_2 from formic acid.

Unsupported Pd nanoparticles in the size range from 9 to 40 nm were also studied in electrooxidation of formic acid (167). The cyclic voltammetry and chronoamperometry studies showed that the most active catalyst contained the smallest (9 and 11 nm) Pd nanoparticles. At X-ray photoelectron spectroscopy analysis these nanoparticles displayed the highest core-level binding energy shift and the highest valence band center downshift with respect to the Fermi level. The shifts can directly be related to the electronic structure of palladium nanoparticles of different sizes A correlation between formic acid oxidation current and these shifts was found. The observed shifts were caused by a weakening of the bond strength of the COOH intermediate adsorption on the catalyst surface. This, in turn, resulted in the increase in the formic acid oxidation rate to CO_2 (and in the associated oxidation current). The results demonstrated the significance of the core-level binding energy and center of the d-band shifts in electrocatalysis and particle size effect on the electronic properties of palladium that yielded different catalytic activity in the HCOOH oxidation.

3.7.3. Other oxidations

Size dependence in the solvent-free aerobic oxidation of various alcohols was studied using zeolite-supported palladium nanoparticles of 2.0–10.5-nm diameter (168). In benzyl alcohol oxidation the TOF reached a maximum at a Pd size of 2.8 nm. For the oxidation of geraniol or 2-octanol without delocalized π-ring, the reaction was structure-insensitive, and the intrinsic TOF did not change significantly with the Pd particles size (Fig. 31).

The effect of palladium particle size on the activity during methane combustion under diesel-engine exhaust conditions was studied (169). The

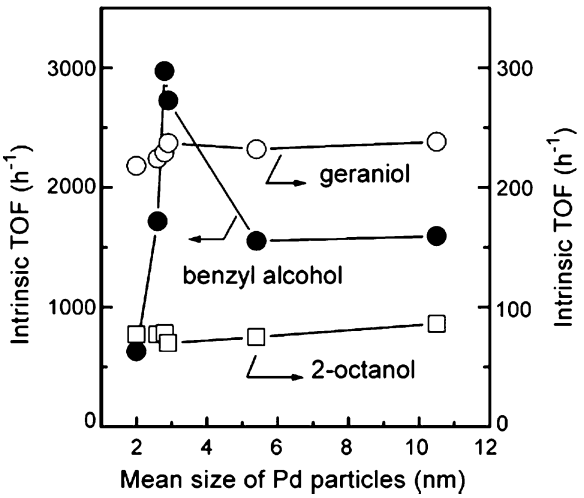

Figure 31: Structure sensitivty and insensitivity in alcohol oxidations over Pd/zeolite catalysts. Reprinted from (168) with permission from Elsevier.

particles were prepared by a microemulsion (ME) technique and used being deposited on alumina together with the catalysts prepared by conventional impregnation. Particles of less than 2 nm exhibited low temperature ignition. Medium-sized particles (about 10 nm) increased the reaction rate, and complete conversion was obtained at a lower temperature. Large particles (up to 40 nm) did not further improve the catalytic activity.

Different morphologies of Ag nanoparticles (nanowires of a mean diameter of 150 nm and nanopolyhedra of ~300 nm diameter) were used supported on α-Al_2O_3 and MgO for the selective gas phase oxidation of styrene (102). Phenylacetaldehyde and styrene oxide were the main products, while the direct combustion was negligible even at near total conversion. The top crystal face of nanoparticles was (111), which was proposed to have a beneficial effect on the selective oxidation of styrene.

Gold nanoparticle size effect in ethylene glycol oxidation was studied using supported Au spherical nanoparticles stabilized by PVA (49) and N-dodecil-N,N-dimethyl-3-amino-1-propan sulfonate (SB) (50). When the PVA-protected particles between 4.3 and 10 nm were deposited on carbon, the highest TOF was observed for 7 nm particles [Fig. 32 (50)]. On the oxides Al_2O_3, TiO_2 the activity of Au nanoparticles increased with decreasing particle size. XPS of the carbon-supported gold revealed that the activity depends not only on the particle size but also on gold surface concentration (49). Using the

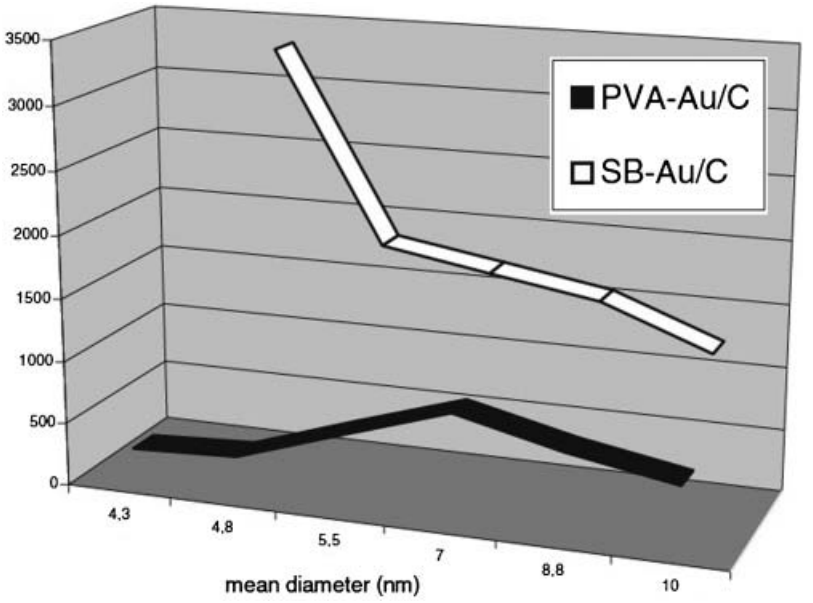

Figure 32: TOFs of ethylene glycol oxidation over carbon-supported 1% Au catalysts prepared by stabilization by polyvinylalcohol (PVA) and N-dodecil-N,N-dimethyl-3-amino-1-propan sulfonate (SB). Reprinted from (50) with permission from Springer.

sulfobetain protective agent, much higher TOFs were found for the catalysts with a lower mean diameter of 4.8 nm but with a high atomic Au/C percentage at the surface. The 4.8-nm SB-protected nanoparticles with the atomic surface concentration of 2.29 at.% Au(4f)/C(2s) were more active than the 4.3-nm PVA-stabilized particles with 0.49 at.% Au(4f)/C(2s) (50). SB was more able than PVA to locate gold particles externally on the surface of carbon, favouring the gold particle activity in the liquid phase oxidation. Supposing that the gold particle activity is not limited by shielding effects, gold-on-carbon activity in the liquid-phase oxidation should increase with decreasing particle dimension as observed for the oxide-supported particles. To confirm this, a catalytic study of support-free nanoparticles would be beneficial, but no such data have been reported. The same authors showed that the carbon-deposited CTAB-protected gold nanoparticles ranged between 5.9 and 28 nm had lower activity in the same reaction (61). This was ascribed to the blocking effect of the surfactant.

3.8. More Examples of Structure Sensitivity Studies

The Pd particle size effect in NO-CO reaction was studied using Pd/MgO(100) model catalysts at low pressure by a pulsed molecular beam technique (170). Three samples with mean clusters sizes of 2.8, 6.9, and 15.6 nm were used. The reaction products were mainly N_2 and CO_2. The largest particles, which exhibit principally (100) facets were the least active; while the medium sized particles exhibiting mainly (111) facets were more active. The smallest particles were less active because of the proportion of strongly adsorbed nitrogen species decreases with the decreased cluster size (the low coordinated sites increased). The strongly bound nitrogen atoms tend to cover the particle surface and decrease the available sites for NO dissociation leading to decreased catalytic activity.

Mechanism of electrocatalytic reduction of nitric oxide in acidic media was studied on Pt(100), Pt(110) and Pt(111) (171). The adsorption of nitric oxide on Pt(100) results in the formation of an adlayer with a structure similar to that formed under ultrahigh vacuum conditions. Ammonia was shown to be the main product of NO_{ads} reduction on Pt(100). Pt(100) is the most active surface for breaking the N-O bond.

Platinum hexagons (6.9 nm), cubes (13.6 nm) and tetrahedrons (14.6 nm) stabilized by PVP, poly(*N*-isopropylacrylamide) (NIPA) and sodium poly (acrylate) (SPA), respectively, were deposited on γ-Al_2O_3 and studied in NO reduction by CH_4 at 350–600°C (28). Similar study was performed for the cubic nanoparticles for NO reduction by C_3H_6 (73). The activity was compared with a conventional Pt/Al_2O_3 catalyst with spherical particles of 2.4 nm diameter. The use of nanocrystals allowed increasing yield to N_2O at the dramatic decrease of NH_3 and CO formation (28): Excerpt from (28) is

reprinted with permission from Springer. The effect was attributed to shape (surface) effect and size (bulk) effect. The proposed explanations were based on the earlier results obtained over clean metal surfaces. The first step of NO conversion is the dissociation of the adsorbed molecule on metal surface:

$$NO_{ads} \rightarrow N_{ads} + O_{ads} \tag{3}$$

The dissociation of NO is very sensitive to the crystallographic orientation. On Pt(100) NO dissociates by 50%; Pt(111) facets are completely inactive at any coverage, while the high index Pt planes are very active, e.g., more than 98% of the adsorbed NO is dissociated on Pt(410) surfaces. NO dissociation is also known to take place at the steps. Small spherical Pt nanoparticles of 2.4 nm have random crystallographic orientation and are rich in high index planes, edges, kinks and steps, so they are expected to show high activity for NO decomposition. In contrast, large crystals of the studied morphologies have limited activity for NO decomposition because of the relatively low concentration of high index planes and surface defects.

NO decomposition is followed by N_2 and N_2O formation:

$$N_{ads} + N_{ads} \rightarrow N_2 \tag{4}$$

$$N_{ads} + NO_{ads} \rightarrow N_2O \tag{5}$$

The generation of N_2O is favoured over large nanocrystals as they exhibit low activity in NO decomposition. In contrast, high selectivity to N_2 was observed over the small spherical particles because of their high efficiency in step (3). Among the nanocrystals, cubes showed the lowest activity in NO decomposition and highest yield to N_2O as these crystals have the least defected (smooth) surface.

The second reactant, methane, adsorbs dissociatively on Pt surface:

$$CH_4 \rightarrow CH_x + (4-x)H_{ads}, \tag{6}$$

followed by oxidation of the CH_x and H_{ads} species by O_{ads} resulted from NO decomposition. The structure sensitivity of the methane oxidation over Pt was ascribed to the different reactivity of the adsorbed oxygen. The catalytic activity of large Pt particle for oxidations is at least one order of magnitude higher than the small and well-dispersed Pt particles. The oxidation of CH_4 on the large ("L") Pt nanocrystals ($\sim$13 nm) was described by equation (7):

$$CH_x + (4+x)/2(O_{ads})_L \rightarrow CO_2 + (x/2)H_2O. \tag{7}$$

Methane continuously removes the pool of O_{ads} then NO dissociation can continue, mainly on high index planes and surface defects.

Small particles give high selectivity to CO and NH_3 as at high temperatures they are converted to PtO, PtO_2 and $PtAl_2O_4$. As a result of the low oxidation activity of $O^{\delta-}$ (PtO_x) species, some of the surface CH_x species undergo only a partial oxidation on small ("S") particles:

$$CH_x + (2+x)\Big/2\left(O^{\delta-}\right)_S \rightarrow CO + (x/2)H_2O. \quad (8)$$

In addition to CO, large amounts of NH_3 are formed during the reduction of NO with methane over small particles. The lifetime of the CH_x and H_{ads} species on the small Pt particles is longer as the result of low oxidation ability of bulk PtO_x. Thus, the reactions responsible for ammonia formation are favoured:

$$CH_x + (x/2)N_{ads} \rightarrow C + (x/3)NH_3 \quad (9)$$

$$3H_{ads} + N_{ads} \rightarrow NH_3. \quad (10)$$

The ammonia formation over nanocrystals of the reported shapes were greatly reduced because the active oxygen chemisorbed on the large Pt particles rapidly removes the carbonaceous and H species from the surface as CO_2 and H_2O.

Thus, for this structure-sensitive NO/CH_4 reaction it was shown than colloidal techniques used for preparation of nanocrystals of different shapes allowed accurate tuning of the catalytic properties (28, 73).

4. OPTIMAL CATALYST DESIGN

The previous subchapters showed that the use of nanostructures with controlled size and shape in catalytic reactions allow better understanding of their mechanism and getting an insight on the structure sensitivity of numerous reactions. Eventually, this knowledge should result in the synthesis of a working catalyst with the optimal crystalline arrangement of atoms on the surface. Ease of the described colloidal techniques and precise control over the nanostructures' size and shape make it possible to fill in the materials gap between the ideal single crystals and working catalysts. However, there are some challenges arising in the practical use of colloidal nanoparticles, which will be discussed below both for unsupported and supported nanostructures. The unsupported particles may be used in liquid-phase catalytic reactions, while the supported ones both in gas- and liquid-phase.

4.1. Unsupported Nanoparticles

The first problem arising for the use of unsupported nanoparticles is their isolation from the colloidal solution in which they were prepared. For many

applications, the stabilized nanostructures are not purified from the synthesis solution, which is added together with nanoparticles to the reaction mixture (24, 25, 51). There was a case, for example, for a Suzuki reaction: PVP-Pd nanoparticles prepared in the aqueous phase were added to the reactants in water (24). This was possible due to the same solvent in synthesis and reaction solutions.

However, this simple approach cannot be applied when the synthesis and reaction solvents are immiscible. The most extreme case in this sense is the use of nanoparticles prepared in reverse microemulsions (ME), which are multicomponent systems (hydrocarbon, water, surfactant, nanoparticles, excess of a reducing agent). Metal concentration in the ME is typically very low to assure aqueous phase solubilisation by a surfactant, so, the volume of a catalyst-containing ME may even exceed by several times the volume of the reaction mixture in order to get reasonable reaction rates. A catalytic reaction may be affected by the presence of ME via the "medium" and "solubilization" effects. An example of the use of a ME in a catalytic reaction was shown for Pt nanoparticles catalyzed hydrogenation of 1-butene, which was introduced into the ME (172). Excess of hydrazine used for platinum reduction poisoned the catalyst, so, H_2O_2 had to be added to the microemulsion to remove the reductant. When a non-ionic surfactant was used for the microemulsion preparation, Pt nanoparticles were much more active than in the presence of a cationic surfactant (CTAB). However, even the most active particles were still about 10 times less active than the same particles deposited on a support. Thus, a surfactant and ME water phase decrease the transport of the reactants to Pt surface atoms (172).

Recovery of a surfactant and hydrocarbon from a nanoparticle-containing reverse ME was claimed to be a challenging task hampering the commercialization of a ME technique for catalyst preparation (55). Several methods were recently proposed to isolate the nanoparticles from the reverse microemulsion without their aggregation. Hydrocarbon evaporation (173, 174) or freeze-drying/sublimation (175) did not allow elimination of surfactant molecules, whereas cross-flow ultrafiltration (176) resulted in a concentrated nanoparticle suspension. Another method involved the hydrocarbon evaporation in vacuum at 50°C, followed by the surfactant dissolution in methanol with the simultaneous flocculation of Pd nanoparticles, which could be isolated by centrifugation (Fig. 33) (57). The obtained precipitate was shown to contain Pd nanoparticles with the initial size. 99.5% of the surfactant was successfully removed by centrifugation, while residuals stabilized the nanoparticles against agglomeration. The nanoparticles could be dried under mild conditions still preserving their monodispersity (56), or ultrasonically redispersed in water (37) or in reaction mixture (57). The method also allows recovery of the surfactant and hydrocarbon. Interesting alternative was proposed for Ag

nanoparticles prepared in reverse ME with recovery achieved by dissolving antisolvent CO_2 in the micellar solution: the Ag particles were precipitated by compressed CO_2 at suitable pressure, while the surfactants remained in hydrocarbon. However, the particles were not tested in a catalytic reaction (177).

To recycle unsupported nanoparticles, ultrafiltration of the reaction mixture may be performed, like it was shown for Pd nanoparticles stabilized in block-copolymer micelles (64). If a repeated catalytic reaction is performed to study the reuse effect on the particles stability, fresh reactants can be simply added to the reaction mixture from a previous run (66). When nanoparticles are stabilized in an ionic liquid and used in biphasic liquid-liquid reactions (e.g., Pt nanoparticles in lower ionic liquid phase and hydrogenation arenes or alkenes in the upper phase), the particles may be easily separated by decantation or distillation (43).

4.2. Supported Nanoparticles

Easy handling of metal nanostructures may be achieved via their deposition on a support that also extends their application area to gas-phase reactions.

For catalytic applications, various metal nanostructures were deposited onto metal oxides, activated carbon, zeolites, etc. A conventional technique

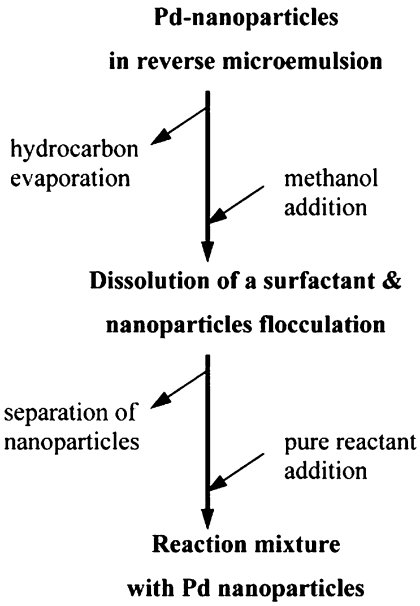

Figure 33: Method for nanoparticle isolation from reverse microemulsion for catalytic applications. Reprinted from (57) with permission from Elsevier.

includes wet or wetness impregnation of a support with a colloidal dispersion, followed by centrifugation or filtration with repeated washing. It was shown for nanoparticles stabilized both by polymers (62, 64), low-weight surfactants (61), and other stabilizers (54). As an example, Pd nanoparticles stabilized in diblock-copolymer micelles were deposited on γ-Al_2O_3 and used in liquid-phase hydrogenation of 2-butyne-1,4-diol. The catalyst showed high activity and selectivity but the nanoparticle-containing micelles leached progressively from the support (64). Sometimes, a support can be prepared in the same micellar solution as nanoparticles, e.g., Pt/SiO_2 catalyst was prepared by tetraethoxysilane hydrolysis in the microemulsion where Pt nanoparticles were forming. This allowed uniform nanoparticle dispersion on the support without aggregation (178). Supports with deposited nanoparticles can be dried under air, in vacuum, or via freeze-drying. These mild immobilization conditions ensure nanoparticles retaining their original shape and size. The obtained catalysts are often calcined to remove an organic stabilizer that can result in particle sintering (36) and loss of their shape and/or size. As an example, polymer-stabilized Pt nanocubes were deposited on alumina, followed by freeze-drying, high temperature activation and tested in gas phase NO reduction with C_3H_6 (73). CTAB-stabilized Au nanoparticles were mixed with activated carbon and used directly for liquid-phase ethylene glycol oxidation, however, the surfactant decreased the catalyst activity (61). Indeed, if a major part of a stabilizer is not removed from the particle surface, it can lead even to the complete loss of activity, e.g., Pd nanoparticles synthesized in microemulsion by AOT and deposited onto metal oxides showed zero activity in allyl alcohol hydrogenation, but the calcined catalysts showed high conversions (60).

Catalytic nanoparticles prepared in ME show the highest activity loss, probably, due to high ratios of surfactant-to-metal (up to several hundred g/g). To remove the excess of a surfactant before deposition on a support, several techniques were proposed. The most widespread one includes addition of tetrahydrofuran (THF) during mixing a nanoparticle-containing ME with a support. THF competes with the surfactant adsorbed on nanoparticles and displace them resulting in an unstable suspension. The particles precipitate and adsorb onto a support (55). However, it is difficult to achieve homogeneous particle distribution on a support, the procedure success depends on support properties. Besides, THF should be added dropwise, and its volume can exceed the volume of initial ME (up to 3-fold) to achieve destabilization.

Another method to deposit surfactant-free nanoparticles onto a solid support consists in spraying ME into an air/acetylene flame. Thus, gold nanoparticles were deposited onto silicon wafers and almost preserved their original structure (179). To recover a surfactant and hydrocarbon from ME, nanoparticles may be isolated using the above described technique (Fig. 33),

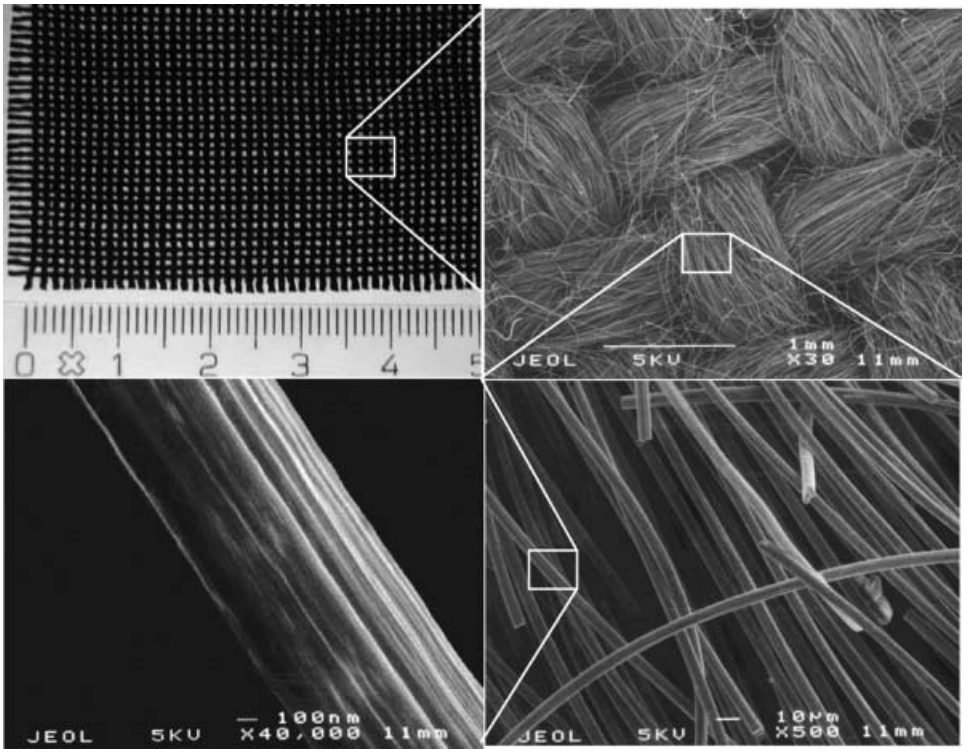

Figure 34: Structure of woven active carbon fibres support. Reprinted from (180) with permission from Elsevier.

ultrasonically redispersed in water and deposited by insipient wetness impregnation onto a support. Upon deposition, nanoparticles maintain their size, shape and monodispersity (37). This technique allowed synthesizing a structured catalyst based on ME-derived Pd nanoparticles deposited on activated carbon fibre (ACF) fabrics, which showed high activity, selectivity and stability in the repeated use in semi-batch three-phase hydrogenation of 1-hexyne, representing an alternative to a traditional Lindlar catalyst (37). The catalyst arranged structure (Fig. 34) makes it a promising material for continuous applications (34), e.g., it can be used as catalytic stages in bubble column reactors (180). In a batch process it can be fixed on a stirrer between metal gauzes; catalyst recycling in this case does not require filtration as for the powdered catalyst. The same procedure was used to deposit Pd nanoparticles onto carbon nanofibers (CNF) grown on sintered metal fibre (SMF) filters. High permeability and low pressure drop allowed using this material for gas-phase acetylene hydrogenation (114).

To ensure particle immobilization on a support, surface modification of the particles and supports may be performed. For example, thiophenol was used to modify a surface of Pd nanoparticles prepared in a reverse ME. The particles

were mixed with metal oxides modified by 3-mercaptopropyltrimethoxysilane (MPS) to create thiol groups as particle-binding sites. Mixing of the modified particles and support resulted in stable particles which did not leach out during liquid-phase allyl alcohol hydrogenation. However, thiol groups poisoned some active sites leading to the decreased activity (60). The colloidal nanoparticles stabilized by PVP can be also captured on metal oxide supported modified with 3-mercaptopropyltrimethoxysilane: the nanoparticles were precipitated in acetone by centrifugation and redispersed in dichloromethane containing MPS to exchange the maximum of PVP with MPS ligand, followed by the support addition. These catalysts showed higher activity than unsupported ones due to the elimination of the adsorbed PVP (181).

Metal particles can be also deposited on a support via ion exchange, e.g., Pd nanoparticles were incorporated in a hydrotalcite via anion exchange between a suspension of hydrotalcite-nitrate and a Pd hydrosol stabilized by sodium dodecyl sulfate. No surface aggregation after Pd deposition was observed. The catalyst showed high activity, selectivity and stability in alkyne hydrogenations (58). Another example includes deposition of tetradecyltrimethylammonium bromide-stabilized Pd nanoparticles on Na-montmorillonite: the surfactant molecules rendered the clay surface hydrophobic via cation-exchange reaction and simultaneously ensured the adsorption of the released Pd particles onto the silicate surface, resulting in the formation of organophilic catalyst used in liquid-phase hydrogenation of 1-phenyl-1-pentyne (38). Again, the surfactant prevented aggregation of the nanosized Pd.

The supported catalyst may contain nanostructures with different size and shape distribution compared to the unsupported particles (35). Colloidal dispersion of Pd cubes, spheres, rods, tetrahedrons, and polyhedric particles prepared via a seed-mediated approach was concentrated by centrifugation, mixed with α-Al_2O_3 and washed to remove the stabilizing CTAB. The resulting solid contained only nanorods and polyhedric particles, which was explained by the selective insertion of some nanostructures in the support pores (35).

When a seed-mediated approach is used for the particle preparation, supported catalysts may be prepared via impregnation of a support with the seeds followed by contacting the solid with the growth solution (35). Pd nanorods and multi-twinned particles prepared in this way on α-Al_2O_3 showed activity higher by several fold than the catalyst prepared by deposition of the before prepared nanostructures onto the support. This effect was attributed to the change in the nanostructure size and fraction of active crystalline surfaces.

To conclude, there are two main challenges in terms of deposition of before prepared metal nanostructures. The first one is to retain the particles size and shape upon immobilization, which often can be ensured by the mild deposition

conditions. The second one is to achieve a strong particles' adhesion to the support to prevent metal leaching during liquid-phase reactions. Rational combination of the support and stabilizer, as well as their surface modification may result in a leaching-resistant heterogeneous catalyst.

5. CONCLUSION

According to "Vision 2020 Catalysis Report" (2, 182), the principle areas of science should include "new methods to synthesize stable, high productivity catalysts with control of active-site architecture". The ultimate goal of synthesizing a catalyst with a surface consisting predominantly of active sites can be attained knowing the nature of active sites required for an eventual reaction. Various crystallographic orientations of catalytically active metal nanoparticles in working catalysts do not allow the turnover frequencies and selectivities, which can be achieved with model single crystals. However, control over nanoparticle size/shape may rend the desirable active surface.

Described colloidal techniques provide an easy way to produce nanocubes, nanotetrahedrons, nanowires and other structures. Nanocubes and nanotetrahedrons are expected to show high performance in structure-sensitive reactions demanding (100) and (111) surfaces, respectively. The use of these particles could help to surpass the material gap between single metal crystals and industrial catalysts. Applications of these structures in catalysis are still limited mostly because of the influence of a stabilizer or change of the active nanoparticle morphology during the catalyzed reaction and/or deposition on a support. Increasing research activity in chemistry, materials science, catalysis, and chemical engineering will lead to the rational design of highly efficient catalysts for an eventual catalytic process.

REFERENCES

[1] Kralik, M., and Biffis, A. (2001) Catalysis by Metal Nanoparticles Supported on Functional Organic Polymers. *J. Mol. Catal. A*, 177: 113–138.

[2] Aiken III, J.D., and Finke, R.G. (1999) A Review of Modern Transition-Metal Nanoclusters: Their Synthesis, Characterization, and Application in Catalysis. *J. Mol. Catal. A*, 145: 1–44.

[3] Gonsalves, K.E., Li, H., Perez, R., Santiago, P., and Jose-Yacaman, M. (2000) Synthesis of Nanostructured Metals and Metal Alloys from Organometallics. *Coord. Chem. Rev.*, 206–207: 607–630.

[4] Shchukin, D.G., and Sukhorukov, G.B. (2004) Nanoparticle Synthesis in Engineered Organic Nanoscale Reactors. *Adv. Mater.*, 16: 671–682.

[5] Bronstein, L.M., Sidorov, S.N., and Valetsky, P.M. (2004) Nanostructured Polymeric Systems as Nanoreactors for Nanoparticle Formation. *Rus. Chem. Rev.*, 73: 501–515.

[6] Burda, C., Chen, X., Narayanan, R., and El-Sayed, M.A. (2005) Chemistry and Properties of Nanocrystals of Different Shapes. *Chem. Rev.*, 105: 1025–1102.

[7] Astruc, D. *Nanoparticles and Catalysis*, Wiley-VCH: Weinheim, 2007; 663 pp.

[8] Corain, B., Schmid, G., and Toshima, N., (eds.) (2008) *Metal Nanoclusters in Catalysis and Materials Science: the Issue of Size Control*, Elsevier: New York, 470 pp.

[9] Nalwa, H.S., (Ed.) (2004) *Encyclopedia of Nanoscience and Nanotechnology*, American Scientific Publishers; California, USA, 10 vol.

[10] Wieckowski, A., Savinova, E.R., and Vayenas, C.G., (eds.) (2003) *Catalysis and Electrocatalysis at Nanoparticle Surfaces*; CRC; New York, USA, 970 pp.

[11] Guczi, L., Peto, G., Beck, A., and Paszti, Z. (2004) Electronic Structure and Catalytic Properties of Transition Metal Nanoparticles: the Effect of Size Reduction. *Top. Catal.*, 29: 129–138.

[12] Toebes, M.L., van Dillen, J.A., and de Jong, K.P. (2001) Synthesis of Supported Palladium Catalysts. *J. Mol. Catal. A*, 173: 75–98.

[13] Corain, B., Centomo, P., Lora, S., and Kralik, M. (2003) Functional Resins as Innovative Supports for Catalytically Active Metal Nanoclusters. *J. Mol. Catal. A*, 204–205: 755–762.

[14] Bennett, C.O., and Che, M. (1989) Some Geometric Aspects of Structure Sensitivity. *J. Catal.*, 120: 293–302.

[15] Coq, B., and Figueras, F. (1998) Structure-Activity Relationships in Catalysis by Metals: Some Aspects of Particle Size, Bimetallic and Supports Effects. *Coord. Chem. Rev.*, 178–180: 1753–1783.

[16] Henry, C.R. (2000) Catalytic Activity of Supported Nanometer-Sized Metal Clusters. *Appl. Surf. Science*, 164: 252–259.

[17] Che, M., and Bennett, C.O. (1989) The Influence of Particle Size on the Catalytic Properties of Supported Metals. *Adv. Catal.*, 36: 55–172.

[18] Molnar, A., Sarkany, A., and Varga, M. (2001) Hydrogenation of Carbon-Carbon Multiple Bonds: Chemo-, Regio- and Stereo-Selectivity. *J. Mol. Catal. A*, 173: 185–221.

[19] Borodzinski, A. (2001) The Effect of Palladium Particle Size on the Kinetics of Hydrogenation of Acetylene-Ethylene Mixtures over Pd/SiO_2 Catalysts. *Catal. Lett.*, 71: 169–175.

[20] Silvestre-Alberto, J., Rupprechter, G., and Freund, H.-J. (2006) Atmospheric Pressure Studies of Selective 1,3-Butadiene Hydrogenation on Well-Defined $Pd/Al_2O_3/NiAl(110)$ Catalysts: Effect of Pd Particle Size. *J. Catal.*, 240: 58–65.

[21] Pradier, C.M., Birchem, T., Berthier, Y., and Cordier, G. (1994) Hydrogenation of 3-Methyl-butenal on Pt(110), Comparison with Pt(111). *Catal. Lett.*, 29 (3–4): 371–378.

[22] Arenz, M., Mayrhofer, K.J.J., Stamenkovic, V., Blizanac, B.B., Tomoyuki, T., Ross, P.N., and Markovic, N.M. (2005) The Effect of the Particle Size on the Kinetics of CO Electrooxidation on High Surface Area Pt Catalysts. *J. Am. Chem. Soc.*, 127: 6819–6829.

[23] Sen, F., and Gokagac, G. (2007) Different Sized Platinum Nanoparticles Supported on Carbon: An XPS Study on These Methanol Oxidation Catalysts. *J. Phys. Chem. C*, 111: 5715–5720.

[24] Li, Y., Boone, E., and El-Sayed, M.A. (2002) Size Effects of PVP-Pd Nanoparticles on the Catalytic Suzuki Reactions in Aqueous Solution. *Langmuir*, 18: 4921–4925.

[25] Le Bars, J., Specht, U., Bradley, J.S., and Blackmond, D.G. (1999) A Catalytic Probe of the Surface of Colloidal Palladium Particles Using Heck Coupling Reactions. *Langmuir*, 15: 7621–7625.

[26] Narayanan, R., and El-Sayed, M.A. (2004) Effect of Nanocatalysis in Colloidal Solution on the Tetrahedral and Cubic Nanoparticle Shape: Electron-Transfer Reaction Catalyzed by Platinum Nanoparticles. *J. Phys. Chem. B*, 108: 5726–5733.

[27] Fukuoka, A., Higashimoto, N., Sakamoto, Y., Inagaki, S., Fukushima, Y., and Ichikawa, M. (2001) Preparation and Catalysis of Pt and Rh Nanowires and Particles in FSM-16. *Microporous and Mesoporous Materials*, 48: 171–179.

[28] Miyazaki, A., Balint, I., and Nakano, Y. (2003) Morphology Control of Platinum Nanoparticles and Their Catalytic Properties. *J. Nanoparticle Research*, 5: 69–80.

[29] Zaera, F. (2001) Probing Catalytic Reactions at Surfaces. *Progress in Surf. Sci.*, 69: 1–98.

[30] Choo, H., He, B., Liew, K.Y., Liu, H., and Li, J. (2006) Morphology and Control of Pd Nanoparticles. *J. Mol. Catal. A*, 224: 217–228.

[31] Kim, F., Connor, S., Song, H., Kuykendall, T., and Yang, P. (2004) Platonic Gold Nanocrystals. *Angew. Chem. Int. Ed.*, 43: 3673–3677.

[32] Bronstein, L.M. (2003) Nanoparticles Made in Mesoporous Solids. *Top. Curr. Chem.*, 226: 55–89.

[33] Schwarz, J.A., Contescu, C.I., and Putyera, K., (eds.) (2004) *Dekker Encyclopedia of Nanoscience and Nanotechnology*; Marcel Dekker, Inc.: New York; 5 vol.

[34] Kiwi-Minsker, L. (2002) Novel Structured Materials for Structured Catalytic Reactors. *Chimia*, 56: 143–147.

[35] Berhault, G., Bisson, L., Thomazeau, C., Verdon, C., and Uzio, D. (2007) Preparation of Nanostructured Pd Particles Using a Seeding Synthesis Approach - Application to the Selective Hydrogenation of Buta-1,3-diene. *Appl. Catal. A*, 327:32–43.

[36] Agrell, J., Germani, G., and Jaras, S.G. Boutonnet, M. (2003) Production of Hydrogen by Partial Oxidation of Methanol over ZnO-Supported Palladium Catalysts Prepared by Microemulsion Technique. *Appl. Catal. A*, 242: 233–245.

[37] Semagina, N., Renken, A., and Kiwi-Minsker, L. (2007) Monodispersed Pd-Nanoparticles on Carbon Fiber Fabrics as Structured Catalyst for Selective Hydrogenation. *Chem. Eng. Sci.*, 62: 5344–5348.

[38] Mastalir, A., Kiraly, Z., Szollosi, G., and Bartok, M. (2001) Stereoselective Hydrogenation of 1-Phenyl-1-Pentyne over Low-Loaded Pd-Montmorillonite Catalysts. *Appl. Catal. A*, 213: 133–140.

[39] Xiong, Y., Cai, H., Wiley, B.J., Wang, J., Kim, M.J., and Xia, Y. (2007) Synthesis and Mechanistic Study of Palladium Nanobars and Nanorods. *J. Am. Chem. Soc.*, 129: 3665–3675.

[40] Van Hardeveld, R., and Hartog, F. (1969) The Statistics of Surface Atoms and Surface Sites on Metal Crystals. *Surf. Sci.*, 15: 189–230.

[41] Teranishi, T., and Miyake, M. (1998) Size Control of Palladium Nanoparticles and Their Crystal Structures. *Chem. Mater.*, 10, 594–600.

[42] Schmid, G. (1992) Large Clusters and Colloids. Metals in the Embryonic State. *Chem. Rev.*, 92: 1709–1727.

[43] Scheeren, C.W., Machado, G., Dupont, J., and Fichtner, P.F.P., Texeira, S.R. (2003) Nanoscale Pt(0) Particles Prepared in Imidazolium Room Temperature Ionic Liquids: Synthesis from an Organometallic Precursor, Characterization, and Catalytic Properties in Hydrogenation Reactions. *Inorg. Chem.*, 42: 4738–4742.

[44] Turkevich, (1985) J. Colloidal Gold. Part I. Historical and Preparative Aspects, Morphology and Structure. *Gold Bulletin*, 18 (3): 86–91.

[45] Henglein, A., and Giersig, M. (1999) Formation of Colloidal Silver Nanoparticles: Capping Action of Citrate. *J. Phys. Chem. B*, 103: 9533–9539.

[46] Telkar, M.M., Rode, C.V., Chaudhari, R.V., Joshi, S.S., and Nalawade, A.N. (2004) Shape-Controlled Preparation and Catalytic Activity of Metal Nanoparticles for Hydrogenation of 2-Butyne-1,4-diol and Styrene Oxide. *Appl. Catal. A*, 273: 11–19.

[47] Rioux, R.M., Song, H., Hoefelmeyer, J.D., Yang, P., and Somorjai, G.A. (2005) High-Surface-Area Catalyst Design: Synthesis, Characterization, and Reaction Studies of Platinum Nanoparticles in Mesoporous SBA-15 Silica. *J. Phys. Chem. B*, 109: 2192–2202.

[48] Song, H., Rioux, R.M., Hoefelmeyer, J.D., Komor, R., Niesz, K., Grass, M., Yang, P., and Somorjai, G.A. (2006) Hydrothermal Growth of Mesoporous SBA-15 Silica in the Presence of PVP-Stabilized Pt Nanoparticles: Synthesis, Characterization, and Catalytic Properties. *J. Am. Chem. Soc.*, 128: 3027–3037.

[49] Bianchi, C., Porta, F., Prati, L., and Rossi, M. (2000) Selective Liquid Phase Oxidation Using Gold Catalysts. *Top. Catal.*, 13: 231–236.

[50] Biella, S., Porta, F., Prati, L., Rossi, M. (2003) Surfactant-Protected Gold Particles: New Challenge for Gold-on-Carbon Catalysts. *Catal. Lett.*, 90: 23–29.

[51] Wilson, O.M., Knecht, M.R., Garcia-Martinez, J.C., and Crooks, R.M. (2006) Effect of Pd Nanoparticle Size on the Catalytic Hydrogenation of Allyl Alcohol. *J. Am. Chem. Soc.*, 128: 4510–4511.

[52] Niu, Y., Yeung, L.K., and Crooks, R.M. (2001) Size-Selective Hydrogenation of Olefins by Dendrimer-Encapsulated Palladium Nanoparticles. *J. Am. Chem. Soc.*, 123: 6840–6846.

[53] Ganesan, M., Freemantle, R.G., and Obare, S.O. (2007) Monodisperse Thioether-Stabilized Palladium Nanoparticles: Synthesis, Characterization, and Reactivity. *Chem. Mater.*, 19: 3464–3471.

[54] Toshima, N., Shiraishi, Y., Teranishi, T., Miyake, M., Tominaga, T., Watanabe, H., Brijoux, W., Bönnemann, H., and Schmid, G. (2001) Various Ligand-Stabilized Metal Nanoclusters as Homogeneous and Heterogeneous Catalysts in the Liquid Phase. *Appl. Organometal. Chem.*, 15: 178–196.

[55] Eriksson, S., Nylen, U., Rojas, S., and Boutonnet, M. (2004) Preparation of Catalysts from Microemulsions and Their Applications in Heterogeneous Catalysis. *Appl. Catal. A*, 265: 207–219.

[56] Semagina, N., Renken, A., and Kiwi-Minsker, L. (2007) Palladium Nanoparticle Size Effect in 1-Hexyne Selective Hydrogenation. *J. Phys. Chem. C*, 111: 13933–13937.

[57] Semagina, N., Renken, A., Laub, D., and Kiwi-Minsker, L. (2007) Synthesis of Monodispersed Palladium Nanoparticles to Study Structure Sensitivity of Solvent-Free Selective Hydrogenation of 2-Methyl-3-butyn-2-ol. *J. Catal.*, 246: 308–314.

[58] Mastalir, A., and Kiraly, Z. (2003) Pd Nanoparticles in Hydrotalcite: Mild and Highly Selective Catalysts for Alkyne Semihydrogenation. *J. Catal.*, 220: 273–381.

[59] Chen, D.-H., Wang, C.-C., and Huang, T.-C. (1999) Preparation of Palladium Ultrafine Particles in Reverse Micelles. *J. Coll. Int. Sci.*, 210: 123–129.

[60] Sato, H., and Ohtsu, T., Komasawa, I. (2002) Preparation of Ultrafine Palladium Particles in Reverse Micelles and Application for Hydrogenation Catalysis. *J. Chem. Eng. Japan*, 35: 255–262.

[61] Porta, F., Prati, L., Rossi, M., and Scari, G. (2002) Synthesis of Au(0) Nanoparticles from W/O Microemulsions. *Colloids Surf., A: Physicochem. Eng. Aspects* 211: 43–48.

[62] Seregina, M.V., Bronstein, L.M., Platonova, O.A., Chernyshov, D.M., Valetsky, P.M., Hartmann, J., Wenz, E., and Antonietti, M. (1997) Preparation of Noble-Metal Colloids in Block Copolymer Micelles and Their Catalytic Properties in Hydrogenation. *Chem. Mater.*, 9: 923–931.

[63] Azzam, T., Bronstein, L., and Eisenberg, A. (2008) Water-Soluble Surface-Anchored Gold and Palladium Nanoparticles Stabilized by Exchange of Low Molecular Weight Ligands with Biamphiphilic Triblock Copolymers. *Langmuir*, DOI: 10.1021/la703719f, 24 (13): 6521–6529.

[64] Semagina, N., Joannet, E., Parra, S., Sulman, E., Renken, A., and Kiwi-Minsker, L. (2005) Palladium Nanoparticles Stabilized in Block-Copolymer Micelles for Highly Selective 2-Butyne-1,4-diol Partial Hydrogenation. *Appl. Catal. A*, 280: 141–147.

[65] Narayanan, R., and El-Sayed, M.A. (2005) Catalysis with Transition Metal Nanoparticles in Colloidal Solution: Nanoparticle Shape Dependence and Stability. *J. Phys. Chem. B*, 109: 12663–12676.

[66] Narayanan, R., and El-Sayed, M.A. (2005) Effect of Colloidal Nanocatalysis on the Metallic Nanoparticle Shape: The Suzuki Reaction. *Langmuir*, 21: 2027–2033.

[67] Sau, T.K., and Murphy, C.J. (2004) Room-Temperature, High-Yield Synthesis of Multiple Shapes of Gold Nanoparticles in Aqueous Solurion. *J. Am. Chem. Soc.*, 126: 8648–8649.

[68] Ahmadi, T.S., Wang, Z.L., Green, T.C., Henglein, A., and El-Sayed, M.A. (1996) Shape-Controlled Synthesis of Colloidal Platinum Nanoparticles. *Science*, 272, 1924–1925.

[69] Narayanan, R., and El-Sayed, M.A. (2004) Shape-Dependent Catalytic Activity of Platinum Nanoparticles in Colloidal Solution. *Nano Lett.*, 4: 1343–1348.

[70] Narayanan, R., and El-Sayed, M.A. (2004) Changing Catalytic Activity During Colloidal Platinum Nanocatalysis Due to Shape Changes: Electron-Transfer Reaction. *J. Am. Chem. Soc.*, 126: 7194–7195.

[71] Petroski, J., and El-Sayed, M.A. (2003) FTIR Study of the Adsorption of the Capping Material to Different Platinum Nanoparticle Shapes. *J. Phys. Chem. A*, 107: 8371–8375.

[72] Teranishi, T., Kurita, R., and Miyake, M. (2000) Shape Control of Pt Nanoparticles. *J. Inorg. Organomet. Polym.*, 10: 145–156.

[73] Balint, I., Miyazaki, A., and Aika, K. (2004) Effect of Platinum Morphology on Lean Reduction of NO with C_3H_6. *Phys. Chem. Chem. Phys.*, 6: 2000–2002.

[74] Miyazaki, A., and Nakano, Y. (2000) Morphology of Platinum Nanoparticles Protected by Poly(N-isopropylacrylamide). *Langmuir*, 16: 7109–7111.

[75] Fu, X., Wang, Y., Wu, N., Gui, L., and Tang, Y. (2002) Shape-Selective Preparation and Properties of Oxalate-Stabilized Pt Colloid. *Langmuir*, 18: 4619–4624.

[76] Song, H., Kim, F., Connor, S., Somorjai, G.A., and Yang, P. (2005) Pt Nanocrystals: Shape Control and Langmuir-Blodgett Monolayer Formation. *J. Phys. Chem. B.*, 109: 188–193.

[77] Sun, Y.G., and Xia, Y.N. (2002) Shape-Controlled Synthesis of Gold and Silver Nanoparticles. *Science*, 298: 2176–2179.

[78] Wiley, B., Herricks, T., Sun, Y., and Xia, Y. (2004) Polyol Synthesis of Silver Nanoparticles: Use of Chloride and Oxygen to Promote the Formation of Single-Crystal, Truncated Cubes and Tetrahedrons. *Nano Lett.*, 4: 1733–1739.

[79] Yang, J., Zhang, Q., Lee, J.Y., and Too, H.-P. (2007) Dissolution–Recrystallization Mechanism for the Conversion of Silver Nanospheres to Triangular Nanoplates. *J. Coll. Int. Sci.*, 308: 157–161.

[80] Tsuji, M., Nishizawa, Y., Matsumoto, K., Miyamae, N., Tsuji, T., and Zhang, X. (2007) Rapid Synthesis of Silver Nanostructures by Using Microwave-Polyol Method with the Assistance of Pt Seeds and Polyvinylpyrrolidone. *Coll. Surf. A*, 293: 185–194.

[81] Nikoobakht, B., and El-Sayed, M.A. (2003) Preparation and Growth Mechanism of Gold Nanorods (NRs) Using Seed-Mediated Growth Method. *Chem. Mater.*, 15: 1957–1962.

[82] Su, X., Zhao, J., Bala, H., Zhu, Y., Gao, Y., Ma, S., and Wang, Z. (2007) Fast Synthesis of Stable Cubic Copper Nanocages in the Aqueous Phase. *J. Phys. Chem. C*, 111: 14689–14693.

[83] Jin, R.C., Cao, Y.W., Mirkin, C.A., Kelly, K.L., Schatz, G.C., and Zheng, J.G. (2001) Photoinduced Conversion of Silver Nanospheres to Nanoprisms. *Science*, 294: 1901–1903.

[84] Compton, O.C., and Osterloh, F.E. (2007) Evolution of Size and Shape in the Colloidal Crystallization of Gold Nanoparticles. *J. Am. Chem. Soc.*, 129: 7793–7798.

[85] Jin, R.C., Cao, Y.C., Hao, E.C., Metraux, G.S., Schatz, G.C., and Mirkin, C.A. (2003) Controlling Anisotropic Nanoparticles Growth through Plasmon Excitation. *Nature*, 425: 487–490.

[86] Zhu, J., Shen, Y., Xie, A., Qiu, L., Zhang, Q., and Zhang, S. (2007) Photoinduced Synthesis of Anisotropic Gold Nanoparticles in Room-Temperature Ionic Liquid. *J. Phys. Chem. C*, 111: 7629–7633.

[87] Ullah, M.H., Il, K., and Ha, C.-S. (2006) Preparation and Optical Properties of Colloidal Silver Nanoparticles at a High Ag^+ Concentration. *Mater. Lett.*, 60: 1496–1501.

[88] Murphy, C.J., Gole, A.M., Hunyadi, S.E., and Orendorff, C.J. (2006) One-Dimensional Colloidal Gold and Silver Nanostructures. *Inorg. Chem.*, 45: 7544–7554.

[89] Murphy, C.J., Sau, T.K., Gole, A.M., Orendorff, C.J., Gao, J., Gou, L., Hunyadi, S.E., and Li, T. (2005) Anisotropic Metal Nanoparticles: Synthesis, Assembly, and Optical Applications. *J. Phys. Chem. B*, 109:13857–13870.

[90] Sau, T.K., and Murphy, C.J. (2004) Seeded High Yield Synthesis of Short Au Nanorods in Aqueous Solution. *Langmuir*, 20: 6414–6420.

[91] Johnson, C.J., Dujardin, E., Davis, S.A., Murphy, C.J., and Mann, S. (2002) Growth and Form of Gold Nanorods Prepared by Seed-Mediated, Surfactant-Directed Synthesis. *J. Mater. Chem.*, 12: 1765–1770.

[92] Jana, N.R., Gearheart, L., and Murphy, C.J. (2001) Seed-Mediated Growth Approach for Shape-Controlled Synthesis of Spheroidal and Rod-Like Gold Nanoparticles Using a Surfactant Template. *Adv. Mater.*, 13: 1389–1393.

[93] Perez-Juste, J., Liz-Marzan, L.M., Carnie, S., Chan, D.Y.C., and Mulvaney, P. (2004) Electric-Field-Directed Growth of Gold Nanorods in Aqueous Surfactant Solutions. *Adv. Funct. Mater.*, 14: 571–579.

[94] Navaladian, S., Janet, C.M., Viswanathan, B., Varadarajan, T.K., and Viswanath, R.P. (2007) A Facile Room-Temperature Synthesis of Gold Nanowires by Oxalate Reduction Method. *J. Phys. Chem. C*, 111: 14150–14156.

[95] Krichevski, O., and Markovich, G. (2007) Growth of Colloidal Gold Nanostars and Nanowires Induced by Palladium Doping. *Langmuir*, 23: 1496–1499.

[96] Kuo, P.-L., and Chen, C.-C. (2006) Generation of Gold Thread from Au(III) and Triethylamine. *Langmuir*, 22: 7902–7906.

[97] Ramanath, G., D'Arcy-Gall, J., Maddanimath, T., Ellis, A.V., Ganesan, P.G., Goswami, R., Kumar, A., and Vijayamohanan, K. (2004) Templateless

Room-Temperature Assembly of Nanowire Networks from Nanoparticles. *Langmuir*, 20: 5583–5587.

[98] Chen, J., Wiley, B.J., and Xia, Y. (2007) One-dimensional Nanostructures of Metals: Large-Scale Synthesis and Some Potential Applications. *Langmuir*, 23: 4120–4129.

[99] Sun, Y., and Xia, Y. (2002) Large-Scale Synthesis of Uniform Silver Nanowires through a Soft, Self-Seeding, Polyol Process. *Adv. Mater.*, 14: 833–837.

[100] Sun, Y., Yin, Y., Mayers, B.T., Herricks, T., and Xia, Y. (2002) Uniform Silver Nanowires Synthesis by Reducing $AgNO_3$ with Ethylene Glycol in the Presence of Seeds and Poly(vinyl pyrrolidone). *Chem. Mater.*, 14: 4376–4745.

[101] Tsuji, M., Matsumoto, K., Miyamae, N., Tsuji, T., and Zhang, X. (2007) Rapid Preparation of Silver Nanorods and Nanowires by a Microwave-Polyol Method in the Presence of Pt Catalyst and Polyvinylpyrrolidone. *Crystal Growth & Design*, 7: 311–320.

[102] Chimentao, R.J., Kirm, I., Medina, F., Rodriguez, X., Cesteros, Y., Salagre, P., and Sueiras, J.E. (2004) Different Morphologies of Silver Nanoparticles as Catalysts for the Selective Oxidation of Styrene in the Gas Phase. *Chem. Comm.*, 7: 846–846.

[103] Caswell, K.K., Bender, C.M., and Murphy, C.J. (2003) Seedless, Surfactantless Wet Chemical Synthesis of Silver Nanowires. *Nano Lett.*, 3: 667–669.

[104] Chen, J., Herricks, T., Geissler, M., and Xia, Y. (2004) Single-Crystal Nanowires of Platinum Can Be Synthesized by Controlling the Reaction Rate of a Polyol Process. *J. Am. Chem. Soc.*, 126: 10854–10855.

[105] Berhault, G., Bausach, M., Bisson, L., Becerra, L., Thomazeau, C., and Uzio, D. (2007) Seed-Mediated Synthesis of Pd Nanocrystals: Factors Influencing a Kinetic- or Thermodynamic-Controlled Growth Regime. *J. Phys. Chem. C*, 111: 5915–5925.

[106] Coq, B., and Figueras, F. (2001) Bimetallic Palladium Catalysts: Influence of the Co-Metal on the Catalyst Performance. *J. Mol. Catal. A*, 173: 117–134.

[107] Singh, U.K., and Vannice, M.A. (2001) Kinetics of Liquid-Phase Hydrogenation Reactions over Supported Metal Catalysts—a Review. *Appl. Catal. A*, 213: 1–24.

[108] Chen, B., Dingerdissen, U., Krauter, J.G.E., Rotgerink, H.G.J.L., Mobus, K., Ostgard, D.J., Panster, P., Riermeier, T.H., Seebald, S., Tacke, T., and Trauthwein, H. (2005) New Developments in Hydrogenation Catalysis Particularly in Synthesis of Fine and Intermediate Chemicals. *Appl. Catal. A*, 280: 17–46.

[109] Hub, S., Hilaire, L., and Touroude, R. (1988) Hydrogenation of But-1-yne and But-1-ene on Palladium Catalysts: Particle Size Effect. *Appl. Catal.*, 36: 307–322.

[110] Ryndin, Y.A., Nosova, L.V., Boronin, A.I., and Chuvilin, A.L. (1988) Effect of dispersion of supported palladium on its electronic and catalytic properties in the hydrogenation of vinylacetylene. *Appl. Catal.*, 42: 131–141.

[111] Rajaram, J., Narula, A.P.S., Chawla, H.P.S., and Dev, S. (1983) Semihydrogenation of Acetylenes. Modified Lindlar Catalyst. *Tetrahedron*, 39: 2315–2322.

[112] Gigola, C.E., Aduriz, H.R., and Bodnariuk, P. (1986) Particle Size Effect in the Hydrogenation of Acetylene under Industrial Conditions. *Appl. Catal.*, 27: 133–144.

[113] Tribolet, P., and Kiwi-Minsker, L. (2005) Palladium on Carbon Nanofibers Grown on Metallic Filters as Novel Structured Catalyst. *Catal. Today*, 105: 337–343.

[114] Ruta, M., Semagina, N., and Kiwi-Minsker, L. (2008) Monodispersed Pd-Nanoparticles for Acetylene Selective Hydrogenation: Particle Size and Support Effects. *J. Phys. Chem. C*, submitted for revision, 112: 13635–13641.

[115] Borodzinski, A. (1999) Hydrogenation of Acetylene-Ethylene Mixtures on a Commercial Palladium Catalyst. *Catal. Lett.*, 63: 35–42.

[116] Borodzinski, A., and Bond, G.C. (2006) Selective Hydrogenation of Ethyne in Ethene-Rich Streams on Pallaium Catalysts. Part 1. Effect of Changes to the Catalyst During Reaction. *Catal. Rev.*, 48: 91–144.

[117] Teschner, D., Vass, E., Havecker, M., Zafeiratos, S., Schnorch, P., Sauer, H., Knop-Gericke, A., Schlogl, R., Chamam, M., Wootsch, A., Canning, A.S., Gamman, J.J., Jackson, S.D., McGregor, J., and Gladden, L.F. (2006) Alkyne Hydrogenation over Pd Catalysts: A New Paradigm. *J. Catal.*, 242: 26–37.

[118] Benedetti, A., Fagherazzi, G., Pinna, F., Rampazzo, G., Selva, M., and Strukul, G. (1991) The Influence of a Second Metal Component (Cu, Sn, Fe) on Pd/SiO_2 Activity in the Hydrogenation of 2,4-Dinitrotoluene. *Catal. Lett.*, 10: 215–224.

[119] Molnar, A., Smith, G.V., and Bartok, M. (1986) Selective Hydrogenation of Alkynes over Metallic Glasses. *J. Catal.*, 101: 67–72.

[120] Silvestre-Albero, J., Rupprechter, G., and Freund, H.-J. (2006) From Pd Nanoparticles to Single Crystals: 1,3-Butadiene Hydrogenation on Well-Defined Model Catalysts. *Chem. Commun*, 1: 80–82.

[121] Doyle, A.M., Shaikhutdinov, S.K., and Freund, H.-J. (2005) Surface-Bonded Presursor Determines Particle Size Effects for Alkene Hydrogenation on Palladium. Angew. *Chem. Int. Ed.*, 44: 629–631.

[122] Boitiaux, J.P., Cosyns, J., and Vasudevan, S. (1983) Hydrogenation of Highly Unsaturated Hydrocarbons over Highly Dispersed Palladium Catalyst. Part I: Behavior of Small Metal Particles. *Appl. Catal.*, 6: 41–51.

[123] Zakarina, N.A., Zakumbaeva, G.D., Toktabaeva, N.F., Dyusenbina, B.B., Litvyakova, E.N., and Kuanyshev, A.S. (1983) Monodispersed Palladium Catalysts in the Hydrogenation of Dimethylethynylcarbinol. *Kinet. Catal*, 24: 733–737.

[124] Zakumbaeva, G.D., Zakarina, N.A., Naidin, V.A., Dostiyarov, A.M., Toktabaeva, N.F., and Litvyakova, E.N. (1983) Properties of Monodisperse Pd/MgO Catalysts. *Kinet. Catal.*, 24: 379–383.

[125] Silvestre-Albero, J., Rupprechter, G., and Freund, H.-J. (2005) Atmospheric Pressure Studies of Selective 1,3-Butadiene Hydrogenation on Pd Single Crystals: Effect of CO Addition. *J. Catal.*, 235: 52–59.

[126] Guo, X.C., and Madix, R.J. (1995) Selective Hydrogenation and H-D Exchange of Unsaturated Hydrocarbons on Pd(100)-P(1×1)-H(D). *J. Catal.*, 155: 336–344.

[127] Ulan, J.G., Maier, W.F., and Smith, D.A. (1987) Rational Design of a Heterogeneous Pd Catalyst for the Selective Hydrogenation of Alkynes. *J. Org. Chem.*, 52: 3132–3142.

[128] Englisch, M., Jentys, A., and Lercher, J.A. (1997) Structure Sensitivity of the Hydrogenation of Crotonaldehyde over Pt/SiO_2 and Pt/TiO_2. *J. Catal.*, 166: 25–35.

[129] Bezemer, G.L., Bitter, J.H., Kuipers, H.P.C.E., Oosterbeek, H., Holewijn, J.E., Xu, X., Kapteijn, F., van Dillen, A.J., and de Jong, K.P. (2006) Cobalt Particle Size Effects in the Fischer-Tropsch Reaction Studied with Carbon Nanofiber Supported Catalysts. *J. Am. Chem. Soc.*, 128: 3956–3964.

[130] Ojeda, M., Rojas, S., Boutonnet, M., Perez-Alonso, F.J., Garcıa-Garcıa, F.G., and Fierro, J.L.G. (2004) Synthesis of Rh Nano-Particles by the Microemulsion Technology. Particle Size Effect on the $CO+H_2$ Reaction. *Appl. Catal. A*, 274: 33–41.

[131] Birchem, T., Pradier, C.M., Berthier, Y., and Cordier, G. (1994) Reactivity of 3-Methyl-Crotonaldehyde on Pt(111). *J. Catal.*, 146: 503–510.

[132] Rocaboy, C., and Gladysz, J.A. (2002) Highly Active Thermomorphic Fluorous Palladacycle Catalyst Precursors for the Heck Reaction, Evidence for a Palladium Nanoparticle Pathway. *Org. Lett.*, 4: 1993–1996.

[133] Astruc, D. (2007) Palladium Nanoparticles as Efficient Green Homogeneous and Heterogeneous Carbon-Carbon Coupling Precatalysts: A Unifying View. *Inorg. Chem.*, 46: 1884–1894.

[134] Yeung, L.K., Crooks, andR.M. . Heck. (2001) Heterocoupling within a Dendritic Nanoreactor. *Nano Lett.*, 1: 14–17.

[135] Pathak, S., Greci, M.T., Kwong, R.C., Mercado, K., Prakash, G.K.S., Olah, G.A., and Thompson, M.E. (2000) Synthesis and Applications of Palladium-Coated Poly(vinylpyridine) Nanospheres. *Chem. Mater.*, 12: 1985–1989.

[136] Gopidas, K.R., Whitesell, J.K., and Fox, M.A. (2003) Synthesis, Characterization, and Catalytic Applications of a Palladium-Nanoparticle-Cored Dendrimer. *Nano Lett.*, 3: 1757–1760.

[137] Gniewek, A., Trzeciak, A.M., Ziolkowski, J.J., Kepinski, L., Wrzyszsz, J., and Tylus, W. (2005) Pd-PVP Collod as Catalyst for Heck and Carbonylation Reactions: TEM and XPS Studies. *J. Catal.*, 229: 332–343.

[138] Na, Y., Park, S., Han, S.B., Han, H., Ko, S., and Chang, S. (2004) Ruthenium–Catalyzed Heck–Type Olefination and Suzuki Coupling Reactions: Studies on the Nature of Catalytic Species. *J. Am. Chem. Soc.*, 126: 250–258.

[139] Augustine, R.L., and O'Leary, S.T. (1995) Heterogeneous Catalysis in Organic Chemistry. Part 10. Effect of the Catalyst Support on the Regiochemistry in the Heck Arylation Reaction. *J. Mol. Catal. A*, 95: 277–285.

[140] Narayanan, R., and El-Sayed, M.A. (2003) Effect of Catalysis on the Stability of Metallic Nanoparticles: Suzuki Reaction Catalyzed by PVP-Palladium Nanoparticles. *J. Am. Chem. Soc.*, 125: 8340–8347.

[141] Narayanan, R., and El-Sayed, M.A. (2004) Effect of Colloidal Catalysis on the Nanoparticle Size Distribution: Dendrimer-Pd vs PVP-Pd Nanoparticles Catalyzing the Suzuki Coupling Reaction. *J. Phys. Chem. B*, 108: 8572–8580.

[142] Narayanan, R., and El-Sayed, M.A. (2005) FTIR Study of the Mode of Binding of the Reactants on the Pd Nanoparticles Surface During the Catalysis of the Suzuki Reaction. *J. Phys. Chem. B*, 109: 4357–4360.

[143] Fukuoka, A., Higashimoto, N., Sasaki, M., Harada, M., Inagaki, S., Fukushima, Y., and Ichikawa, M. (2000) Templating Fabrication and Catalysis of Platinum Nanowires in Mesoporous Channels of FSM-16. *Stud. Surf. Sci. Catal.* **2000**, 130: 3041–3046.

[144] Somorjai, G.A. (1997) New Model Catalysts (Platinum Nanoparticles) and New Techniques (SFG and STM) for Studies of Reaction Intermediates and Surface Restructuring at High Pressures During Catalytic Reactions. *Appl. Surf. Science*, 121–122: 1–19.

[145] Zuegg, H., and Kramer, R. (1983) Particle Size Effect on Catalysis Caused by Adlining Metal-Support Sites. *Vacuum*, 33: 697–699.

[146] Zuegg, H., and Kramer, R. (1984) The Influence of Ammonia Poisoning on the Selectivity of the Hydrogenolysis of Methylcyclopentane on Platinum. *Appl. Catal.*, 9: 263–268.

[147] Kramer, R., and Zuegg, H. (1983) The Hydrogenolysis of Methylcyclopentane on Platinum Model Catalysts: Particle Size Effect Due to a Reaction Occuring at the Phase Boundary Metal-Support. *J. Catal.*, 80: 446–456.

[148] Li, Y., Petroski, J., and El-Sayed, M.A. (2000) Activation Energy of the Reaction between Hexacyanoferrate(III) and Thiosulfate Ions Catalyzed by Platinum Nanoparticles *J. Phys. Chem. B*, 104: 10956–10959.

[149] Narayanan, R., and El-Sayed, M.A. (2003) Effect of Catalytic Activity on the Metallic Nanoparticle Size Distribution: Electron-Transfer Reaction between $Fe(CN)_6$ and Thiosulfate Ions Catalyzed by PVP-Platinum Nanoparticles. *J. Phys. Chem. B*, 107: 12416–12424.

[150] Sharma, R.K., Sharma, P., and Maitra, A. (2003) Size-Dependent Catalytic Behavior of Platinum Nanoparticles on the Hexacyanoferrate(III)/Thiosulfate Redox Reaction. *J. Colloid Interface Sci.*, 265: 134–140.

[151] Clint, J.H., Collins, I.R., Williams, J.A., Robinson, B.H., Towey, T.F., and Khan-Lodhi, P.C.A. (1993) Synthesis and Characterisation of Colloidal Metal and Semiconductor Particles Prepared in Microemulsion. *Faraday Discuss.*, 95: 219–233.

[152] Mayrhofer, K.J.J., Blizanac, B.B., Arenz, M., Stamenkovic, V.R., Ross, P.N., and Markovic, N.M. (2005) The Impact of Geometric and Surface Electronic Properties of Pt-Catalysts on the Particle Size Effect in Electrocatalysis. *J. Phys. Chem. B*, 109: 14433–14440.

[153] Tang, Z., Geng, D., and Lu, G. (2005) Size-Controlled Synthesis of Colloidal Platinum Nanoparticles and Their Activity for the Electrocatalytic Oxidation of Carbon Monoxide. *J. Coll. Int. Sci.*, 287: 159–166.

[154] Sun, Y., Zhuang, L., Lu, J., Hong, X., and Liu, P. (2007) Collapse in Crystalline Structure and Decline in Catalytic Activity of Pt Nanoparticles on Reducing Particle Size to 1 nm. *J. Am. Chem. Soc.*, 129: 15465–15467.

[155] Gong, Y., Hou, Z., and Xin, H. (2004) Optimal Particle Size for Reaction Rate Oscillation in CO Oxidation on Nanometer-Sized Palladium Particles. *J. Phys. Chem. B*, 108: 17796–17799.

[156] Lopez, N., and Norskov, J.K. (2002) Catalytic CO Oxidation by a Gold Nanoparticle: A Density Functional Study. *J. Am. Chem. Soc.*, 124: 11262–11263.

[157] Bulushev, D.A., Yuranov, I., Suvorova, E.I., Buffat, P.A., and Kiwi-Minsker, L. (2004) Highly Dispersed Gold on Activated Carbon Fibers for Low-Temperature CO Oxidation. *J. Catal.*, 224: 8–17.

[158] Haruta, M. (1997) Size- and Support-Dependency in the Catalysis of Gold. *Catal. Today*, 36: 153–166.

[159] Chusuei, C.C., Lai, X., and Luo, K. (2000) Goodman, D.W. Modeling Heterogeneous Catalysts: Metal Clusters on Planar Oxide Supports. *Top. Catal.*, 14: 71–83.

[160] Overbury, S.H., Schwartz, V., Mullins, D.R., Yan, W., and Dai, S. (2006) Evaluation of the Au Size Effect: CO Oxidation Catalyzed by Au/TiO_2. *J. Catal.*, 241: 56–65.

[161] Hayden, B.E., Pletcher, D., Rendall, M.E., and Suchsland, J.-P. (2007) CO Oxidation on Gold in Acidic Environments: Particle Size and Substrate Effects. *J. Phys. Chem. C*, 111: 17044–17051.

[162] Guczi, L., Peto, G., Beck, A., Frey, K., Geszti, O., Molnar, G., and Daroczi, C. (2003) Gold Nanoparticles Deposited on SiO_2/Si(100): Correlation between Size, Electron Structure, and Activity in CO Oxidation. *J. Am. Chem. Soc.*, 125: 4332–4337.

[163] Jena, B.K., and Raj, C.R. (2007) Shape-Controlled Synthesis of Gold Nanoprism and Nanoperiwinkles with Pronounced Electrocatalytic Activity. *J. Phys. Chem. C*, 111: 15146–15153.

[164] Chrzanowski, W., and Wieckowski, A. (1998) Surface Structure Effects in Platinum/Ruthenium Methanol Oxidation Electrocatalysis. *Langmuir*, 14: 1967–1970.

[165] Bergamaski, K., Pinheiro, A.L.N., Teixeira-Neto, E., and Nart, F.C. (2006) Nanoparticle Size Effects on Methanol Electrochemical Oxidation on Carbon Supported Platinum Catalysts. *J. Phys. Chem. B*, 110: 19271–19279.

[166] Park, S., Xie, Y., and Weaver, M.J. (2002) Electrocatalytic Pathways on Carbon-Supported Platinum Nanoparticles: Comparison of Particle-Size-Dependent Rates of Methanol, Formic Acid, and Formaldehyde Electrooxidation. *Langmuir*, 18: 5792–5798.

[167] Zhou, W.P., Lewera, A., Larsen, R., Masel, R.I., Bagus, P.S., and Wieckowski, A. (2006) Size Effects in Electronic and Catalytic Properties of Unsupported Palladium Nanoparticles in Electrooxidation of Formic Acid. *J. Phys. Chem. B*, 110: 13393–13398.

[168] Li, F., Zhang, Q., and Wang, Y. (2008) Size Dependence in Solvent-Free Aerobic Oxidation of Alcohols Catalyzed by Zeolite-Supported Palladium Nanoparticles. *Appl. Catal. A*, 334: 217–226.

[169] Pocoroba, E., Pettersson, L.J., Agrell, J., Boutonnet, M., and Jansson, K. (2001) Exhaust Gas Catalysts for Heavy-Duty Applications: Influence of the Pd Particle Size and Particle Size Distribution on the Combustion of Natural Gas and Biogas. *Top. Catal.*, 16–17: 407–412.

[170] Piccolo, L., and Henry, C.R. (2001) NO–CO Reaction Kinetics on Pd/MgO Model Catalysts: Morphology and Support Effects. *J. Mol. Catal. A*, 167: 181–190.

[171] Rosca, V., and Koper, M.T.M. (2005) Mechanism of Electrocatalytic Reduction of Nitric Oxide on Pt(100). *J. Phys. Chem. B*, 109: 16750–16759.

[172] Boutonnet, M., Kizling, J., Touroude, R., Maire, G., and Stenius, P. (1986) Monodispersed Colloidal Metal Particles from Non-Aqueous Solutions: Catalytic Behavior for the Hydrogenation of But-1-ene of Platinum Particles in Solution. *Appl. Catal.*, 20: 163–177.

[173] Pillai, V., Kumar, P., Hou, M.J., Ayyub, P., and Shah, D.O. (1995) Preparation of Nanoparticles of Silver Halides, Superconductors and Magnetic Materials Using Water-in-Oil Microemulsions as Nano-Reactors. *Adv. Coll. Int. Sci.*, 55: 241–269.

[174] Arcoleo, V., Goffredi, M., Longo, A., and Turco Liveri, V. (1998) Physico-Chemical Characterization of Pd Nanoparticles Synthesized in W/O Microemulsions. *Mat. Sci. Eng. C*, 6: 7–11.

[175] Zarur, A.J., and Ying, J.Y. (2000) Reverse Microemulsion Synthesis of Nanostructured Complex Oxides for Catalytic Combustion. *Nature*, 403: 65–67.

[176] Higgins, R.J., and Goldsmith, R.L. (1999) Process and System for Production of Inorganic Nanoparticles. Patent WO 99/11243.

[177] Zhang, J., Han, B., Liu, J., Zhang, X., He, J., Liu, Z., Jiang, T., and Yang, G. (2002) Recovery of Silver Nanoparticles Synthesized in AOT/$C_{12}E_4$ Mixed Reverse Micelles by Antisolvent CO_2. *Chem. Eur. J.*, 8: 3879–3883.

[178] Miyao, T., Toyoizumi, N., Okuda, S., Imai, Y., Tajuma, K., and Naito, S. (1999) Preparation of Pd/SiO_2 Ultra-Fine Particles in Reversed Micelles and Their Catalytic Activity. *Chem. Lett.*, 28 (10): 1125–1126.

[179] Bonini, M., Bardi, U., Berti, D., Neto, C., and Baglioni, P. (2002) A New Way to Prepare Nanostructured Materials: Flame Spraying of Microemulsions. *J. Phys. Chem. B*, 106: 6178–6183.

[180] Kiwi-Minsker, L., Joannet, E., and Renken, A. (2004) Loop Reactor Staged with Structured Fibrous Catalytic Layers for Liquid-Phase Hydrogenations. *Chem. Eng. Sci.*, 59: 4919–4925.

[181] Brayner, R., Viau, G., and Bozon-Verduraz, F. (2002) Liquid-Phase Hydrogenation of Hexadienes on Metallic Colloidal Nanoparticles Immobilized on Supports via Coordination Capture by Bifunctional Organic Molecules. *J. Mol. Catal. A*, 182–183: 227–238.

[182] The Council for Chemical Research, Inc.: Chemicals Industry Catalysis Workshop Report http://www.ccrhq.org/vision2020/catalysis. Last accessed 25 March 2009.